Modeling of Waste Tire Pyrolysis and Hydrotreatment for Jet Fuel Applications

André Gonçalo Ferreira da Silva

Thesis to obtain the Master of Science Degree in

Chemical Engineering

Supervisors:
Dr. Ana Catarina Gouveia Braz
Dr. Maria Cristina de Carvalho Silva Fernandes

Examination Committee

Chairpeson: Dr. Maria de Fátima Grilo da Costa Montemor
Supervisor: Dr. Ana Catarina Gouveia Braz
Member of Committee: Dr. Henrique Aníbal Santos de Matos

December 2022

Declaration of Originality

I declare that this document is an original work of my own authorship and that it fulfills all the requirements of the Code of Conduct and Good Practices of the Universidade de Lisboa.

Acknowledgments

To start, I'd like to thank Prof. Catarina Braz and Prof. Cristina Fernandes for their support, advice and availability as I worked on this project. I'd like to thank my family for their love and support over the years, as well as my colleagues and friends for making these years more enjoyable and fruitful. Finally, I would like to thank a special friend who has been with me for many years and hopefully more to come.

Abstract

This thesis investigated the pyrolysis modeling of the waste tires and the hydrotreatment modeling of pyrolysis oil and analyzed the potential of the oil resulting from both processes for jet fuel applications using *Aspen Plus*® V11.

Waste tires are a major problem, with 1 billion tires being scrapped yearly. Their pyrolysis produces oil that has the ingredients needed for jet fuel application. As a result, the obtained oil by pyrolysis was studied for jet fuel replacement.

The tire pyrolysis modeling was done using Ismail et al. 2017 kinetic model. It was found that the implementation of this model could not reproduce the literature results. To improve the implemented model, parameter estimation was performed using *gPROMS ModelBuilder V7.07*®. The model with the new parameter estimated gave a 3% improvement over the literature data Afterward, a sensitivity analysis was performed on the pyrolysis reactor conditions. It was concluded that jet fuel specifications could not be met.

Hydrotreatment was performed to improve the pyrolysis oil. Olmo 2015 kinetic model was used to model the hydrotreatment. When mixing the pyrolysis oil with the hydrogen at the ratio mentioned in the literature, total vaporization occurred, contrary to what was predicted. To model the hydrotreatment process, multiple alternatives were studied. Adding a custom term to the kinetic model was the best solution. Changing the temperature and amount of catalyst in a sensitivity analysis led to a hydrotreated oil that was almost as good as jet fuel.

Keywords: pyrolysis modeling, hydrotreatment modeling, jet fuel, sensitivity analysis.

Resumo

Nesta tese investigou-se a modelação da pirólise de pneus usados, do hidrotratamento de óleo de pirólise, e analisou-se o potencial do óleo resultante para jet fuel, utilizando o simulador *Aspen Plus*® V11

Pneus usados são um problema atualmente com cerca de 1 bilião de pneus a serem descartados anualmente. A sua pirólise produz óleo com conteúdo útil para a produção de jet fuel. Desta forma, o potencial da utilização de óleo de pirólise para substituir jet fuel foi estudada.

Utilizou-se o modelo cinético de Ismail et al. 2017 para modelar a pirólise. Não se conseguiu reproduzir os dados da literatura através da implementação do modelo cinético. Como tal estimaram-se novos parâmetros com o *gPROMS ModelBuilder V7.07*®. O modelo com os novos parâmetros permitiu um melhoramento de 3% em relação ao modelo da literatura.

Efetuou-se uma análise de sensibilidade às condições do reator de pirólise, tendo-se concluído que as especificações do jet fuel não podiam ser cumpridas.

Realizou-se hidrotratamento para melhorar o óleo de pirólise. O modelo cinético de Olmo 2015 foi utilizado para modelar o processo. Ao misturar óleo de pirólise com hidrogénio na proporção mencionada na literatura, ocorreu vaporização total, ao contrário do que acontece na realidade. Para modelar o processo de hidrotratamento, foram estudadas múltiplas alternativas. A adição de um termo personalizado ao modelo cinético correspondeu à melhor situação. Através de análise de sensibilidade à temperatura e quantidade de catalisador, concluiu-se que o óleo hidrotratado se encontrava perto das especificações exigidas para utilização como jet fuel.

Palavras-chave: modelação de pirólise, modelação de hidrotratamento, jet fuel, análise de sensibilidade.

Table of Contents

List of Figures

List of Tables

Acronyms

BTEX	Mixture of benzene, toluene, ethylbenzene, and xylene
NR	Natural rubber
SR	Synthetic rubber
BR	Butadiene rubber
SBR	Styrene-butadiene rubber
TT	Truck tires
PCT	Passenger car tires
NATO	North Atlantic Treaty Organization
ASTM	American Society For Testing And Materials
AJF	Alternative Jet Fuel
CB	Carbon black
CSBR	Conical Spouted Bed
TPO	Tire pyrolysis oil
FCC	Fluid catalytic cracking
RPlug	Reactor Model Based On Plug Flow With Rate Based Kinetics
RYield	Reactor Model Based On Product Yields
RGibbs	Multiphase Equilibrium Reactor Model
HT	Hydrotreatment
HDS	Hydrodesulfurization
HDN	Hydrodenitrification
HDA	Hydrodearomatization
HDM	Hydrodemetallization
HDO	Hydrodeoxygenation
WHSV	Weight hourly space velocity (hr^{-1})
LHSV	Liquid hourly space velocity (hr^{-1})
ULSD	Ultra-low-sulfur diesel
HDS	Hydrodesulfurization
BTZ	Benzothiazole
REquil	Reactor Model based on reaction stochiometry and phase equilibrium
RStoic	Reactor Model Based On Reaction Stoichiometry
PR-BM	Peng Robinson with Boston-Mathias alpha function equation of state
HCOALGEN	Enthalpy Model For Coal
DCOALIGT	Density Model For Coal
API	American Petroleum Institute
TTO	Truck tires oil
PCTO	Passenger car tires oil
GCxGC	Gas Chromatography
1DRT	1st Dimension Retention Time, Min
2DRT	2nd Dimension Retention Time, Min
HC	Hydrocracking
SSTPO	Simulated scrap tire oil
NBP	Normal Boiling Point
MW	Molecular weight

1 Introduction

The world's population growth directly impacts the global development of the automobile industry. As a result, the global tire market, the foundation of the automotive industry, is expanding. Approximately 1.6 billion new tires are produced globally, but the recycling sector processes only 100 million, and approximately 1 billion waste tires are generated. (Jansen, van der Walt, and Crouse 2022) In 2015, 386 800 tons of waste tires were produced in Europe.(Balaban, Smejda, and Onur 2022)

Tires are produced from a complex mixture of synthetic and natural metal, fabric, and additives. Due to their complex chemistry, organic polymers, metals, and other inorganic chemicals are not biodegradable and pose a significant environmental threat. Stockpiling of waste tires serves as breeding grounds for disease-carrying mosquitoes and presents a high fire risk. Due to negative effects on health and the environment, European Union issued 1991/311/EC, which banished the disposal of tires in landfills in any form. This led to a 92% recovery rate of waste tires in Europe in 2018. (Eskandarinia, Esmailzade, and Aslani n.d.; Balaban, Smejda, and Onur 2022)

However, on the global estimation of waste tire management, 3–15% of tires are recycled, 5–23% reused, 20–30% landfilled/stockpiled, and 25–60% incinerated annually. (Abbas-Abadi et al. 2022) Despite significant progress in waste tire management, more study is required to improve current practices and create better alternatives. Pyrolysis is a method of waste tire treatment that is becoming increasingly popular and has been the focus of numerous articles.

According to T. Dick et al. 2020, pyrolysis and gasification are the most effective processes for converting used tires into helpful energy and other chemical products. Pyrolysis is a thermochemical process that causes the cracking of polymeric chains in the absence of oxygen, resulting in a liquid fraction, a gas phase, and a solid fraction. The gas is composed primarily of C1–C4 hydrocarbons and hydrogen and can be burned to provide energy for the industrial process or directly power the pyrolysis process. The char can be used to create activated carbon or carbon black.

According to numerous studies, oil accounts for 40–60 %wt of the pyrolysis products. Due to its high calorific value (38–45 MJ/kg), it has been considered an alternative to fossil fuels. In addition to limonene, BTEX (a mixture of benzene, toluene, ethylbenzene, and xylene), and aromatic hydrocarbons, the pyrolysis oil also contains chemicals with high added value. (Han, Stankovikj, and Garcia-Perez 2017; G. Zhang et al. 2021; Martín et al. 2022)

Figure 1 shows the valorization pathways available for tires and the different petrochemical industry manufacturing stages to which each recovered product can be recycled. (Olmo 2015)

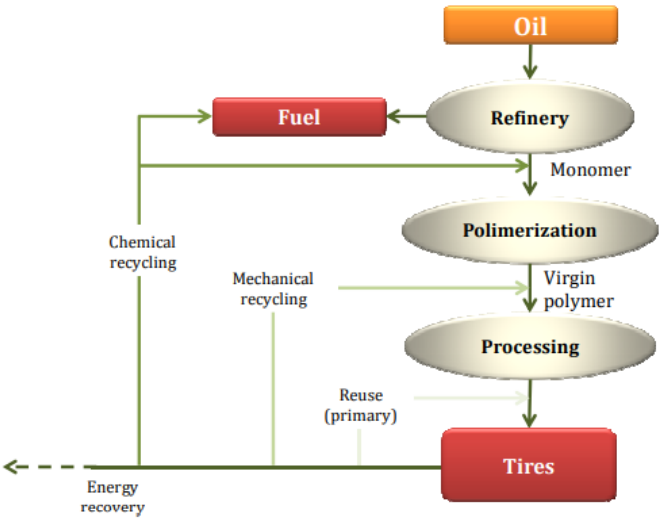

Figure 1 - Valorization pathways available for tires and the different petrochemical industry manufacturing stages to which each recovered product can be recycled. (Olmo 2015)

1.1 Motivation

Modern industrial society relies heavily on fossil fuels, which causes significant environmental issues, including global warming. In 2018, aviation accounted for 2.4 % of worldwide carbon dioxide emissions, equivalent to 905 billion kg of CO_2. If no action is taken to reduce emissions, this number might triple by 2050.

The global aviation community has set a goal of lowering net aviation carbon emissions by 50 % by 2025 compared to 2005. Alternative low-emission fuels, CO_2 certification of new aircraft, and aerodynamic and motor system improvements have been recommended to reduce emissions.

This is where pyrolysis oil as a potential alternative fuel comes into play. The oil produced by pyrolysis has a very high calorific value (44 MJ/kg), a very low ash content (0.05 %wt), and a relatively low sulfur content (0.8-1.5 %wt). The composition of pyrolysis oil has been described as having 3 %wt paraffin&isoparaffin content, more than 55 %wt aromatic compounds, and more than 20 %wt naphthenes. (Olmo 2015) Currently, available jet fuel derived from fossil petroleum contains approximately 20 % paraffin, 40 % isoparaffin, 20 % naphthene, and 20 % aromatic compounds. (Han, Stankovikj, and Garcia-Perez 2017)

As a result, pyrolysis oil contains all components needed to produce jet fuel. However, it must be improved because it cannot be used directly. By hydrotreating and hydrocracking, the pyrolysis oil composition can be upgraded to meet the required standard. This procedure aims to 1) create new oil products or improve existing ones, 2) convert low-quality or inferior resources into valuable products, and 3) convert higher molecular-weight components into lower molecular-weight compounds. (Speight 1999; Somsri 2018)

1.2 Problem statement

This thesis aims to simulate waste tire pyrolysis and upgrading, specifically by hydrotreatment using *Aspen Plus*®, and to assess waste tire potential to be used as jet fuel. Chapter 2 (pag.4) provides a review of tires, jet fuel, pyrolysis, and hydrotreatment. The overview of pyrolysis process modeling, the modeling used, the sensitivities made, and the conclusions are presented in Chapter 3 (pag.22). The overview of hydrotreatment process modeling, the modeling used, the sensitivities made, and conclusions are presented in Chapter 4 (pag.41). Chapter 5 (pag.66) summarizes the key findings and recommendations for future research.

2 Literature Review

This literature review gives an overview of tire composition, Section 2.1 (pag.4) types of jet fuels, and jet fuel specifications. Section 2.2 (pag.5), the pyrolysis process, conditions, types of reactors, and simulation of the process in *Aspen Plus*®, Section 2.3 (pag.8) and the hydrotreatment process, as well as simulation of this process in *Aspen Plus*®, Section 2.4 (pag.17)

2.1 Tires Composition

The primary function of a tire is to provide secure contact between the vehicle and the road surface. Tire compositions vary significantly due to the wide variety of tire applications. More than 200 distinct raw materials are used to manufacture a tire. Tires contain carbon black, steel, natural rubber (NR), and synthetic rubber (SR) as primary components. Synthetic rubber examples include butadiene rubber (BR) and styrene-butadiene rubber (SBR). The combination of these materials enables the production of tires with a wide range of properties suitable for any application. The addition of carbon black to rubber improves and reinforces its physical properties. In order to increase its hardness, rubber is also vulcanized. This procedure forms disulfide bonds between the chains of rubber molecule chains. (Battista et al., 2021)

According to J. D. Martínez 2021, the most important classification factor for tires is their size. For instance, tires can be categorized as truck tires (TT) or passenger car tires (PCT). Table 1 shows the approximate proportions of tires raw materials for truck tires (TT) and passenger car tires (PCT) in the USA and EU. (J. D. Martínez 2021)

Table 1 - Shows the approximate proportions of these raw materials for TT and PCT in the USA and EU. (J. D. Martínez 2021)

Raw materials	USA (%wt)		EU (%wt)	
	PCT	TT	PCT	TT
Natural Rubber	14	27	22	30
Synthetic Rubber	27	14	23	15
Carbon Black	28	28	28	20
Steel	15	15	13	25
Others (fabric, fillers, accelerators, etc.)	16	16	14	10

2.1.1 Tires elemental composition

Waste tire compositions are determined by analyses suitable for solid materials characterization, such as proximate and ultimate analyses. Proximate analysis is used to determine the weight percentages of moisture, volatile matter, fixed carbon, and ash. In contrast, ultimate analysis determines the weight percentages of chemical elements (carbon, hydrogen, nitrogen, oxygen, and sulfur). In the ultimate analysis, the carbon weight includes the carbon present in organic material and any other originally present as mineral carbonate. As for hydrogen weight, it includes the hydrogen in

organic materials and water associated with the organic feedstock. Nitrogen weight present in the ultimate analysis is assumed to be part of the organic material. As for sulfur, it is assumed to exist in organic matter in three forms: organic sulfur compounds, inorganic sulfides, which primarily exist as iron sulfide pyrite and marcasite, and inorganic sulfates. The oxygen content of given tires is usually determined by difference. (Antoniou and Zabaniotou 2013)

2.2 Jet fuel

There are numerous varieties of jet fuel, but they can be divided into two categories: military fuel and civilian fuel. Jet A-1, Jet A, and Jet B are the three types of jet fuel used for commercial aviation. The main difference between them is their freezing points, with the first at -47 °C, the second at -40 °C, and the third at -60 °C. Jet A is mostly used in the United States, Jet A1 is more common in the rest of the world, and Jet B is mostly used in extremely cold regions like Canada and Alaska. As for military jet fuel, JP-5 and JP-8 are two examples of military jet fuel. JP-8 fuel is similar to Jet A1 but contains additional anti-icing and corrosion inhibitor additives to compensate for the logistical and operational differences between military and commercial aircraft. JP-5 fuel is a complex blend of hydrocarbons that includes naphthene and alkanes. This mixture gives JP-5 a high flashpoint of 60 °C, allowing it to avoid the fire risk associated with aircraft carrier transportation. JP-8 is used primarily by NATO air forces and the United States military, whereas JP-5 is used in aircraft carriers. (Goh et al. 2022; iJET and ijet 2021)

Jet A/A-1 alternative fuels are already commercially available, and alternative jet fuel (AJF) has been used on over 300 000 flights since 2011. ASTM International has already approved seven conversion pathways, and as these pathways reach commercial maturity, it is anticipated that AJF's market share will reach a tipping point in 2025 when it accounts for 2 % of global aviation fuel stock. This is equivalent to producing 3.5 billion liters annually by 2025, thereby avoiding 7 $MtCO_2$. (Soria Baledón, Trudel, and Kosoy 2022)

2.2.1 Specifications

The main specifications for jet fuel are flash point, smoke point, freezing point, aromatics content, olefin content, and sulfur content. Jet fuel contains maximum levels of aromatics (25 vol%), sulfur (3000 ppm), and olefins (5 vol%) to control the freezing point, sulfur oxide emissions, and the formation of gums and sediments during storage. (Cheng and Brewer 2017)

2.2.1.1 Kinematic Viscosity

It is critical to maintain the viscosity of jet fuel at a low level. This allows for faster atomization of the fuel spray and, thus, a shorter ignition delay time. Previous research found that fuel viscosity increased as the molecular weight of chemical compounds increased and decreased as the number of double-bond molecules increased. (Why et al. 2022)

2.2.1.2 Density

Density is one of the most important jet fuel parameters because it affects the range of the fuel. Depending on the aircraft type, either high-density or low-density fuel is preferred. A fuel with a high volumetric energy content is preferred for military aircraft that take off with their tanks full, as it maximizes the amount of energy that can be stored in a fixed volume. However, for commercial flights, as most do not have their fuel tank full, choosing between a high-density volumetric fuel and a low-density high gravimetry energy content to minimize fuel weight is dependent on several factors. (Hemighaus et al. 2004) According to the literature, cyclic compounds with longer carbon chains (such as naphthene) and non-paraffinic compounds with higher molecular weight may improve final fuel density. (Why et al. 2022)

2.2.1.3 Freezing Point

The freezing point of jet fuel is another important characteristic. It is necessary to ensure the fluidity of the fuel so that it can be pumped without error from the tank to the engines. As aircrafts can be subjected to extremely low temperatures at altitude and in cold weather, the fuel must remain liquid at these temperatures.

The freezing point is defined based on the temperature at which waxy crystals are formed as the jet fuel is cooled. The composition of jet fuel affects its freezing point, with a higher paraffin content decreasing the freezing point and cyclic compounds, especially aromatics, increasing it. However, as the smoke point decreases due to an increase in aromatics, the freezing point improves, so there is always a trade-off between these two properties. (Kushwaha et al. 2022; Why et al. 2022)

2.2.1.4 Smoke Point

The smoke point of aviation turbine fuels and kerosene indicates the propensity of fuel to produce a smoky flame when burned. This smoky flame is caused by the incomplete combustion of jet fuel, which releases particulates and unburned hydrocarbons. Consequently, the smoke point is an essential criterion for evaluating the combustion properties of jet fuel. Jet fuel with a high smoke point is defined as having a low ignition propensity. (Hui et al. 2021; Why et al. 2022)

2.2.1.5 Aromatics

Aromatics play an important role in aviation fuel as they increase energy density and reduce fuel leakage issues. However, high levels of aromatic hydrocarbons may result in increased smoke formation, which can damage the combustion chambers or turbine blades and shorten the engine's lifespan. The aromatic hydrocarbons in the existing jet fuel are typically in the range of 8–25 v/v%. (Cheng and Brewer 2017; Zhu et al. 2017; Oßwald et al. 2021)

2.2.1.6 Flash Point

The flash point of a hydrocarbon or fuel is defined as the lowest temperature at which the hydrocarbon's vapor pressure is sufficient to produce the vapor required for the spontaneous combustion of the hydrocarbon with air in the presence of an external source, such as a spark or flame. This definition shows that hydrocarbons with higher vapor pressures (lighter compounds) have lower flash points. In general, the flash point rises as the boiling point rises.

The flashpoint is used as a metric to define the highest temperature at which fuel may be handled and stored without posing a significant fire hazard. The temperature surrounding a storage tank should always be lower than the fuel's flash point to prevent ignition. This specification outlines the rules and insurance requirements for safely transporting, storing, and handling jet fuel. (Riazi 2005; Why et al. 2022)

2.2.1.7 Calorific Value

The calorific value of jet fuel is determined by its net heating value. (D02 Committee n.d.) According to Blakey, Rye, and Wilson 2011, a high net heating value and high density would be the most desirable for flight, as they would provide the greatest energy release per unit volume and per unit mass.

2.2.1.8 Olefins

Olefins are reactive compounds that can cause deposits in jet engines; therefore, they are not allowed components in Jet fuel. They are the most reactive type of hydrocarbon and are only allowed in JP-4 at 5% by volume. (Riazi 2005)

2.2.1.9 Sulfur content

The presence of sulfur in fuels may result in the release of toxic gases that react with water to form acid rain, as well as the formation of cooling sulfate aerosols, which increases the net warming effect of aviation emissions. As a result, the amount of sulfur in jet fuel is limited. (Kapadia et al. 2016)

The summary of jet fuel specifications for Jet A or Jet A1 can be seen in Table 2.

Table 2 - Summary of Jet fuel (Jet A or Jet A1) specifications by ASTM D1655. (D02 Committee n.d.)

Aromatics, percent by volume	max	25
Sulfur, total percent by mass weight	max	0.3
Distillation temperature of 10% recovered, temperature, ºC	max	205
Final Boiling point, temperature, ºC	max	300
Flashpoint, ºC	min	38
Density at 15ºC, kg/m^3	Min/max	775-840
Freezing Point,ºC	max	-40 ºC (Jet A/-47 Jet A-1)
Viscosity -20ºC cP	Min/max	2.6/8
Net Heat of combustion MJ/kg	min	42.8
One of the following requirements shall be met:		
Smoke point, mm, or	min	25
Smoke point, mm, and Naphtalenes vol%	min/max	18, 3

2.3 Pyrolysis

The pyrolysis process consists of the thermochemical decomposition of organic matter in the absence of oxygen and at high temperatures ranging from 400 to 800°C. The absence of oxygen prevents the combustion of the products of the decomposition reaction. (Lombardi, Carnevale, and Corti 2015)

Pyrolysis, in general, results in total mass recovery as solid (non-volatile material), liquid (condensable fraction), and gaseous (non-condensable fraction) products. These three products are consistently produced regardless of the apparatus, heating source, operating temperature, or heating rate. (Januszewicz et al. 2020; Jadav et al. 2022)

The gas phase in tire pyrolysis is a mixture of H_2, H_2S, CO, CO_2, CH_4, C_2H_4, C_3H_6, and other substances with a calorific value ranging from 29.9–42.1 MJ/m^3. (Nkosi et al. 2021) Typically, these gases serve as an additional source of heat for the pyrolysis process or as a raw material to produce syngas.

The oil produced has a high energy content and is a chemically complex mixture of aromatic, aliphatic heteroatom, and polar fractions. Nonetheless, its high sulfur content prevents its use as a fuel. In addition, it can be used as a feedstock to produce valuable chemicals after processing. (Sathiskumar and Karthikeyan 2019)

The solid residue consists of steel, carbon black, and unreacted organic matter (char). The solid residue can be used in cement manufacturing as a bitumen additive or transformed into activated carbon with a high surface area. Several researchers have recently investigated the use of carbon-derived tire waste in energy storage applications such as Na, K, and Li-ion batteries, supercapacitors, and biodiesel production catalysts. (Ariri, Alva, and Hasbullah 2020; Januszewicz et al. 2020; Jadav et al. 2022)

Pyrolysis can also be done in the presence of a catalyst. Catalytic use leads to an enhancement in the production or performance of a specific type of product. Through the use of a catalyst, heavy hydrocarbons are transformed into pyrolytic oils with a lower molecular weight. In contrast to the results obtained without the catalyst, tire pyrolysis oil has a higher boiling point. According to the literature, the effect of the catalyst on the tire pyrolysis process promotes the gas yield and decreases tire pyrolysis oil rather than increasing the light oil fraction, with no changes in the char yield. (Sathiskumar and Karthikeyan 2019)

The pyrolysis process product distribution depends on precise parameter settings, including the type of reactor, temperature, retention time, and pressure. Several authors in the scientific literature, including Williams 2013 and J. D. Martínez et al. 2013, have published extensive reviews on the treatment of used tires using various reactors and conditions. It is widely accepted that the input waste tires and the numerous operating conditions of the pyrolysis process must be carefully regulated in relation to the yield and quality of the end products.

Furthermore, waste tire pyrolysis is seen as an energy-efficient process, as well as a relatively clean treatment that limits the production of residual waste and/or emissions.

Figure 2 shows the flux diagram for the pyrolysis process. (Akbas and Yuhana 2021)

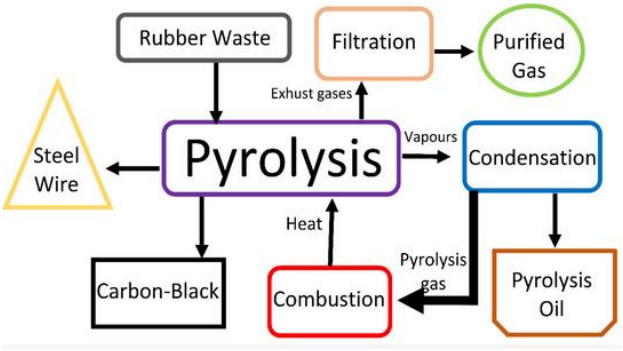

Figure 2 - Pyrolysis process flux diagram. (Akbas and Yuhana 2021)

The pyrolysis mechanisms are extremely complex, consisting of a combination of chemical and physical mechanisms, but they can be described in general terms as follows:

Primary reactions: Original bonds are broken by thermal action, forming free (atoms or molecules whose structure is unstable).

Secondary reactions with bond breaks: If the test pressure is not excessively high, the free radicals are diluted (low partial pressures) and can re-enter the pyrolysis process, forming smaller radicals, H_2, CO, and CO_2. These radicals can react with H_2 to form longer molecules like methane, ethane, ethene, and propane.

Secondary reactions with recombination: When free radicals collide, they can recombine to form larger, more stable compounds, which can then form macromolecules. (Pereira 2016)

2.3.1 Types of pyrolysis

Pyrolysis can be classified as slow, rapid, or flash pyrolysis based on operational characteristics such as reaction residence time. Based on the pyrolysis conditions, it is classified as oxidation pyrolysis, hydrogenation pyrolysis, steam pyrolysis, catalytic pyrolysis, and vacuum pyrolysis. It can be classified as microwave pyrolysis, plasma pyrolysis, or gas fuel heating pyrolysis, depending on the heater system. (Bi et al. 2022)

2.3.1.1 Slow pyrolysis

This type of pyrolysis, as the name implies, has a slow heating rate (0.1-0.8 °C/s), operates at a low temperature (300-500 °C), and has a long residence period (5–30 minutes or more). (Gupta and Mondal 2022) Slow pyrolysis is commonly known as carbonization, and coke is the principal product. Long residence time is believed to be the primary reason for the production and creation of secondary products through the conversion of primary ones, leading to the production of other coke, tar, and heat-stabilized products. (dos Santos et al. 2020; Hoang, Nguyen, and Nguyen 2020; Bi et al. 2022)

Fixed bed, batch and semi-batch reactors, rotary ovens, auger reactors, and stirred tank reactors are associated with slow pyrolysis because these reactors are frequently operated at low temperatures, low heating rates, and with a long residence time for solid and vapor products. (Bi et al. 2022; Mavukwana and Sempuga 2022)

2.3.1.2 Fast pyrolysis

In contrast, to slow pyrolysis, fast pyrolysis is conducted at high heating rates (more than 100 °C/s) and at short vapor residence time to avoid vapor cracking and undesired gasification, which reduces oil production. The previously stated vapor residence time represents the time required for pyrolysis gases to be removed from the pyrolysis zone and reach the quenching unit. (Okoro et al. 2019)

Small particles are required for rapid pyrolysis since this process relies on the rapid release of vapors. This process provides liquid fuel with a higher calorific value and other valuable compounds. (dos Santos et al. 2020; Hoang, Nguyen, and Nguyen 2020; Bi et al. 2022)

Fast pyrolysis reactors include fluidized bed reactors (bubbling and circulating), rotary kilns, spouted reactors, and ablative reactors in which the residence time of volatile matter is shorter than 2 seconds, and the pyrolysis temperature varies from 400 to 600°C. (Bi et al. 2022; Mavukwana and Sempuga 2022)

2.3.1.3 Flash Pyrolysis

Flash pyrolysis is characterized by rapid heating, temperatures between 450°C and 600°C, and residence durations of less than one second. These conditions prevent the cracking of the vapors into

non-condensable gases, maximizing the liquid product yield. The short residence time of the gas volume favors the recovery of a liquid fraction with a high calorific value (the heavy volatile compounds are condensed before undergoing a probable thermal cracking). This process necessitates a reduced feedstock (usually tire in the form of powder) and a particular reactor design that allows for the rapid removal of the vapors produced. Currently, entrained, free fall, and fluidized bed reactors are suitable for this process. (Antoniou and Zabaniotou 2013)

Table 3 summarizes the operating conditions and reactor types of the slow, fast, and flash pyrolysis.

Table 3 - Summary of the operating conditions and reactor types for the slow, fast, and flash pyrolysis. (Parthasarathy et al. 2016; Mavukwana and Sempuga 2022; Bi et al. 2022)

Pyrolysis	Slow Pyrolysis	Fast Pyrolysis	Flash Pyrolysis
Product	Carbon black	Tire-oil	Tire-oil
Temperature (ºC)	300-500	400-600	450-600
Pressure (atm)	1	1	1
Heating Rate (ºC/min)	5-50	15-50	700-1100
Particle Size (mm)	1-4	~4	0.3-1.18
Solid residence time(min)	30-60	15-60	<1s
Catalyst	Not essential	Not essential, However, catalyst improves oil yield and quality	Not essential, However, catalyst improves oil yield and quality
Reactor	Fixed bed, batch and semi-batch reactors, rotary ovens, auger reactors, and stirred tank	Fluidized bed (bubbling and circulating), rotary kilns, spouted and ablative	Entrained, free fall, and fluidized bed

2.3.2 Operating Conditions:

2.3.2.1 Temperature

Temperature is regarded as one of the most influential factors in the yields and properties of pyrolysis products. (Akbas and Yuhana 2021; Bowles and Fowler 2022) From a conversion standpoint and based on a literature review by J. D. Martínez et al. 2013, 500°C appears to be the optimal temperature at atmospheric pressure since complete tire conversion is achieved. At lower temperatures, the primary tire compounds (SBR, BR, and NR) are still present in the pyrolytic carbon black (CB), exhibiting a heterogeneous, sticky-gummy appearance.

The pyrolysis process, however, cannot be controlled solely by changing the temperature, although the temperature has been described as the governing variable in pyrolysis. Product yields are also influenced by system characteristics such as heating rate, carrier gas type, and flow rate and pressure, which directly influence the promotion of secondary reactions. Figure 3 depicts the temperature-dependent behavior of pyrolysis yields. (J. D. Martínez et al. 2013)

Type I: Only considers single break and formation of chemical bonds, constituting a usual yield behavior in which secondary reactions do not occur.

Type II: Results of the mass transfer from the liquid into the gas phase caused by liquid–gas secondary reactions.

Type III: Results from solid–gas secondary reactions followed by the mass transfer from the liquid into the gas phase. Long-term contact between the solid phase (char) and the pyrolysis vapors must produce secondary reactions due to the char catalytic properties. (dos Santos et al. 2020)

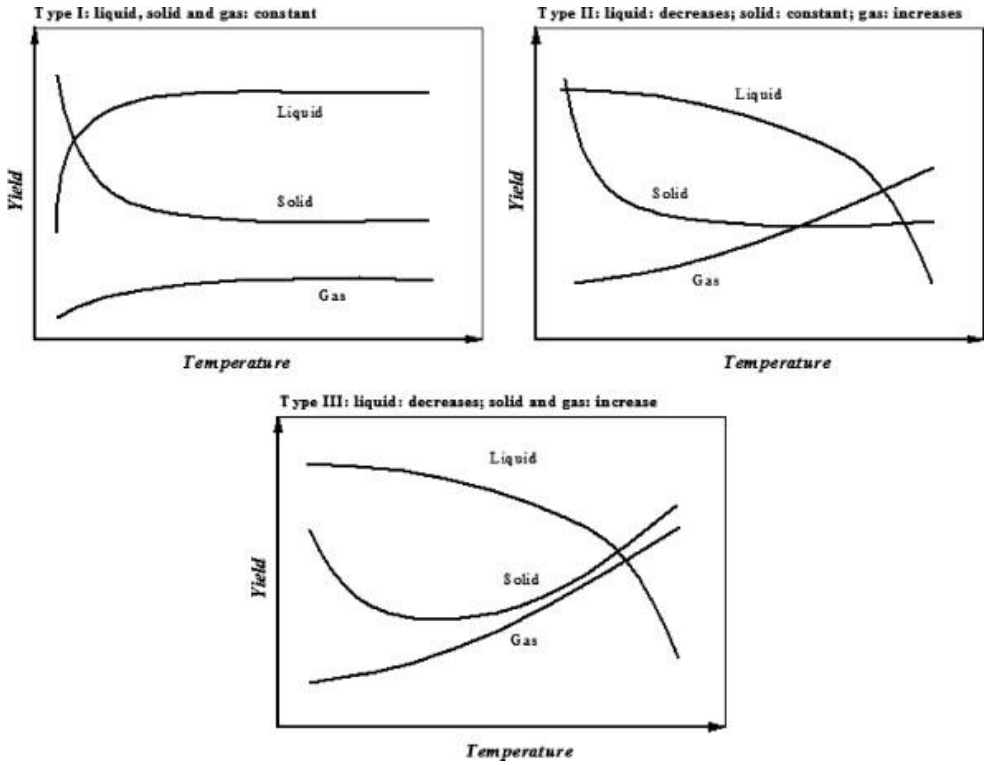

Figure 3 - Yields of tire pyrolysis products at different conditions. (J. D. Martínez et al. 2013)

In general, during the initial stages of pyrolysis, oil production rises steadily with rising temperature, peaking at about 500°C. As the temperature rises, the pyrolysis oil goes through secondary decomposition, producing more gaseous products and less solid and liquid. (X. Zhang, Tang, and Chen 2022)

2.3.2.2 Heating Rate

The heating rate is defined as the change in reactor temperature per unit of time. Increasing the rate of heating increases the rate of degradation and affects the temperature at which maximum volatilization begins and ends. This phenomenon can be attributed to the combined effects of heat transfer and changes in decomposition kinetics, resulting in delayed decomposition.

High heating rates result in higher processing temperatures; for example, when slow pyrolysis is compared to fast pyrolysis, the latter has a higher processing temperature. As a result, in fast pyrolysis, volatiles' residence time in the reactor is minimized in order to prevent secondary reactions,

which would result in an increase in gaseous compounds and a decrease in liquid oil produced. (J. D. Martínez et al. 2013; Alsaleh and Sattler 2014)

The heating rate is not a direct process parameter of control for continuous reactors, such as fluidized beds, conical spouted beds, bubbling fluidized beds reactors, and the ablative process, in which the temperature is set to a certain value and maintained throughout the process. The heating rates in this type of reactor are extremely high and depend primarily on the reactor's characteristics. For instance, the continuous ablative reactor heats solid particles to a high temperature by ablation on a hot surface in less than 1 s. Even so, the heating rate is one of the most researched parameters in pyrolysis because, in addition to influencing the product yields, it also impacts the pyrolysis degradation time and the energy required to drive the process. (J. D. Martínez et al. 2013)

2.3.2.3 Particle Size

Due to the fact that heat and mass transfer occurs during the pyrolysis process, particle size influences the yield. Large particles slow down the heating process and lead to the pyrolysis reaction occurring at a lower temperature and contribute to the possibility of incomplete combustion, as heat can only penetrate a certain depth of the particle depending on the reaction time. On the other hand, small particles are assumed to exhibit isothermal behavior and have no limitations on internal matter transfer, i.e., there are no temperature or mass gradients within the material in thermochemical processes. (Larsen et al. 2006)

2.3.2.4 Residence time

The residence time of the pyrolysis process is another crucial factor. Residence time is proportional to particle size; larger particles require, on average, a longer residence period than smaller particles to undergo the same conversion. Additionally, the residence time influences the extent of secondary reactions. Long residence times combined with high temperatures create favorable conditions for secondary reactions. Consequently, solid and liquid product yields will decrease, while gas product yields will rise.

The residence time is also influenced by the gas flow rate and the reactor design. When the flow rate is high, the gas residence time and subsequent pyrolysis processes are shortened. (Rahman, Yu, and Wu 2022)

2.3.2.5 Types of reactors

Several different criteria can be used to classify pyrolysis reactors. They can be classified, for example, based on the feedstock feeding mode (continuous or periodic operation), the energy supply mode (heat supplied by feedstock combustion, an added inert gas or material, heat transfer from external walls or internal radiators), or the force used to move the feedstock within the reactor (i,e, pneumatic, mechanic, or gravitational). (Costa et al. 2022; X. Zhang, Tang, and Chen 2022)

Even though numerous other reactors have been described in the literature, the primary ones are described.

Stirred tanks

In batch-type stirred pyrolizers, a mechanical agitator actively mixes the charge, increasing the heat transfer rate and reducing temperature variations inside the reactor. The waste tires are delivered intermittently, while the inert gas and pyrolysis products are continuously delivered. (Olmo 2015; Lewandowski, Januszewicz, and Kosakowski 2019)

Williams, Besler, and Taylor 1990 pyrolyzed waste tires in a nitrogen atmosphere using a static batch reactor with pyrolysis temperatures between 300 and 720 °C and heating rates between 5 and 50°Cmin^{-1}. The maximum conversion of the tire, 55% oil, 10% gas, and 35% char, occurred at a temperature of 600 °C. de Marco Rodriguez et al. 2001 studied the pyrolysis of tires under an N_2 atmosphere at 300 ºC, 400 ºC, 500 ºC, 600 ºC, and 700 ºC, with a heating rate of 15 ºC/min for 30 mins. At 300°C, char produced the maximum yield under these circumstances, 87.6 %wt. In contrast, liquid and gas yields rose with temperatures up to 38.5% and 17.8 %wt, respectively, at 700 °C.

Fixed bed

A fixed bed reactor consists of a type of equipment where the catalyst is placed in a fixed position with respect to the reactor, remaining immobile. The fixed bed reactor has several advantages, including high carbon conversion efficiency, the ability to process feedstock with a wide range of ash content, melt ash, produce clean gas with a low tar composition, and wide temperature distribution. The disadvantages are low specific capacity, a long heat-up time, and limited scalability. The tire feed size of this reactor must be small to prevent uneven heating. Due to the low heat transfer of this reactor, as well as the limitations of continuous operation and scalability, its industrial application is not economically viable. (X. Zhang, Tang, and Chen 2022)

In order to research the role of temperature in the pyrolysis process, Kar 2011 carried out pyrolysis on a 10 g tire in a nitrogen-purged atmosphere using a fixed bed reactor with a heating rate of 10ºC/min in a temperature range of 375 to 500 ºC. In this study, 425 ºC was found to have the highest oil yield (60 %wt).

In a fixed bed reactor operating at a temperature range of 400 to 700 ºC in a nitrogen atmosphere Aydın and İlkılıç 2012 examined the pyrolysis procedure. At 500 ºC, the maximum liquid yield of 40.26 %wt was discovered.

Fluidized Bed

Fluidized bed reactors overcome some of the drawbacks of fixed-bed reactors. In contrast to fixed-bed reactors, the fluidized bed reactor's catalyst rests atop a distributor plate through which the fluidizing gas flows, carrying the particles in a fluid state. As a result, because the catalyst is well-mixed with the fluid, there is improved access to it, resulting in a larger surface area for the reaction. This reduces the variability of the process conditions while still allowing for adequate heat transfer. (X. Zhang, Tang, and Chen 2022)

Some disadvantages of this type of reactor include the need for high catalyst levels to homogenize the reactor volume and the wear of the solids and the reactor itself due to friction generated by particle movement in the bed. (Obando 2016; X. Zhang, Tang, and Chen 2022)

The fluidized bed is a type of fast pyrolysis reactor that has a high heating rate, a short reaction time, a short gas residence time, and a low secondary reaction amount. Typically, this type of reactor is used to produce liquid products. (X. Zhang, Tang, and Chen 2022) A fluidized bed reactor is the best reactor for pilot plants, according to Anuar Sharuddin et al. 2016, because it has lower operating costs.

Screw/rotary kiln

The screw-type reactor comprises of an intake hopper through which the reagents are introduced, a screw that transports the feedstock to the hot zone of the reactor, where it is carbonized, as well as an extractor and condenser for the gases and vapors. (Campuzano, Brown, and Martínez 2019; X. Zhang, Tang, and Chen 2022) It is distinguished by the ability to adjust the residence time based on the rotational speed of the feeding screw. Unlike the other reactors discussed, it permits continuous operation without obvious scaling issues, making it an industrially viable alternative. (Obando 2016)

Conical Spouted Bed (CSBR)

Another reactor utilized in the pyrolysis of tire waste is the conical spouted bed reactor. The principal components of the CSBR are the solid feed system, which consists of a hopper, the gas mixture and feeding system, the gas pre-heater, the reactor, the condenser, and the filter system. The most important component of this reactor is the conical spouted bed reactor, which has a conical bottom and a cylindrical top. (Anuar Sharuddin et al. 2016) The advantages of CSBR are (i) a simple design that does not require a gas distributor, (ii) low-pressure drop, (iii) versatility to be used with particles of different geometries and densities, (iv) vigorous gas-solid contact for avoiding clogging of the reactor due to the stickiness of melted waste tire and (v) uniform and low residence time of the volatiles in the reactor. As a result, secondary reactions of the volatiles produced in the reactor are diminished. In addition, the conical spouted bed reactor is suitable for continuous operation, which is crucial for the implementation of large-scale tire pyrolysis. (López et al. 2010)

In practice, some of the problems that this reactor faces are the difficult addition and utilization of catalysts and the collection of products, which, in addition to the required design and high operating costs, makes it less desirable for use. (Olmo 2015)

2.3.2.6 Pyrolysis products

Gas fraction

The gaseous component of waste tire pyrolysis products typically consists of C1-C4 hydrocarbons (paraffins and olefins), H_2, CO, CO_2, and trace quantities of SH_2, SO_2, and NH_3. The COx components result from cracking organic and inorganic tire components, including stearic acid, extender

oils, $CaCO_3$, and metal oxides, among others. In contrast, sulfur is added during the vulcanization of tires to produce the sulfur component of the gas mixture, which is frequently in the form of H_2S. Since the essential monomer of BR and SBR is butene, methane and butenes are the most prevalent hydrocarbons (specifically butadiene). (Antoniou and Zabaniotou 2013; Olmo 2015)

The generated gases have high net heating values ranging from 34.6 to 40.0 MJ/mm^3 and can be used as a combustible fuel to generate the energy necessary for the pyrolysis process. (Antoniou and Zabaniotou 2013) The production of hydrogen from used tires is a popular topic of discussion. Hydrogen is considered a more environmentally friendly fuel than fossil fuels due to its carbon-free energy and lack of greenhouse gas emissions. Y. Zhang et al. 2015 investigated the synthesis of carbon nanotubes and H_2 from waste tires using a two-stage fixed bed reactor and Ni/Al_2O_3 as a catalyst.

Liquid fraction

Pyrolysis oil is a dark, cloudy, dense liquid with a strong odor. The liquid fraction consists of a mixture of C6-C24 hydrocarbons, aromatic hydrocarbons, BTEX (mixture of benzene, toluene, ethylbenzene, and xylene), or limonene, aliphatic, and some oxygenated, nitrogenous, and sulfur compounds predominate. (Martín et al. 2022)

Due to its high heating value, which ranges from 35 to 45 MJ/kg^1, tire pyrolysis oil (TPO) has been considered an alternative fuel. However, its sulfur content of approximately 1 % is the primary drawback to its direct use. Once TPO has been blended with conventional refinery feedstocks, hydroprocessing and fluid catalytic cracking (FCC) are regarded as viable TPO valorization routes. In addition, several desulfurization processes for TPO have been investigated. (Arabiourrutia et al. 2020)

Char fraction

The pyrolysis char mainly consists of carbon black filler and inorganic compounds initially present in the tire and carbonaceous deposits formed during the pyrolysis. Char produced from the pyrolysis of waste tires accounts for 35–55%wt of all products. Among the potential applications of recovered carbon black, its use as a substitute for commercial carbon black stands out. However, some authors study its use as a precursor to obtain activated carbon. (Choi et al. 2014; Martín et al. 2022)

It can be used as a solid fuel due to its high calorific value of 29.1-34.2 MJ/kg. However, high levels of sulfur and ash in char make its use problematic. Untreated char can be used as a low-grade filler in the production of plastics, low-quality rubber, and ink pigments. Although waste tire char has a similar composition to biochar, its use in agriculture is limited due to environmental contaminants such as zinc, sulfur, ash, and certain minerals, which severely limit its application area. As a result, the direct use of waste tire char has yet to gain widespread acceptance.(Rahman, Yu, and Wu 2022)

2.3.3 Simulation of waste tire pyrolysis

Numerous articles on the simulation of waste tire pyrolysis systems were published in the literature. For example, Altayeb 2015; Ismail et al. 2017; Mulaudzi 2017; Wu et al. 2022; Bi et al. 2022, implemented the pyrolysis process in *Aspen Plus®.* Although compared to experiments on the pyrolysis process of waste tire parameters, distributions, and reactor types, the number of articles on pyrolysis simulation is limited, and additional research is needed in this area.

2.3.3.1 *Aspen Plus®* simulation of waste tire pyrolysis

Olazar et al. 2008 proposed a kinetic model for the pyrolysis of waste tires in terms of the reaction modeling of the pyrolysis process. Based on the kinetic rate equations of Olazar et al. 2008, Ismail et al. 2017 deduced the kinetic equation applicable to the *Aspen Plus®* and used an RPlug reactor to simulate the pyrolysis process.

Altayeb 2015 simulated the pyrolysis reaction using an RGibbs. Wu et al. 2022 assessed waste tire pyrolysis and upgrading pathways to produce high-value products. To make this assessment, the authors used *Aspen Plus®* to simulate the pyrolysis process. In this article, the authors used an RYield to make the pyrolysis of waste tires by introducing the experimental pyrolysis yield. Bi et al. 2022 performed a techno-economical analysis of the pyrolysis process of the waste tire with the *Aspen Plus®* simulator, using the reaction rates present in Ismail et al. 2017 work. Multiple capacities were used in this study, and the authors concluded that the profit of waste tire pyrolysis treatment is low at a low processing capacity of 20 000 tons per year. The investment payback period is as long as 76 years, whereas when the processing capacity reaches 50 000 tons per year, the profit is high. The investment payback period is reduced to 3.6 years.

Mulaudzi 2017 modeled and studied the economic potential of pyrolyzing waste tires to produce limonene. An RYield reactor with experimental data yields was used to model the pyrolysis products from waste tires.

Adeniyi and Ighalo 2020 modeled the pyrolysis of rubber sawdust using *Aspen Plus®*. An RYield was used to deconstruct the non-conventional material into conventional components, and then an RGibbs was used to produce the products by minimizing Gibbs free energy. When it came to the yield of the product, the model matched the research, but not when it came to the composition of the product.

2.4 Hydroprocessing

Although pyrolysis-derived liquid oil is viewed as a promising feedstock for producing chemicals and fuels, it is typically distinguished by its high viscosity and high nitrogen and sulfur content. Before the oil can be used, it must undergo additional processing to reduce its N and S concentrations and viscosity. (Liu et al. 2019) Hydrotreating and hydrocracking are viable strategies for decreasing viscosity and sulfur content.

2.4.1 Hydrotreating

Hydrotreatment (HT) refers to several catalytic hydrogenation processes that saturate unsaturated hydrocarbons and remove S, N, O, and metals from different petroleum streams in a refinery, thereby increasing cetane number, density, and smoke point. Hydrogenolysis reactions eliminate heteroatoms, and polycyclic aromatic hydrocarbons undergo partial hydrogenation, while unsaturated hydrocarbons such as olefins and diolefins are also hydrogenated. Hydrodesulfurization (HDS), hydrodenitrification (HDN), hydrodearomatization (HDA), hydrodemetallization (HDM), and hydrodeoxygenation (HDO) are the primary subreactions in hydrogenolysis. HDS, HDN, HDA, and HDM are particularly relevant for feedstock derived from petroleum, while HDO is more interesting for feedstock derived from biomass. HDS, HDN, and HDA are waste tire oil's most important hydrogenolysis reactions. The extent of the reaction for various component classes varies based on the nature of the catalyst and the operating conditions. (Lødeng et al. 2013, 11; Olmo 2015)

This process generally occurs in a trickle bed reactor where hydrogen reacts with oil in the presence of a catalyst. A trickle-bed reactor is a fixed-bed reactor in which liquid oil and gaseous hydrogen are supplied simultaneously from the top. In the trickle-flow regime, the liquid trickles over the catalyst pellets, but the gas phase is continuous. As dry areas result in reduced conversions, preventing the maldistribution of gas and liquid and maintaining a proper wetting of the catalyst particles is the primary issue for these reactors. (Boesen 2011; Olmo 2015)

The reactor is divided into multiple beds to redistribute the liquid so that the wetting of the catalyst in each bed is more homogeneous, using the voids between the beds as quenching boxes for two purposes: 1) cooling the feed to achieve higher conversions in reversible exothermic reactions such as hydrogenations and some hydrogenolysis, and 2) decreasing the concentration of H_2S and NH_3 by-products that reduce the activity of the catalyst. Due to exothermic processes, the temperature in each bed may rise to as high as 30°C; thus, H_2 streams that have been recirculated are often used to quench the heat. (Boesen 2011; Olmo 2015)

Figure 4 shows a simple illustration of a trickle-bed hydrotreating reactor. The typical catalysts for hydrotreating are sulfided $CoMo/Al_2O_3$ and $NiMo/Al_2O_3$. (Boesen 2011)

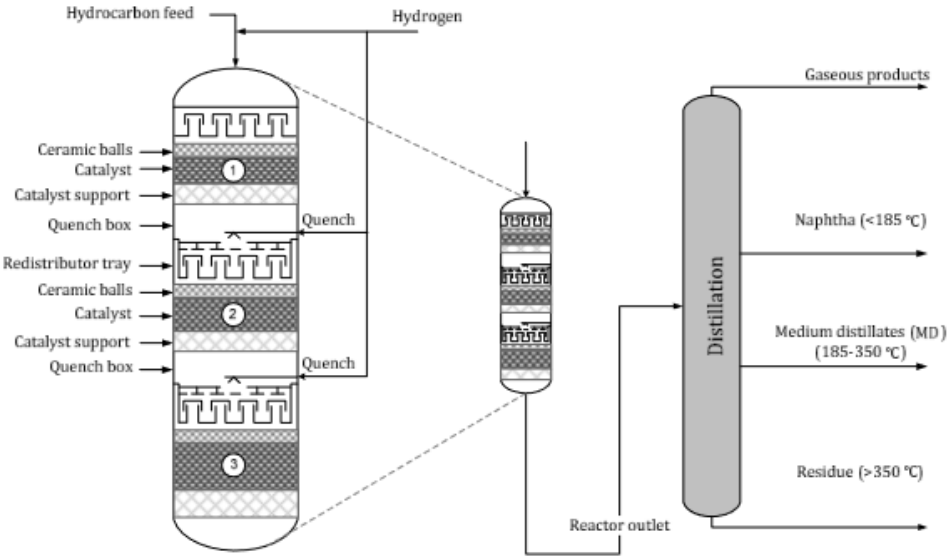

Figure 4 – Trickle bed reactor. (Olmo 2015)

Typically, atmospheric gas oils have been hydrotreated at temperatures ranging from 315 to 400ºC and pressures ranging from 30 to 100bar. The hydrogen flow is often designed to be 3-4 times more than what is used in the process. The hydrogen to liquid feed ratio is commonly in the 70-1000 Nm^3 hydrogen per m^3 liquid feed range. (Boesen 2011; Ortega 2021)

The reaction mixture-catalyst contact time may be represented in weight hourly space velocity (WHSV) or liquid hourly space velocity (LHSV). The latter is calculated as the volumetric liquid feed flow in m^3/hr divided by the catalyst volume in m^3. In contrast, the first is defined as the mass flow rate of feed (kg/hr) supplied to the reactor divided by the mass of the catalyst (kg) in the catalytic reactor. LHSV values for ultra-low-sulfur diesel (ULSD) typically range between 0.5 and 3 hr^{-1}. (Boesen 2011)

2.4.1.1 HDS

Hydrodesulfurization (HDS) is the most widely used technology to lower sulfur content and effectively remove various sulfur compounds. According to the research, the HDS process is a highly successful process in improving TPO quality by decreasing viscosity and increasing TPO saturated fraction content. It is a hydrotreating process that uses a hydrogen gas source to produce ultralow-sulfur fuel oil. However, it is extremely expensive due to the high temperature and pressure conditions and the significant hydrogen consumption. (Bandyopadhyay and Upadhyayula 2018; Hossain, Choi, and Choi 2021)

The basic chemical concept of the process is to convert organic sulfur in the feedstock to hydrogen sulfide through hydrogenation and hydrogenolysis, as described by Equation (1).

$$Feedstock_{Sulfur} + H_2 \rightarrow H_2S + products_{sulfur-deficient} \quad (1)$$

2.4.1.2 HDN

The predominant form of nitrogen in waste tire pyrolysis is benzothiazole (BTZ), which is also classified as a sulfur compound. (G. Zhang et al. 2021) As a result, denitrification is often accompanied by desulfurization. Nitrogenous chemicals are the most prevalent toxins in hydrotreating owing to their strong adsorption ability on catalytic sites. Because of their basic nature, they adsorb reversibly or irreversibly onto acidic catalytic sites, depending on the reaction circumstances. In particular, basic nitrogen molecules in the feedstock are known to lead to catalyst deactivation. (Boesen 2011; Olmo 2015; G. Zhang et al. 2021)

The aromatic ring saturation is typically slightly more thermodynamically preferred than the N ring saturation in HDN of aromatic nitrogen compounds, but the N ring is always hydrogenated first due to kinetic factors. In this manner, S and N are removed from BTZ using an amine intermediate, resulting in the production of H_2S and NH_3. (Boesen 2011; Olmo 2015)

Figure 5 shows the HDN pathway schematic.

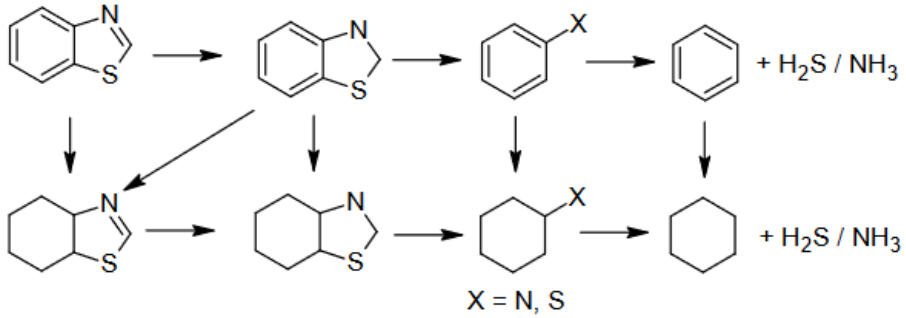

Figure 5 - HDN pathway schematic. (Olmo 2015)

2.4.1.3 HDA

Hydrodearomatization reactions involve the saturation of aromatic rings with hydrogen. Hydrogenation of the first ring of polycondensed aromatic hydrocarbons is typically the quickest, with subsequent rings hydrogenating at a slower rate and the final ring being the least reactive. The partial pressure of H_2 is the most important factor governing HDA. Depending on the feedstock type, the H_2 partial pressure required to reduce the aromatic content to 10 vol% can vary by as much as 40 vol%. Another important aspect, according to the literature, is that the hydrogenation of aromatic hydrocarbons is reversible, with the equilibrium conversion often less than 100% under the operating conditions of industrial reactors. (Boesen 2011; Olmo 2015; Bandyopadhyay and Upadhyayula 2018)

2.4.1.4 Modeling of Hydrotreatment in *Aspen Plus*®

Plazas-González, Guerrero-Fajardo, and Sodré 2018 developed a model for the hydrotreatment of palm oil components to create green diesel. An equilibrium reactor (REquil) was used in the *Aspen Plus*® program to predict how these reactions would behave. Mederos-Nieto et al., 2019 used *Aspen Plus*® process simulator to simulate a hydrotreating process involving two separate feedstocks from the same plant: crude castor oil and castor oil methyl esters. This process was represented by two stoichiometric reactors (RStoic) connected in series.

Cavalcanti et al., 2022 proposed a model for the hydrotreatment of soybean oil for the production of green diesel. The process was simulated in *Aspen Plus*® v10; the decarboxylation, decarbonylation, and hydrodeoxygenation processes were simulated using a stoichiometric reactor, Alaei Kadijani and Narimani 2016 simulated an Ultra-Deep Hydrodesulfurization reactor with a trickling bed reactor. In order to model this hydrotreatment, the general reactor mode was selected in *Aspen HYSYS*®, and the appropriate reactions were defined in accordance with the conversion reactor model.

Bandyopadhyay and Upadhyayula 2018 studied in *Aspen Plus*® the HDS, HDN, and HDA reactions with representative compounds to gain insight into the equilibrium conversion of these reactions, utilizing an RGibbs reactor with the temperature, pressure, and stoichiometric ratios typically used in an industrial hydrotreating reactor. Using the Aspen Hysys Hydroprocessor Bed® module, Sbaaei and Ahmed 2018 created a rigorous model of an existing trickle bed reactor for hydrotreatment. The trickle bed reactor model includes equations for HDS, HDN, saturation, cracking, and ring opening. The rate expression for each reaction is encoded to correspond with published data. All processes except aromatic saturation are irreversible. The typical reaction network has 97 kinetic lumps and 177 reactions. This paper illustrates the specifics and interplay of the responses. Using the model yields, the findings for the next three months after calibration were compared to the plant yields. The article concluded that the model was a good way to track how well plants were doing for three months after calibration.

Gutiérrez-Antonio et al., 2016 used an Aspen Plus® Rplug module to simulate the hydrotreating process of jatropha curcas oil using kinetic models from the literature. For the hydrotreatment process of bio-oil, Peters, Iribarren, and Dufour 2015 employed an RYield module of Aspen Plus® to convert the feed to the corresponding products using experimental data from the literature.

Based on previously reported research, Shemfe, Gu, and Ranganathan 2015 constructed a two-stage hydrotreating process in Aspen Plus® by modeling the process through two continuous stirred-tank reactor using a pseudo-first-order reaction model of lumped bio-oil species based on previously published research.

3 Waste Tire Pyrolysis

This chapter provides an overview of how kinetic modeling of the pyrolysis process is done in Section 3.1 (pag.22). How the kinetic modeling has been implemented is explained in Section 3.2 (pag.24). The results of reproducing the experimental results of Laresgoiti et al., 2004 and Olazar et al., 2008 using Ismail et al., 2017 reaction rates and *Aspen Plus*® files reactions are presented in Section 3.3 (pag.25). What is parameter estimation and how it was done towards the pyrolysis reactions is explained in Section 3.4 (pag.29). Finally, a sensitivity analysis was made to understand the impact of multiple independent variables on the pyrolysis process in Section 3.5 (pag.33)

3.1 Kinetic modeling

Most studies have primarily focused on the kinetics of rubber decomposition (devolatilization) without establishing a kinetic model for the formation of secondary products. For reactor design and process optimization, it is essential to develop kinetic models that accurately predict product distributions under pyrolysis conditions. Due to the wide variety of structures present in such mixtures, compound-by-compound identification and quantification are, if not impossible, challenging. Considering the mixture in terms of selected lumps whose properties, such as boiling range, molecular weight ranges, carbon number ranges, solubility class fractions, and other structural characteristics, can be specified. Olazar et al., 2008 applied discrete lumping schemes for the kinetic modeling of complex reactions for the pyrolysis of waste tires, involving series and parallel reactions based on carbon numbers. Continuous lumping is an alternative approach that can be considered for the kinetic modeling of thermal and catalytic processing of complex feedstocks.

3.1.1 Discrete Lumping

An example of a discrete kinetic model is Olazar et al. 2008 work, which modeled the complex reactions of pyrolysis of waste tires involving series and parallel reactions, involving the lumping of compounds into groups according to their carbon number and aromaticity. These are non-condensable gases C1-C4, non-aromatics C5-C10, aromatics C5-C10, and tar (includes aromatics and non-aromatics) C11-C24.

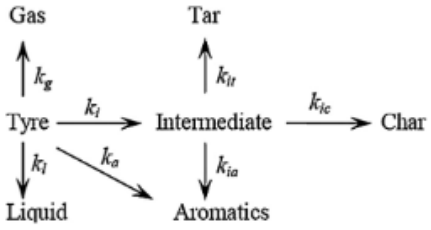

Figure 6 - Kinetic schematic of the pyrolysis of waste tires proposed by *Olazar et al., 2008.*

The kinetic modeling scheme in Figure 6 is based on the supposition that the decomposition reaction is first order concerning the amount of tire not yet converted. Equations (2)-(8) represent the mathematical modeling of the proposed kinetic scheme.

$$\frac{dX_n}{dt} = \left(k_g + k_l + k_a + k_i\right)(1 - X_n) \quad (2)$$

$$\frac{dX_g}{dt} = k_g(1 - X_n) \quad (3)$$

$$\frac{dX_l}{dt} = k_l(1 - X_n) \quad (4)$$

$$\frac{dX_a}{dt} = k_a(1 - X_n) + k_{ia}X_i \quad (5)$$

$$\frac{dX_t}{dt} = k_{it}X_i \quad (6)$$

$$\frac{dX_c}{dt} = k_{ic}X_i \quad (7)$$

$$\frac{dX_i}{dt} = k_i(1 - X_n) - k_{ia}X_i - k_{it}X_i - k_{ic}X_i \quad (8)$$

where,X_n =Overall mass conversion (kg converted/kg initial),

$X_g, X_l, X_a, X_t, X_c, X_i$ = Mass fraction gas yield of gas, oil, aromatics, tar, char, and intermediates, respectively,

$k_g, k_l, k_a, k_i, k_{ia}, k_{it}, k_{ic}$ = Rate constants for tire-gas, tire-liquid, tire-aromatic, tire-intermediate, intermediate-aromatic, intermediate-tar, and intermediate-char kinetic (1/s).

Ismail et al. 2017 performed a parameter estimation based on this kinetic modeling, but since the reaction rate used in *Aspen Plus*® has to be in the specific form presented in Equations (9) and (10) in order to implement it, various approximations regarding the previous kinetic scheme were realized.

$$\mathrm{r} = [\text{Kinetic factor}][\text{ Driving Force}] \quad (9)$$

$$\text{Kinetic factor}_i = A_i \times \mathrm{T}^{\mathrm{n}} \exp\left(-\frac{Ea_i}{RT}\right) \quad (10)$$

Where, r is the rate expression (mol/m^{3}s), A_i is the pre-exponential constant for reaction i (1/s), Ea_i is the activation energy for reaction i (J/mol), T temperature in the reactor (K), n temperature exponent (dimensionless), and R is the universal gas law constant (J/Kmol).

First, the intermediate compounds were eliminated by assuming pseudo-steady-state conditions, followed by introducing a new variable X' (the mass percentage of tire remaining) which would be equal to $1 - X_n$. Finally, the Arrhenius parameters for the new kinetic scheme were calculated to obtain the global reaction for each grouping.

As in *Aspen Plus*®, the tire feed is defined in terms of its elemental components; thus, the X' has to be defined in terms of elemental components. As such, a division was made in terms of X' by the limiting reagent ultimate analysis weight, in this case, hydrogen weight. The final global kinetic model for each lump is represented in equations (11)-(14).

$$r_g: C_1 - C_4 = 0{,}40428 \cdot \exp\left(\frac{-23010}{RT}\right) \cdot X_{\mathrm{H2}} \text{ (gas)} \quad (11)$$

$$r_l: C_5 - C_{10}(\text{ non-aromatics }) = 0{,}2 \cdot \exp\left(-\frac{1590}{RT}\right) \cdot X_{\mathrm{H2}}(\text{ oil }) \quad (12)$$

$$r_a: C_5 - C_{10}(\text{ aromatics }) = 8{,}4214 \cdot \exp\left(-\frac{32890}{RT}\right) \cdot X_{\mathrm{H2}}(\text{ oil }) \quad (13)$$

$$r_t: C_{11+}(\text{aromatics \& non-aromatics}) = 537{,}28 \cdot T^{-1{,}089} \cdot \exp\left(-\frac{6300}{RT}\right) \cdot X_{\mathrm{H2}}(\text{ oil }) \quad (14)$$

Where r_g (mol/m^{3}s), is the rate expression for the production of $C_1 - C_4$ (mol/m^{3}s), r_l is the rate expression for the production of $C_5 - C_{10}$(non-aromatics) (mol/m^{3}s), $r_a$is the rate expression for the production of $C_5 - C_{10}$(aromatics) (mol/m^{3}s), r_t is the rate expression for the production of C_{11+}(aromatics & non-aromatics) (mol/m^{3}s),and X_{H2} the mass fraction of hydrogen in the liquid.

After obtaining the global kinetic equations associated with each lump, Ismail et al., 2017, used data from the literature to make a parameters estimation based on the work of Laresgoiti et al., 2004 and Williams 2013, the first of which described over 100 tire pyrolysis products, obtaining 116 reaction rates which explained the pyrolysis process.

The kinetic reaction rates and parameters were validated using experimental measurements from Laresgoiti et al., 2004 and Olazar et al., 2008. The average relative error was found to be 24.61 % at 400 °C, 17.95 % at 500 °C, 9.93 % at 600 °C, and 9.09 % at 700 °C, when compared to Laresgoiti et al., 2004 data. The authors attributed this discrepancy to the different heating rates used by Laresgoiti et al., 2004. For Olazar et al., 2008, the simulation results presented an average error of 15 %.

3.2 Pyrolysis modeling

The modeling of the pyrolysis process was made in *Aspen Plus*® V11. Here, the thermophysical properties were acquired using built-in parameters in the software database. Peng Robinson with Boston-Mathias alpha function equation of state (PR-BM) has been cited in multiple articles (Altayeb 2015; Mulaudzi 2017; Adeniyi and Ighalo 2020) as the preferred property method to be used for the pyrolysis process. Alpha is a temperature-dependent parameter that improves the pure component vapor pressure correlation at very high temperatures. For this reason, PR-BM is suitable for the pyrolysis process since relatively high temperatures are involved. The enthalpy model for coal (HCOALGEN) and the density model for coal (DCOALIGT) property models were used to estimate the density and enthalpy of non-conventional components. (Kabir, Chowdhury, and Rasul 2015; Mulaudzi 2017) Missing thermophysical properties were estimated using the UNIFAC group contribution model (Fredenslund, Jones, and Prausnitz 1975) and the process simulator's Property Constant Estimation System.

The Ismail et al., 2017 kinetics was used to simulate the pyrolysis of waste tires. The decision to use these reaction rates to model the pyrolysis process was made because they were the only ones available in the literature with such a high degree of product explanation for the pyrolysis of waste tires.

3.3 Experimental Results Reproduction

The flowsheet implemented in *Aspen Plus*® is presented in Figure 7 . The reactor was simulated using an RPlug block with the same characteristics as the one Ismail et al., 2017 used, with 0.15 m diameter and 1.7 m length. The pyrolysis process was simulated at temperatures ranging from 300 °C to 700 °C.

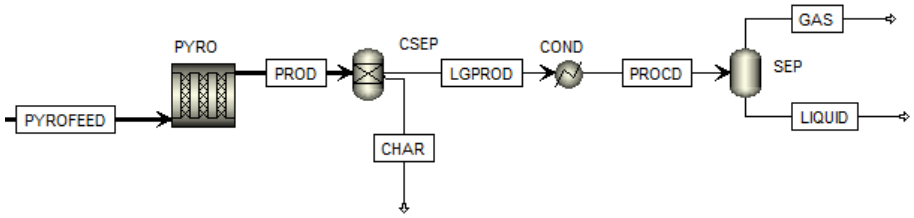

Figure 7 – Pyrolysis flowsheet implemented in *Aspen Plus*®.

The elemental composition of the tire fed in the reactor PYRO was defined in the PYROFEED stream. The effluent from the reactor was sent to the separator CSEP, where the vapor was separated from the ashes, carbon, and sulfur that did not react, and then cooled in condenser COND to separate non-condensables from condensables in the flash drum SEP.

Ismail et al. 2017 kinetics was implemented to reproduce his simulation results. The simulations were performed for *Ismail et al. 2017* 116 reactions, and later with 38 reactions based on an existing *Aspen Plus*® file entitled “Pyrolysis of waste tires” (waste_tires_pyrolysis-V11.apw), with different kinetic parameters. The results were compared with the experimental results from Laresgoiti et al., 2004 and Olazar et al., 2008. The 38 and 116 kinetic parameters used can be seen in Table 17 (pag.77) of the Appendix.

Table 4, presents the elemental composition of the waste tire feeds used in the simulations, where Ashes were defined as a non-conventional compound.

Table 4 – Ultimate analysis of the tires used for parameter estimation.

	(Olazar et al., 2008)	(Laresgoiti et al 2004)
Carbon	82.5	74.2
Hydrogen	6.4	5.8
Nitrogen	0.5	0.3
Sulfur	1.1	1.5
Oxygen	5.7	4.7
Ashes	3.8	13.5 [a]

a = Steel + other inorganics instead of ashes.

The average relative error of both works was used as a metric used for deciding which kinetic model was the best at reproducing the experimental results. Equations (15) and (16) show how each average relative of each work was calculated, and Equation (17) the average relative error of both works.

$$\bar{\sigma}_{\text{Laresgoiti et al.,2004}} = \frac{\sum_{\text{c=c7}}^{\text{c15}} \frac{\sum_{TL=400}^{700} \frac{|\exp_c - \text{sim}_c|}{\exp_c}}{\text{ntemp}}}{\text{nlumps}} \cdot 100 \quad (15)$$

$$\bar{\sigma}_{\text{Olazar et al.,2008}} = \frac{\sum_{\text{b=tar}}^{\text{aromatic}} \frac{\sum_{TO=425}^{610} \frac{|\exp_b - \text{sim}_b|}{\exp_b}}{\text{ntemp}}}{\text{nlumps}} \cdot 100 \quad (16)$$

$$\bar{\sigma}_{\text{Total}} = \frac{\sum_{TO=425}^{610} \frac{|\exp_b - \text{sim}_b|}{\exp_b} + \sum_{TO=425}^{610} \frac{|\exp_b - \text{sim}_b|}{\exp_b}}{ntemps \cdot nlumps(\text{Laresgoiti et al., } 2004) + ntemps \cdot nlumps(\text{Olazar et al., } 2008)} \cdot 100 \quad (17)$$

where

TL	Temperatures used in Laresgoiti et al. 2004 work, 400, 500, 600, 700 ºC
TO	Temperatures used in Olazar et al. 2008, 425, 500, 550, 610 ºC
Ntemps	Number of temperatures, dimensionless
Nlumps	Number of lums, dimensionless
c	Laresgoiti et al. 2004 experimental values in lumps, c7..c15, dimensionless
b	Olazar et al. 2008 experimental values in lumps, tar, liquid, gas aromatic, dimensionless
$\bar{\sigma}_{\text{Laresgoiti et al.,2004}}$	Average relative error for Laresgoiti et al. 2004 work
$\bar{\sigma}_{\text{Olazar et al.,2008}}$	Average relative error for Olazar et al. 2008,work
$\bar{\sigma}_{\text{Total}}$	Average relative error for both works

3.3.1 Results

The experimental results from the works of Laresgoiti et al. 2004 and Olazar et al. 2008 and the simulation results from Ismail et al. 2017 were extracted from the later author, using the digitizer software (WebPlotDigitizer), and can be seen in Figure 8 and Figure 9, together with this work's simulation results for the 116 and 38 reactions.

To make the comparison between the simulated results and Olazar et al. 2008 work, the products were grouped into four groups, liquid (non-aromatic), gas, tar, and aromatic, previously mentioned in Section 3.1 and the yield of each group in relation to the initial tire was plotted for the range of temperatures used in the work (425 ºC, 500 ºC, 550 ºC, 610 ºC).

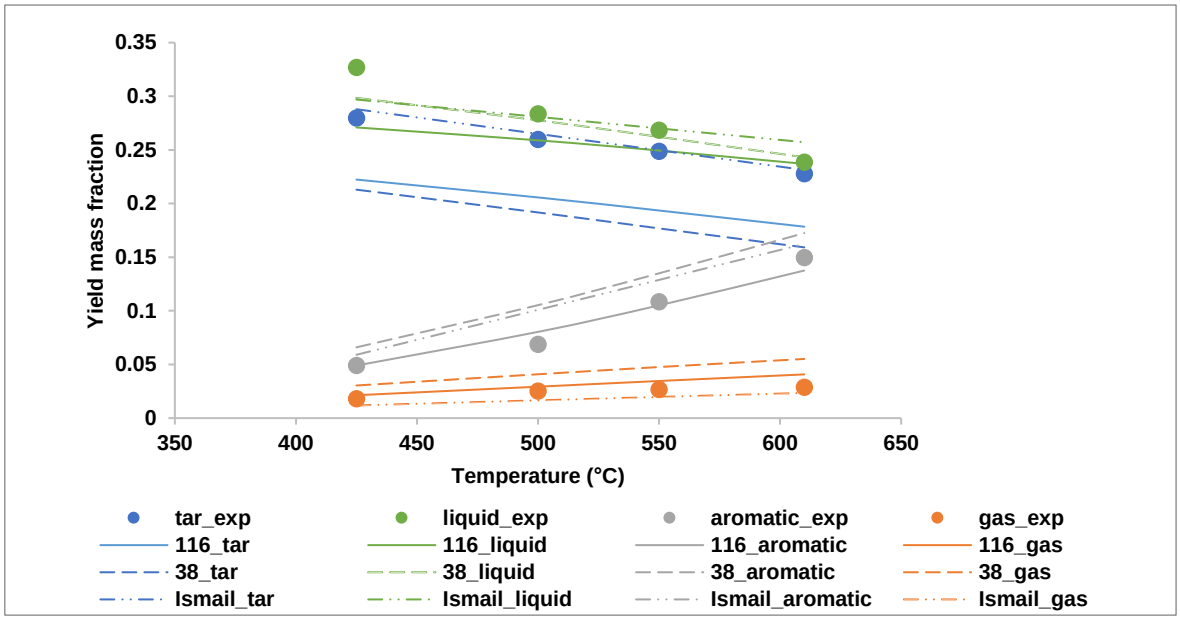

Figure 8 - The experimental (Olazar et al. 2008) and simulated product for the 116 , 38, and Ismail et al. 2017 results yields at temperatures of 425, 500, 550, and 610 °C

Figure 8 analysis reveals that all models appear to be able to simulate the behavior of the gas and aromatic groups with temperature. Whereas for the tar and aromatic groups, Ismail et al. 2017 model gives better results.

In regard to the comparison with the experimental data present in Laresgoiti et al. 2004. The products were classified between C7-C15, and the yield of each individual group was plotted for the temperatures used in the work (400ºC, 500ºC, 600ºC and 700 °C), present in Figure 9.

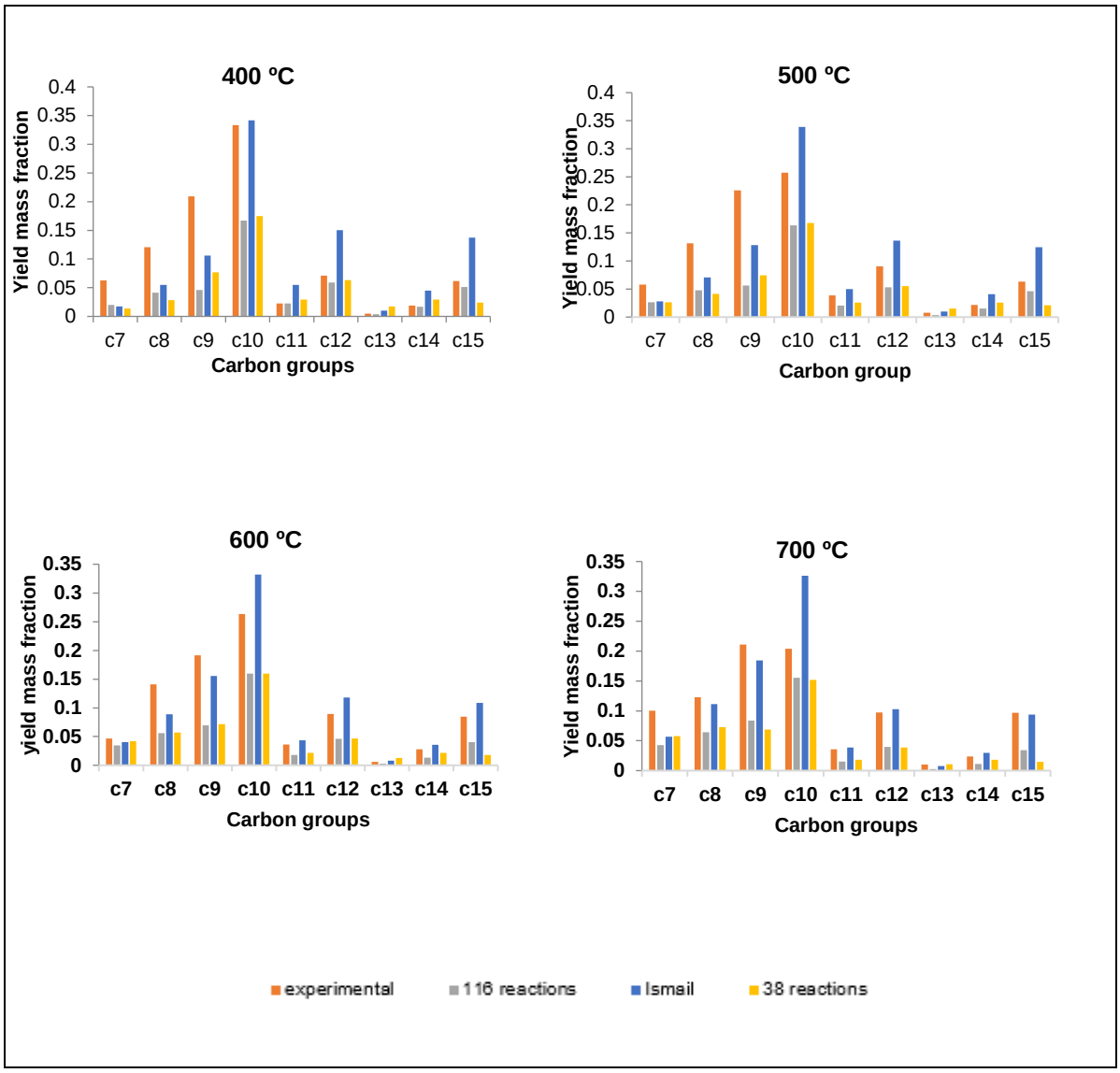

Figure 9 - Simulated product for 116 and 38 reactions, Ismail et al. 2017 and Laresgoiti et al. 2004 experimental results for C7-C15 yield mass fractions of the oil and gas products at temperatures of 400, 500, 600 and 700 °C.

Figure 9 analysis shows that all models exhibit a noticeably high relative error in comparison to the experimental findings for all temperatures.

Table 5 shows the new average relative errors obtained from the figures of Ismail et al., 2017 article, the Aspen Plus® simulation results with 116 reactions and Ismail et al., 2017 kinetic parameters, and the Aspen Plus® simulation results with 38 reactions and the waste_tires_pyrolysis-V11.apw original kinetic parameters. It is possible to see that the average error for the 38 reaction implementation is significantly high in comparison with the other two situations. This might be due to the fact that there were not enough reactions used to adequately represent the experimental findings or that the new parameters estimated by Aspen Plus® significantly affected the reaction rate. The latter could be the main cause, as the reaction rate constant of limonene, one of the main products of pyrolysis, in Ismail et al. 2017 work (0.619) is nearly double that of Aspen File (0.35). The difference between the 116 reactions implemented results and Ismail et al., 2017 results could be due to some parameters being incorrectly inserted.

Table 5 – Average relative error comparison between Ismail et al. 2017 simulation results and the implementation of 116 and 38 reactions results with the experimental results of Laresgoiti et al. 2004 and Olazar et al. 2008.

	$\bar{\sigma}_{\text{Laresgoiti et al.,2004}}$ (%)	$\bar{\sigma}_{\text{Olazar et al.,2008}}$ (%)	$\bar{\sigma}_{\text{Total}}$ (%)
Ismail et al 2017 work	47	15	37
116 Reactions	47	31	42
38 Reactions	57	63	59

It was also possible to see that the average relative error calculated using Ismail simulation results differed significantly from the average relative error stated by the author for the Laresgoiti et al. 2004 work, which was 24.61% at 400 °C, 17.95% at 500 °C, 9.93% at 600 °C, and 9.09% at 700 °C. Instead, 89, 52, 26 and 21% were calculated, respectively.

To reduce the disparity between the current implementation and the results of Ismail et al. 2017, parameter estimation was performed, to find new pre-exponential constants. Ai, for equation (10).

3.4 Parameters Estimation

The *gPROMS ModelBuilder V7.07*® software was used to perform the Parameter Estimation to estimate from experimental data the values of unknown model parameters. Through the implementation of the model and the addition of experimental data, it is possible to associate this measured data with the model variables and use it as an input for parameter estimation. Parameter Estimation refers to fitting model parameters to a given data collection. In *gPROMS ModelBuilder*®, parameter estimation on the Maximum Likelihood formulation, which in *gPROMS ModelBuilder*® accounts for the physical model of the process and the variance model of the measuring instruments. *gPROMS ModelBuilder*® aims to identify values for the unknown physical and variance model parameters that maximize the likelihood that the mathematical model will predict the measurement values received from the experiments while solving a Maximum Likelihood Parameter Estimation issue. Assuming independently distributed, normally distributed measurement errors, ϵ_{ijk}, with zero means and standard deviations σ_{ijk} , this maximum likelihood goal is achieved by minimizing the objective function. Equation (18) represents the objective function.

$$\Phi = \frac{N}{2}\ln(2\pi) + \frac{1}{2}\min_{\theta}\left(\sum_{i=1}^{NE}\sum_{j=1}^{NV_i}\sum_{k=1}^{NM_{ij}}\left[\ln\left(\sigma_{ijk}^2\right) + \frac{\left(\tilde{z}_{ijk} - z_{ijk}\right)^2}{\sigma_{ijk}^2}\right]\right) \quad (18)$$

N	Total number of measurements taken during all the experiments
θ	Set of model parameters to be estimated. The acceptable values may be subject to given lower and upper bounds, i.e $\theta^t \leq \theta \leq \theta^u$
NE	Number of experiments performed
NV_i	Number of variables measured in the *i* th experiment
NM_{ij}	Number of measurements of the *jth* variable in the *ith* experiment
σ^2_{ijk}	Variance of the *kth* measurement of variable *j* in experiment *i*. This is determined by the measured variable's variance model
$\tilde{z}_{ijk}$	*kth* measured value of variable *j* in experiment *i*
z_{ijk}	*kth* predicted value of variable *j* in experiment *i*

Prior to estimating the parameters, a mathematical model was required. The mathematical model of the RPlug for the kinetic model presented in the work of Ismail et al., 2017 was implemented in gPROMS® and is described by Equations (19)-(21).

$$\frac{\partial F_i}{\partial z} = \frac{A}{m} \times \sum_{j=i}^{No\ Reac} v_{ij} R_j \tag{19}$$

$$\frac{\partial m_i}{\partial z} = \frac{\partial F_i}{\partial z} \times Mw_i \tag{20}$$

$$m = \sum_{i=2}^{No\ Comp} F_i Mw_i \tag{21}$$

where:

i	The number of components, aside from carbon, i = 2… Nocomp, where in this modeling,i=1 is the carbon element (dimensionless)
z	reactor tube axial position, ∈]0, L[,(m)
L	Reactor length (m)
Nocomp	number of compounds, dimensionless
R_i	reaction rate of species i at the position z, mol/m^{3}s
Fi	molar flow rate of species *i* at the position z,mol/s
mi	mass flow rate of species *i* at the position z,kg/s
m	total flow rate at position z,kg/s
Mwi	Molecular mass of species *i*, kg/kmol
v_{ij}	stoichiometric coefficient of species *i* in reaction *j*, (dimensionless)
j	1,,,, NoReact, (dimensionless)
NoReact	number of reactions, (dimensionless)

Equations (19)-(21) are responsible for the mass balance within the reactor, while Equation (22) for the reaction rate.

$$R_j = A_j e^{\frac{-Ea}{RT}} T^{n_j} \prod_{I=1}^{No\ comp} {F_i}^{O_{ij}} \prod_{i=1}^{No\ Comp} {Mw_i}^{O_{ij}} \tag{23}$$

Where:

Ea	Activation Energy (J/mol)
A_j	Rate pre-exponential constant of reaction j, (1/s)
R	Universal gas law constant, (J/Kmol)
T	Temperature, (K)
n_j	temperature exponent of reaction *j*, (dimensionless)
O_{ij}	Reaction order of component *i* in reaction *j*, (dimensionless)
R_j	Reaction rate of reaction *j,* (mol/m^{3}s)

The parameters were estimated using the described model and experimental data from Laresgoiti et al., 2004 and Olazar et al., 2008.

3.4.1 Results

The results for Olazar et al., 2008 and Laresgoiti et al., 2004 work for the 116 and 38 models with the new kinetic parameters can be seen in Figure 10 and Figure 11.

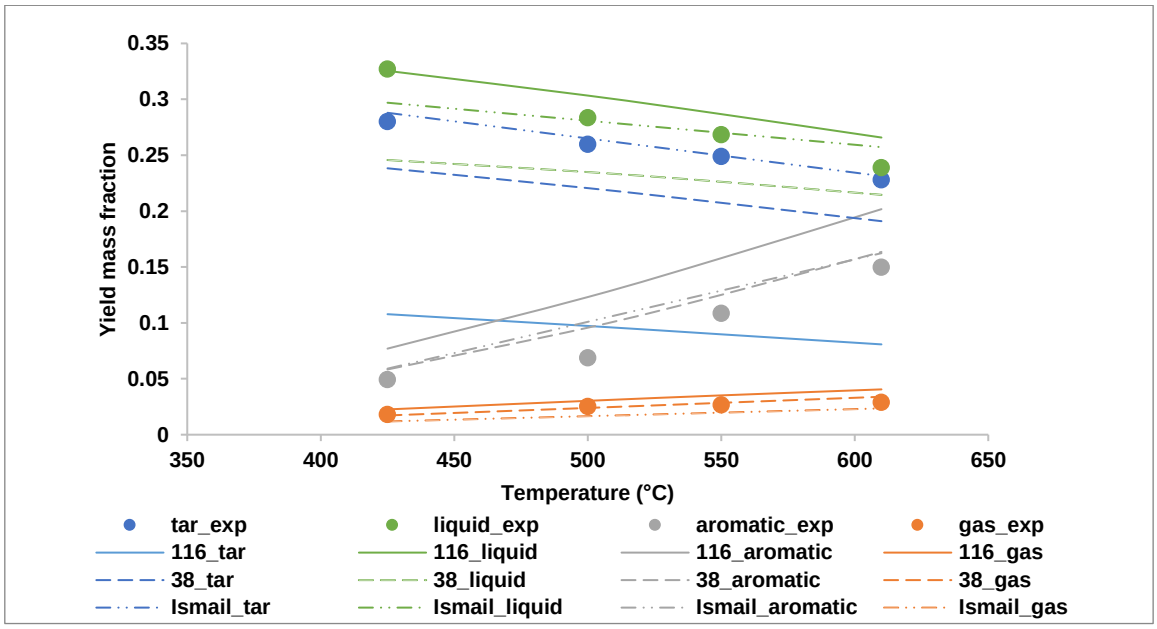

Figure 10 - The experimental (Olazar et al. 2008) and simulated product for the 116 (new parameters), 38 (new parameters), and Ismail et al. 2017 results yields at temperatures of 425, 500, 550, and 610 °C

As can be seen, the new parameters for the 116 reactions model produce worse results when modeling the tar group and slightly worse when simulating the aromatic group. The 38 reactions model with the new parameters produced better results, with the tar and liquid groups being better modelled. However, even though the 38 reactions modeled has been improved, it is still not able to model the experimental data as well as Ismail simulation results. It does however provide better results at estimating the tar group than the 116 reactions shown in Figure 8.

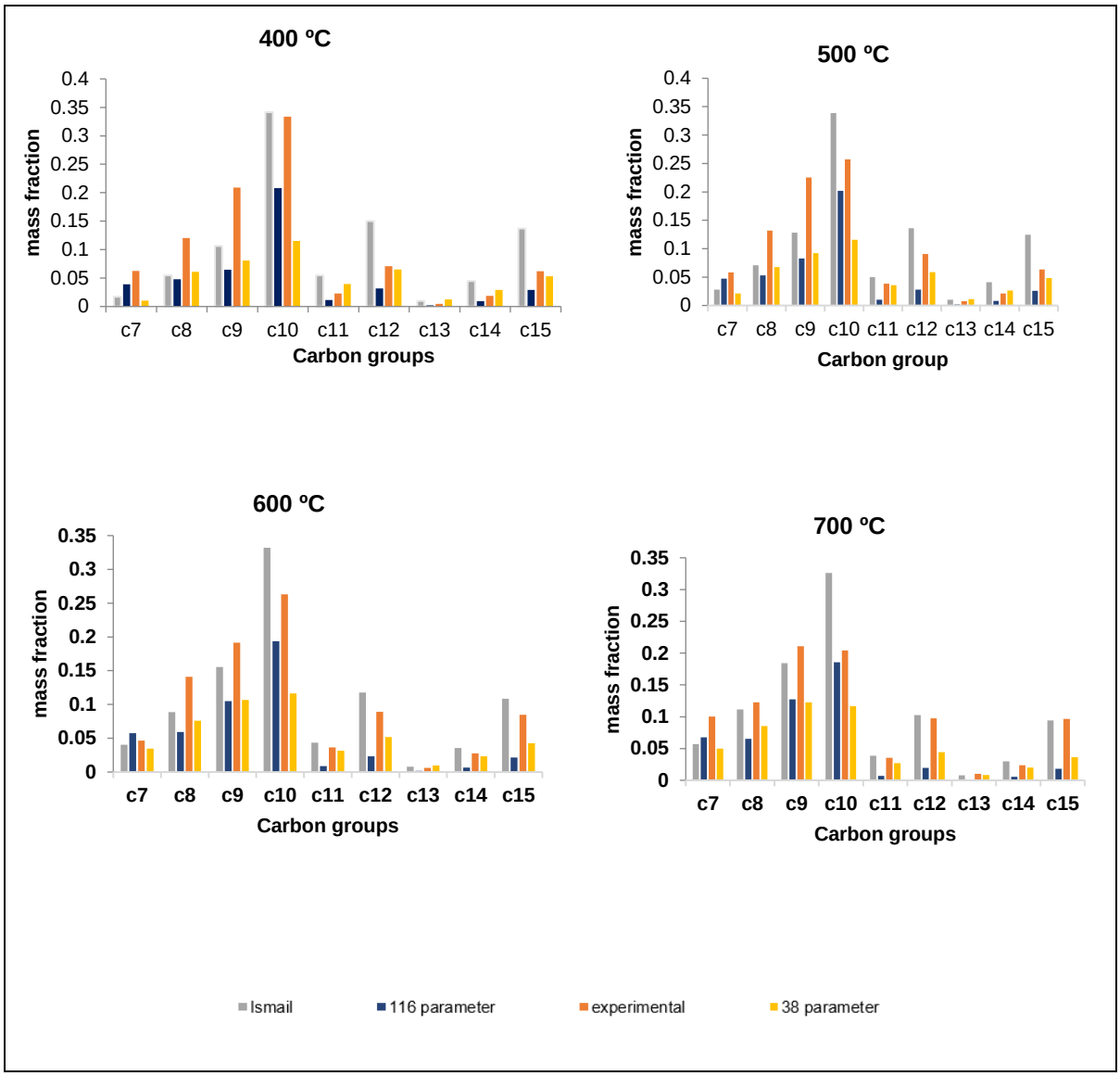

Figure 11 - Simulated product for 116 and 38 models with new parameters, Ismail et al. 2017 and Laresgoiti et al. 2004 experimental results for C7-C15 yield mass fractions of the oil and gas products at temperatures of 400, 500, 600 and 700 °C.

For the reproduction of and Laresgoiti et al. 2004 experimental data, the new 116 and 38 reaction parameters model still show that the experimental data cannot be well modelled, with disparities between the estimated models and Ismail simulation results.

Table 6 shows the average relative error for each work and the total average error. It can be seen that through the parameter estimation it was possible to obtain a 3% improvement in relation to the Ismail et al. 2017 simulation results.

The reason for the lack of a higher improvement might have been due to the fact that only the pre-exponential constants were varied, whereas the activation energy and the temperature coefficient were maintained constant. Since this variables were optimized for the Olazar et al. 2008 work, which was made using a conical spouted bed reactor, the fact that data from a different reactor was used to estimate the parameters (Laresgoiti et al. 2004 work was conducted using a autoclave batch reactor),

not varying this variables might be the reason as to why there was practically no improvement. This indicates that using data from different reactors as the basis for parameter estimation is not the best option. Also, the kinetic scheme used to create the pyrolysis modeling may be too simple and increasing complexity may result in better results.

Table 6 – Average relative error to Olazar et al. 2008 and Laresgoiti et al. 2004 results.

	$\bar{\sigma}_{\text{Laresgoiti et al.,2004}}$ (%)	$\bar{\sigma}_{\text{Olazar et al.,2008}}$ (%)	$\bar{\sigma}_{\text{Total}}$ (%)
gPROMS 116 Parameters Estimation	38	52	51
gPROMS 38 Parameters Estimation	15	45	36

Whereas previously, a lower specification of the products (38 reactions) gave the worst results, in this situation, it did better. This might be due to the fact that, contrary to what was proposed previously, a simpler approach can lead to a better situation since the number of parameters is lower. The parameters obtained for the 38 reactions model can be seen in Table 17 (pag.77).

3.5 Sensitivity Analysis

After choosing the kinetic parameters to be used (38 reactions parameters estimation), a base case scenario for the pyrolysis of waste tires was decided upon for the rest of the current work. It was decided to continue with the ultimate analysis values present in the *Aspen Plus*® file shown in Table 7 and the feed quantity used to simulate the process was based on the most frequent value of capacity for waste tire pyrolysis plants found in the literature, 20 000 tone/year, Table 16 (pag.77). For the reactor temperature, 500 ºC was selected because, according to J. D. Martínez et al. 2013, this is the optimal temperature at atmospheric pressure where complete tire conversion is achieved. At lower temperatures, the primary tire compounds (SBR, BR, and NR) persist in the pyrolytic CB with a heterogeneous, gum-like appearance. As for the condensation temperature, 30ºC was chosen, the same as Ismail et al 2017.

The pyrolysis products were categorized using the classification used by Pires et al. 2018. However, a new classification, cycloparaffin, was introduced because the pyrolysis oil produced using this kinetic model results in products outside the classification range presented in the literature. Using this classification system, an assumption was made where all polycyclic aromatic compounds, including biphenyl, were classified as naphthalene, even though they are not naphthalene's. The classification of the pyrolysis products can be seen in Table 18 (pag.83) of the Appendix.

In the industrial setting, inert gases like nitrogen are frequently added to the pyrolysis reactor to make the reactor atmosphere inert. Nitrogen addition to the pyrolysis process was not considered in this study, as it does not affect the simulation of the pyrolysis reaction. At the same, since no economic evaluation was performed, its addition has no effect.

The operating conditions for the sensibility can be seen in Table 8.

Table 7 – Ultimate analysis of a tire from the *Aspen Plus*® V11 file.

Carbon	74.8
Hydrogen	7
Nitrogen	0.3
Sulfur	1.5
Oxygen	2.7
Ashes	13.7

Table 8 – Operating conditions used for the sensibility analysis.

	Min	Max	Units
Residence Time	50	500	kg/hr
Condenser Temperature	0	100	ºC
Pyrolysis Reactor Temperature	200	700	ºC

To assess the pyrolysis oil's potential for jet fuel application, the Jet A requirements that could be obtained via *Aspen Plus*®, were applied:

- Volumetric amount of aromatic (4ºC);
- Net Heating Value (Lower heating value), calculated based on the equation (24);

$$\sum_{I} -Hcom(i) \cdot Rates(i) \tag{24}$$

  Where, $Hcom(i)$is the molar standard heat of combustion at 25°C and 1 bar of component i and $Rates(i)$ (dimensionless) is the component mole fraction.

- Flash Point API (Riazi 1986)*;*
- Naphthalene Volumetric amount (15ºC);
- Viscosity at -20ºC;
- Density at 15ºC;
- Sulfur total, by mass.

The values for each requirements mentioned above can be seen in Table 2 (pag.8).

The aromatic volume was obtained at 4ºC since that is the maximum temperature at which a hydrocarbon mixture can be sampled in the ASTM D1319-15 test used to determine the aromatic content in liquid petroleum. As for the naphthalene volume, it was obtained at 15ºC, since that is the temperature mentioned in the ASTM D1840 test, used to calculate the naphthalene volume in aviation turbine fuels.

The value of Shell SPK, 5729 viscosity, 2.6 cP at -20ºC was used to establish a minimum viscosity allowed in jet fuel so that it could be determined whether the pyrolysis oil was within the industry's range of jet fuel viscosity.(Kang et al. 2019)

3.5.1 Reaction Temperature

Figure 12 depicts the mass fraction of the compounds class in the reactor effluent. The results show that increasing the temperature leads to increased gas quantity and aromatic content, whereas the rest of component classes decrease with temperature. Also, it is possible to see that the rate at which aromatics are being produced is higher than the rest of the class of compound. The same trends can be seen in Figure 13, which represent the mass fraction of the compounds class in the pyrolysis oil, obtained after condensing the vapor product.

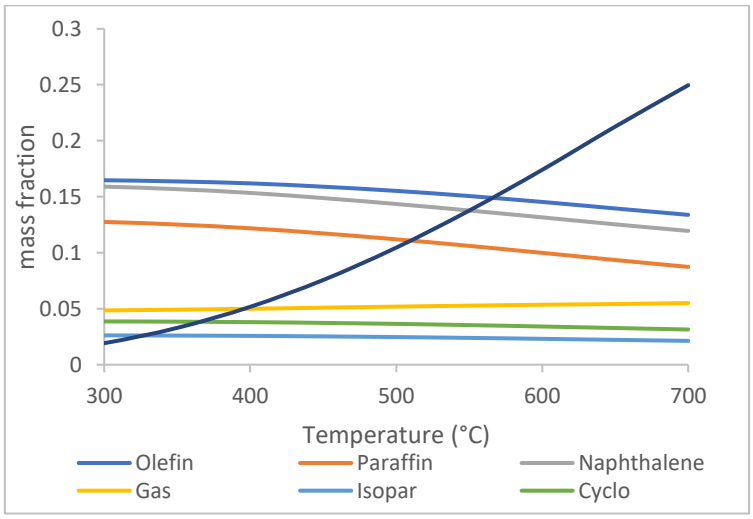

Figure 12 – Impact of temperature variation on the mass fraction at the reactor effluent for the multiple compounds class.

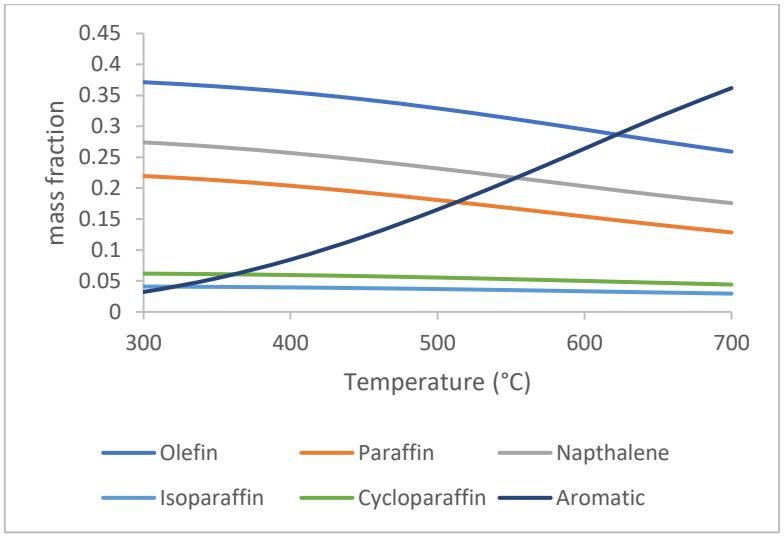

Figure 13 – Impact of temperature variation on the mass fraction in the pyrolysis oil obtained after the condenser for the multiple compounds class.

Figure 14 shows that the volumetric fraction of naphthalene is always above the maximum value allowed for jet fuel, indicating that further processing of the pyrolysis oil is necessary to meet this specification.

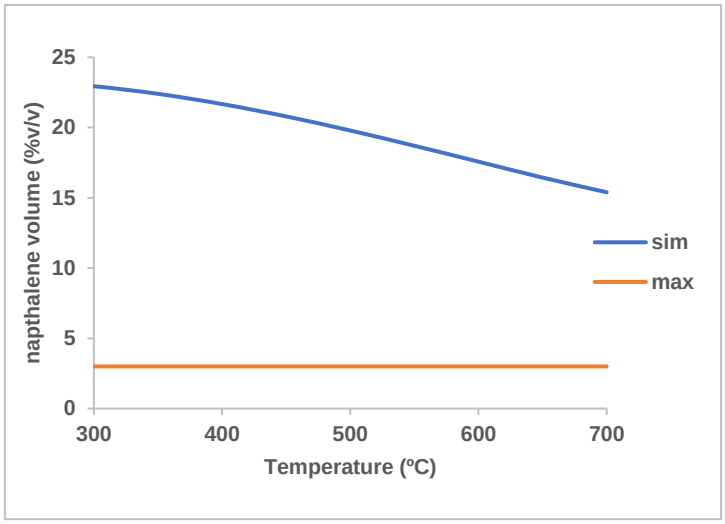

Figure 14 – Impact of temperature variation on the naphthalene volume of the pyrolysis oil condensed at 30ºC, obtained at 4ºC and compared with the maximum naphthalene volume allowed.

Additionally, another interesting aspect that can be seen in Figure 15 where through this variation, density increases with temperature.

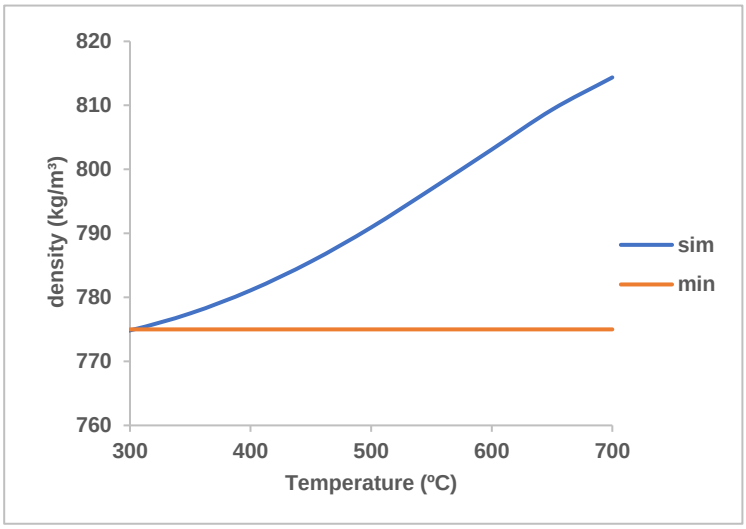

Figure 15 - Impact of temperature variation on the density of the pyrolysis oil condensed at 30ºC, obtained at 15 ºC, and compared with the maximum density and minimum density allowed for jet fuel.

According to the literature, density is a measure of the aromaticity of hydrocarbon oil. As pyrolysis oil is indeed a hydrocarbon oil, the increase in aromatic content in the oil leads to this trend. (Diebold et al. 1997; Karonis et al. 1998)

Table 9 – Jet fuel specification metrics obtained for the temperature range studied.

	Viscosity (-20 ºC)	Net Heating Value (Mj/kg)	Flashpoint (ºC)	Aromatic (v/v%)	Sulfur (m/m%)
300	3.3	42.6	25.0	2.8	0.1
350	3.3	42.5	24.6	4.7	0.2
400	3.2	42.4	24.8	7.3	0.3
450	3.1	42.3	27.5	10.6	0.4
500	3.0	42.1	30.3	14.6	0.6
550	2.9	41.9	30.1	18.9	0.8
600	2.8	41.8	29.4	23.6	1.0
650	2.8	41.6	28.9	28.4	1.1
700	2.7	41.4	28.3	32.9	1.2

Analyzing Table 9, it is possible to understand that viscosity decreases as temperature rises. This is due to increased aromatic compounds, which have double bounds. As stated in the literature review (pag.5), an increase in the formation of double-bound compounds decreases viscosity.

Flashpoint increases until 500ºC until it decreases. The increase is due to the decrease in lower molecular weight compounds such as olefins and paraffins, as seen in Figure 13. However, the subtle decrease is mainly due to the impact of the decrease in naphthalene content (higher molecular weight compounds) at this temperature. The aromatic volume increase is explained by the increase formation along the temperature of aromatic compounds. As for the net heating value decrease, this is expected given that as temperature increases, more gaseous compounds form, and less carbon and hydrogen elements become available. The equations (25) and (26) support this justification. Equation (25) was obtained from Alsheyab et al. 2013 and Equation (26) from Cooper, Kim, and MacDonald 1999.

$$HHV = 10^{-5}(33{,}827\mathrm{C} + 144{,}267\mathrm{H} - 18{,}033\mathrm{O} + 9{,}420S) \quad (25)$$

$$LHV = HHV - 2 * \Delta H_V water \quad (26)$$

Where, HHV is the higher heating value (J/kg), H, C,O and S are the weight fraction of the elements in the ultimate analysis, LHV the lower heating value (J/kg) and $\Delta H_V water$ the heat of vaporization of water (J/mol).

The sulfur mass fraction increases as the temperature rises. This is due to the formation of more gas compounds as temperature rises, as shown in Figure 12, which reduces the amount of pyrolysis oil produced and increases the amount of sulfur per unit of pyrolysis oil produced.

3.5.2 Residence Time

In order to understand the impact of the residence time, the feed flowrate was changed between 50 and 500 kg/hr. As shown in equation (27), residence time alters with the total volumetric flow rate of the process stream. By changing the mass quantity, this variable changes, making it possible to analyze the residence time.

$$\theta = \frac{\pi D^2 N}{4} \int_{z=0}^{z=L} \frac{dz}{F_z \sum_j \phi_{j,z}} \tag{27}$$

Where, θ is the reactor residence time *(s), D* the tube diameter *(m),* N is the number of tubes *(dimensionless), Z is* the axial position in reactor of length *L (m), F_z is* the total volumetric flow rate of process stream at axial location *z (m^3/s), $\phi_{j,z}$* volume fraction of phase *j* at axial location *z (dimensionless), j* the phase *(vapor, liquid, solid).*

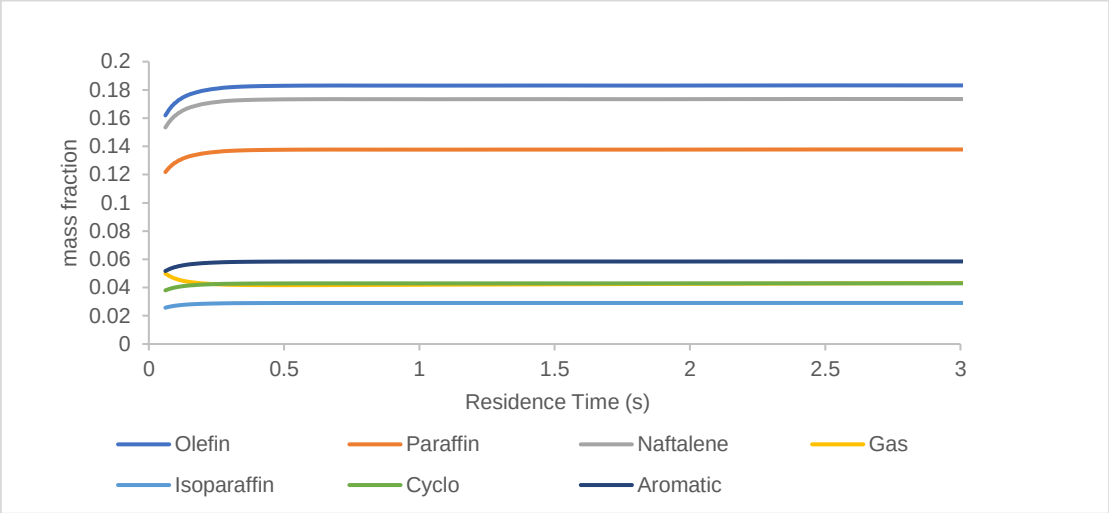

Figure 16 – Residence time variation and impact in the multiple compounds class present in the tire in terms of the mass fraction at the reactor end.

Analyzing Figure 16 reveals that the reaction appears to occur instantaneously, in less than one second, for all of the classification lumps and that there is no change in the composition of the product regardless of how long the product remains in the reactor; increasing the time residence from 10 to 50 seconds has no effect. This is due to the fact that the kinetic model is only dependent upon the elemental composition of the tire and not the decomposition of higher molecular compounds to lower molecular compounds. As such, all the product formation happens at the same time. This analysis leads to the conclusion that regulating the formation of a specific product via residence time using the current kinetic model should be avoided.

3.5.3 Condenser temperature

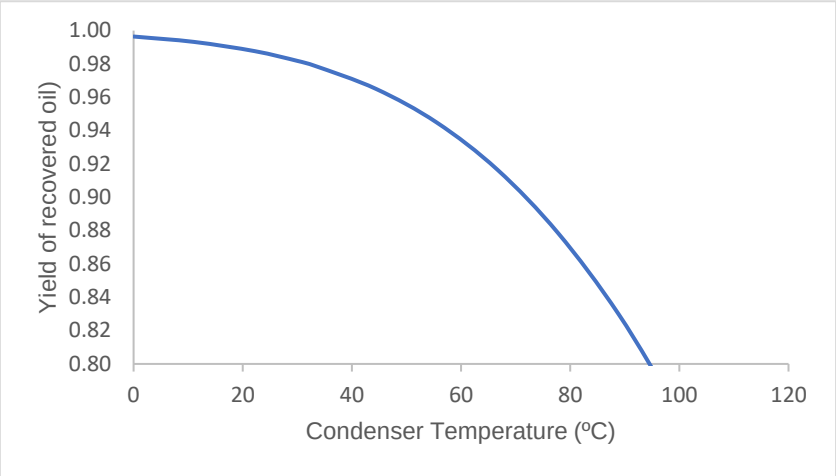

Figure 17 – Mass yield of oil condensed at the condenser temperature per the oil produced in the pyrolysis reactor.

Figure 17 shows how the mass yield of oil condensed per oil produced changed with temperature. It can be seen that below 70 ºC, a yield of more than 90% is obtained and at 40ºC a yield of over 95% can be obtained. Looking at the way the condenser temperature dictates the yield of oil produced obtained, it is indicative of the importance of this variable.

3.5.4 Different Type of Tires

To see how the present kinetic model responded to the use of different types of tires, a sensitivity study was done. The ultimate analysis of the different tires used in this work can be seen in Table 19 (pag.84)

Analyzing Figure 18 reveals that there is no difference between the composition of each tire pyrolysis oil. This is due to the present kinetic limitation, where hydrogen weight fraction in the ultimate analysis is the main factor influencing the product outcome, as seen in equation (28), so as long as the carbon element is in excess. Equation (28) represents the general reaction rates for this pyrolysis model.

$$r_i = \mathrm{A}_i \cdot \exp\left(\frac{Ea_i}{RT}\right) \cdot X_{\mathrm{H2}} \tag{28}$$

Where r_i is the reaction expression for the production of product i (mol/m^{3}s), A_i the kinetic constant for the production of product i (1/s), Ea_i the activation energy for the production of product i (J/mol), R the universal gas constant, (J/Kmol), T temperature in the reactor (K) and X_{H2}, the mass fraction of hydrogen in the reactor (dimensionless).

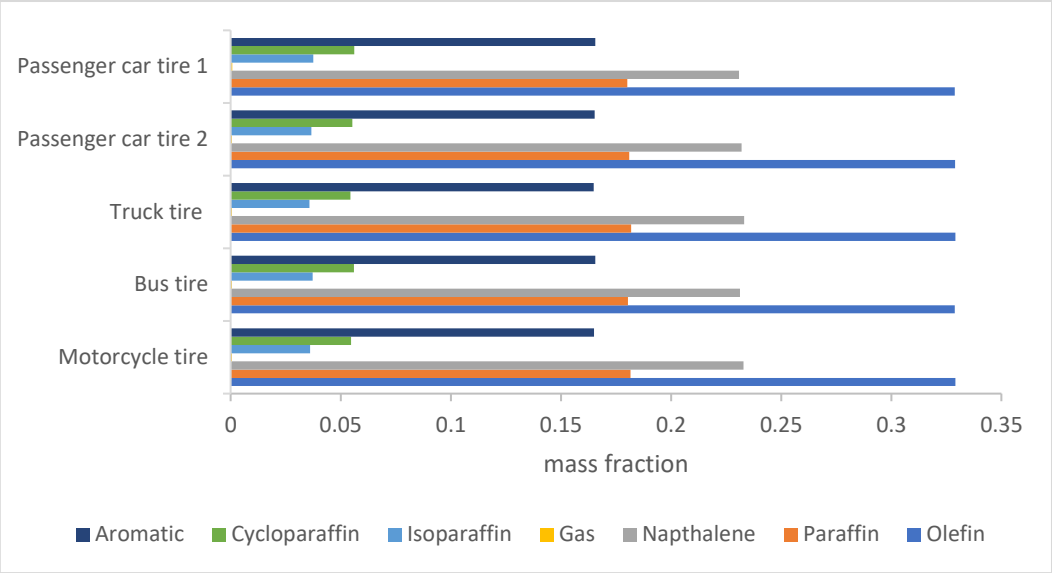

Figure 18 - Representation of how each classification lumps mass fraction changes for the different types of tires, for the oil obtained in the condenser for the case scenario.

As the hydrogen weight fraction in the ultimate analysis for all the different tires is similar, around ±7 %wt, and carbon is in excess, this led to similar results. However, the literature indicates that the use of different types of tire feeds affects the product's composition. For instance, in the study by Ucar et al. 2005, which utilized two distinct types of feed tires, truck tires and passenger car tires, truck tires oil (TTO) yielded a higher aromatic content than passenger car's tires oil (PCTO). At 550 ºC, PCTO yielded 41.5 %vol of aromatic content, while TTO yielded 15.4 %vol.

4 Pyrolysis Oil Hydrotreatment

This chapter introduces how kinetic modeling is done in the hydrotreatment process, Section 4.1 (pag.41), and how it was done in this thesis, Section 4.2 (pag.43). The reproduction of the experimental results of the hydrotreatment model is explained in Section 4.3 (pag.44) and the lumping methodology in Section 4.4 (pag.50). Finally, the sensitivity analysis toward the independent variables is done in Section 4.6 (pag.61) using the base case pyrolysis oil from the previous section.

4.1 Approach by Lumping

The development of a lumping approach usually proceeds through the following steps indicated in Oliveira et al. 2016 :

- Selecting a set of lumps to characterize the feedstock;
- Constructing a kinetic network of lumped reactions to characterize the relationship between lumps;
- Determination of rate equations and their corresponding parameters by optimizing the model using experimental data,

The lumping kinetics have multiple advantages, such as:

- Lumped kinetic models are easy to develop (number of lumps and number of reactions are limited;
- Reaction pathways are global with no intermediaries;
- Kinetic rate equations are simple (pseudo-order reactions, Langmuir approach in heterogeneous kinetics, etc.),

In this type of modeling, the kinetic parameters are frequently determined by minimizing the deviations between model and experimental data from pilot units or industrial plants. Because of this simplicity, high-speed kinetic models with few computational resources are possible, which is useful for optimizing and controlling petroleum operations. However, the lumped kinetics have drawbacks:

- Lumps are frequently defined as groups of compounds that have similar physicochemical properties (as determined by analytical techniques) but not necessarily similar reactivities;
- Modeling is long and expensive since it is dependent upon experimental data coming from the plant;

4.1.1 Examples of Lumped Kinetic Models

Olmo 2015 studied the upgrading of waste tire pyrolysis through hydrotreating and hydrocracking. The study was done in a trickle bed reactor, which is a fixed bed reactor with liquid and gas feeding.

The authors' work lumping was derived from the bi-dimensional GCxGC (Gas Chromatography) chromatogram of analysis of the liquid products of the HT of STPO (scrap tire pyrolysis oil), coupled with its matching projections based on the retention time. A boiling point criterion based on the projection of the retention time in the first dimension (1DRT projection) was used to identify three separate fractions: naphtha (35-216 °C), diesel (216-350 °C), and gasoil (>350 °C). In addition, five lumps were

recognized according to their reactivity through the retention time projection in the second dimension (2DRT projection): (i) paraffins and isoparaffins (P+iP), (ii) olefins (O), (iii) naphthenes (N), (iv) 1-ring aromatics (A1), and (v) 2-ring aromatics (A2). To quantify each lump, a Gaussian deconvolution was applied.

The author proposed a simple kinetic scheme for the hydrotreating stage, where the hydrotreatment can be modeled as three independent kinetic pathways, the hydrodearomatization (HDA), the hydrodesulfurization (HDS), and the hydrocracking (HC).

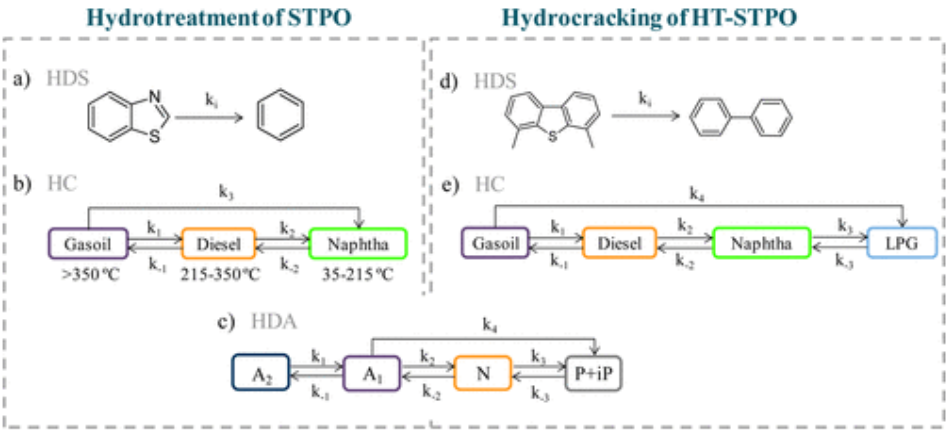

Figure 19 – Hydroprocessing kinetic schematic proposed by Olmo 2015.

The kinetic expression for the formation and decomposition was assumed to be first order in relation to each lump and hydrogen mass fraction. However, the HDS kinetic model was based on Langmuir–Hinshelwood expression.

The HDA kinetic model is presented in Equations (29)-(34).

$$K_1 = \frac{k_1}{k_{-1}} \tag{29}$$

$$K_2 = \frac{k_2}{k_{-2}} \tag{30}$$

$$K_3 = \frac{k_3}{k_{-3}} \tag{31}$$

$$\frac{dx_{A2}}{d\tau} = -k_1 x_{A2} x_H + k_{-1} x_{A1} x_H \tag{32}$$

$$\frac{dx_{A1}}{d\tau} = k_1 x_{A2} x_H - k_{-1} x_{A1} x_H - k_2 x_{A1} x_H + k_{-2} x_N x_H - k_4 x_{A1} x_H \tag{33}$$

$$\frac{dx_N}{d\tau} = k_2 x_{A1} x_H - k_{-2} x_N x_H - k_3 x_N x_H + k_{-3} x_P x_H \tag{34}$$

Where, k_1, k_2, k_3, k_4 $(g_{feed} {g_{cat}}^{-1} h^{-1})$, are direct kinetic constants, k_{-1}, k_{-2}, k_{-3} $(g_{feed} {g_{cat}}^{-1} h^{-1})$, reverse kinetic constants, K_1, K_2, K_3 (dimensionless) equilibrium constants, x_{A2} (dimensionless) the mass fraction of A_2 lump in the liquid phase, x_{A1}(dimensionless) the mass fraction of A_1 lump in the liquid phase, x_N (dimensionless) the mass fraction of N lump in the liquid phase, x_P

(dimensionless) the mass fraction of P lump in the liquid phase, x_H (dimensionless) the mass fraction of H_2 in the liquid phase and τ ($g_{cat} h g_{feed}{}^{-1}$) the spacetime.

The equilibrium constants were established according to the Van't Hoff equation, equation (35), and the kinetic constant were defined by the reparametrized Arrhenius equation, considering T_{ref} as 390 °C, equation (35).

$$K_i = \frac{k_i}{k_{-i}} = K_{i,T_{ref}} \exp\left[\frac{\Delta H_i}{R}\left(\frac{1}{T} - \frac{1}{T_{ref}}\right)\right] \quad (35)$$

$$k_i = k_{i,T_{ref}} \exp\left[\frac{-E_i}{R}\left(\frac{1}{T} - \frac{1}{T_{ref}}\right)\right] \quad (36)$$

Where, K_i (dimensionless) is the thermodynamic equilibrium constant for the reaction *i,* k_i ($g_{feed} g_{cat}{}^{-1} h^{-1}$) the direct kinetic constant of reaction *i,* k_{-i} ($g_{feed} g_{cat}{}^{-1} h^{-1}$) the inverse reaction constant of reaction *i,* ΔH_i (J/mol) the standard reaction enthalpy, T the temperature in the reactor, T_{ref} the reference temperature, $k_{i,T_{ref}}$ ($g_{feed} g_{cat}{}^{-1} h^{-1}$) the direct kinetic constant of reaction *i* at the reference temperature, E_i (J/mol) the activation energy for the reaction i and R (J·K^{-1}·mol^{-1}) the universal gas law constant.

4.2 Hydrotreatment modeling

The Olmo 2015 kinetic model, whose kinetic parameters were obtained for a NiMo/Al_2O_3 catalyst and are present in Table 20 (pag.84), was used to simulate the hydrotreatment of pyrolysis oil. This model was selected because it is the only kinetic model available for the hydrotreatment of used tires. The hydrotreatment process was modeled in *Aspen Plus*® V11, and the same property method (PR-BM), and missing thermophysical properties (UNIFAC), as in the pyrolysis process, were used.

This kinetic model requires the lumping of the pyrolysis oil into various lumps. When separating the compounds into different lumps, it was possible to discern that compounds present in a certain lump of the HDA pathway, for example, compounds in the A1 lump, some might in the Gasoil lump of the HC process, whereas others might be in the Diesel lump.

It was decided to only simulate the HDA pathway over the others since the HDA kinetic model, aside from taking into account the cracking of the compounds, as illustrated in Figure 19, where naphthene cracks into paraffin, it also allows for a more precise characterization of the stream composition. The HDS kinetic model was not implemented because the sulfur component in the pyrolysis oil simulated does not have associated kinetic parameters.

The trickle bed reactor model could not be implemented in *Aspen Plus*® since the model is not available, and as a result, the ideal plug flow reactor model was used. This choice was based on the literature findings, where a trickle bed reactor has been mentioned to be simulated using and ideal plug flow reactor. (Yadav and Roy, 2022)

As in *Olmo 2015* kinetic model, the inverse reaction constants are derived from the equilibrium constant, whose value varies with temperature, a custom equation was developed to account for the calculation of this term in *Aspen Plus*®.

The reaction rate expression present in *Aspen Plus*® is show in equation (37) and an example of the way the inverse pre-exponential constant was calculated can be seen in Figure 20.

$$r = [\text{Kinetic Factor}][\text{Driving Force}][\text{Custom Term}] \quad (37)$$

Custom Term	Equation
K1	k1ref*EXP(-EA1/R*(1/T-1/TREF))
KEQ1	KEQ1REF*EXP(-HF1/R*(1/T-1/TREF))
KMINUS1	k1/keq1

Figure 20 - Custom Equation introduced *Aspen Plus*®.

Where EA1 (J/mol) is the activation energy of one of the direct reactions, Tref (K) is the reference temperature, K1ref ($g_{feed}{g_{cat}}^{-1}h^{-1}$) the direct kinetic rate value at the reference temperature, R ($J{\cdot}K^{-1}{\cdot}mol^{-1}$) the universal gas constant, KEQ1 (dimensionless) is the ratio between the direct kinetic constant and reverse kinetic constant at the reference temperature, HF1 (J/mol) the standard enthalpy of reaction, k1 ($g_{feed}{g_{cat}}^{-1}h^{-1}$) the direct kinetic rate value at the reactor temperature, T (K) the reactor temperature, keq1 (dimensionless) the thermodynamic equilibrium constant at the reactor temperature, KMINUS1 ($g_{feed}{g_{cat}}^{-1}h^{-1}$) the reverse kinetic rate value at reactor temperature.

In addition, for the implementation of the reaction kinetics in *Aspen Plus*®, it was assumed that all direct reactions react with hydrogen and all reverse reactions produce hydrogen. This is in accordance with the knowledge of aromatic saturation and naphthene ring opening. (Robinson 2011) Additionally, mass balance was used to determine the stoichiometry of each component in each reaction.

In order to understand if the implementation of the HDA kinetic model was well done, a reproduction of the experimental data was made.

4.3 Reproducing Experimental Data

The flowsheet implemented in *Aspen Plus*® is presented in Figure 21. The reactor was simulated using an RPlug block with a 1 m diameter and a 1 m length. Since these values do not impact the product formation, arbitrary values were chosen (The kinetic is based on catalyst weight and not on volume). The hydrotreatment experimental reproduction involved simulating the reaction at 300-370°C, 65 bar pressure, a condenser temperature of 0ºC and changing the catalyst weight to obtain a spacetime from 0-0.5 (kgcat·h/kgfeed).

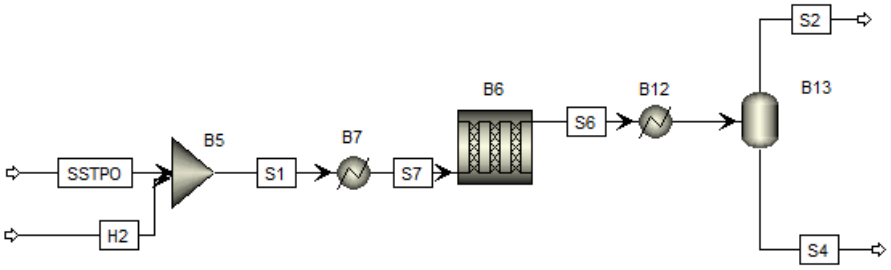

Figure 21 - *Aspen Plus*® Schematic used to compare the results with the literature

The simulated tire pyrolysis stream (SSTPO) was mixed in a Mixer (B5) with a hydrogen stream (H2), then sent to a Heater (B7) that controlled the temperature of the reactor prior to entering the RPlug reactor (B6). The product was then condensed (B12), and via a flash (B13), the condensables were separated from the non-condensables.

In order to make the experimental reproduction, the scrap tire composition used by *Olmo 2015* had to be obtained. It was found that composition was indeed available in the literature (Hita et al. 2015), however, when considering that for two ring aromatics, which account for 17.7% of the STPO, the only available compound was biphenyl, which accounts for 0.12% of the STPO it made more sense to find a more in depth characterization of the scrap tire. In the same article, a composition of a simulated scrap tire oil (SSTPO) was described in greater detail, and this composition served as the basis for the experimental reproduction.

Each compound present (D-limonene, toluene, dibenzothiophene, 1H-Indene) in the simulated scrap tire was assumed to be one of the lumps present in the HDA kinetic model. However, because no paraffinic compounds were used in the SSTPO, the solvent (NC10) was assumed to represent the paraffinic lump.

D-limonene was classified as being the N lump, toluene as A1, NC10 as P, and 1-h Indene as A2. Although 1h-Indene lacks two aromatic rings, it was decided to use the compound closest to having two aromatic rings present in the simulated scrap tire oil as a basis for the lumping, instead of replacing the compounds.

During the initialization of the experimental reproduction, it was found that when mixing the simulated pyrolysis oil with the hydrogen ratio mentioned in *Olmo 2015,* 1000 Nm^3/m^3, the resulting mixture was in the vapor phase at the operating conditions of the literature. Since, in reality, the pyrolysis oil is introduced in the trickle bed reactor in the liquid phase, as mentioned in the literature review (pag.18), the total vaporization of the feed stream when using the ratio of the article is a problematic situation.

In order to deal with this issue, multiple situation strategies were tested. Their description and results are presented in the next sections. The total average relative error was used as the model performance criteria, and its calculation can be seen in Equation (38).

$$\bar{\sigma}_{\text{Olmo 2015}} = \frac{\sum_{T=300}^{375} \frac{\sum_{l=P}^{A2} \frac{\sum_{k=1}^{nexp} \frac{|exp_k - sim_k|}{exp_k}}{nexp}}{nlumps}}{ntemps} \cdot 100 \quad (38)$$

Where, ntemps is the number of temperatures (dimensionless), T the temperatures used in *Olmo 2015 work (*300, 340 and 375ºC), nexp = the number of experiments (dimensionless), k =1,,,nexp (dimensionless), l the lumps (P,N,A1,A2) (dimensionless) and nlump = the number of lumps (dimensionless).

4.3.1 Liquid phase

As previously stated, mixing the feed with hydrogen in the proportion used by *Olmo 2015* results in total vaporization of the stream. As such, the H_2/feed ratio was adjusted so the mixture entering the reactor was only partially vaporated. The lowest H_2/feed ratio found in the literature for hydrotreatment processes was 70 Nm^3/m^3. At this value the pyrolysis oil is 38% vaporized at 300ºC, 63% at 340 ºC and totally vaporized at 375 ºC.

. The simulation results for the hydrotreatment with a hydrogen ratio of 70 Nm^3/m^3 and 300 ºC are presented in Figure 22.

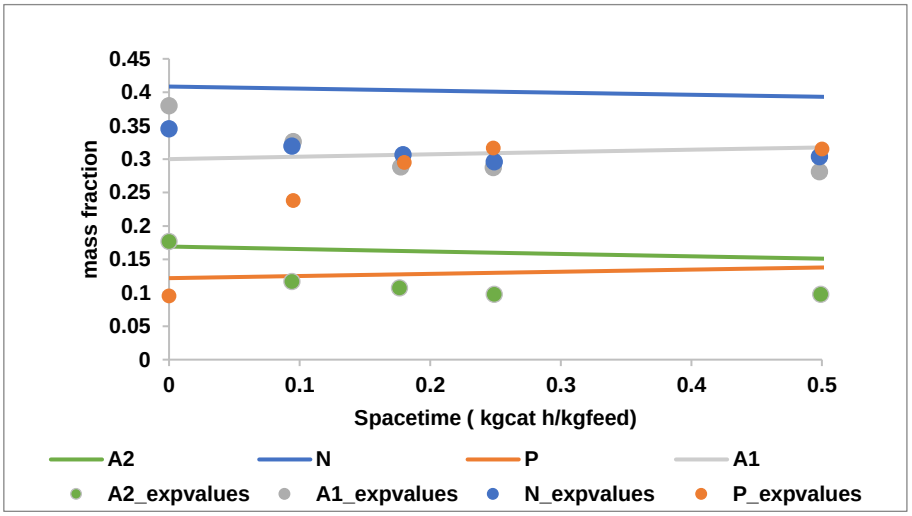

Figure 22 - Reproduction of Olmo 2015 experimental results and comparison of simulation and experimental data for 300 ºC and 65 bar for a liquid phase kinetic rate.

Figure 22 shows that this approach leads to a linear trend of the simulation results, in contrast with the experimental results, which have a curved trend. This might be due to a low conversion rate brought on by having a small amount of feed in the liquid phase. The associated total average relative error for this approach is 36 %.

4.3.2 Vapor phase (1000 Nm³/m³ ratio)

In this approach, the ratio of H_2/feed was kept at 1000 Nm^3/m^3. However, to bypass the total vaporization of the feed problem, the reactions were set to be taken on the vapor phase instead of the liquid phase to try to reproduce the extent of the reaction.

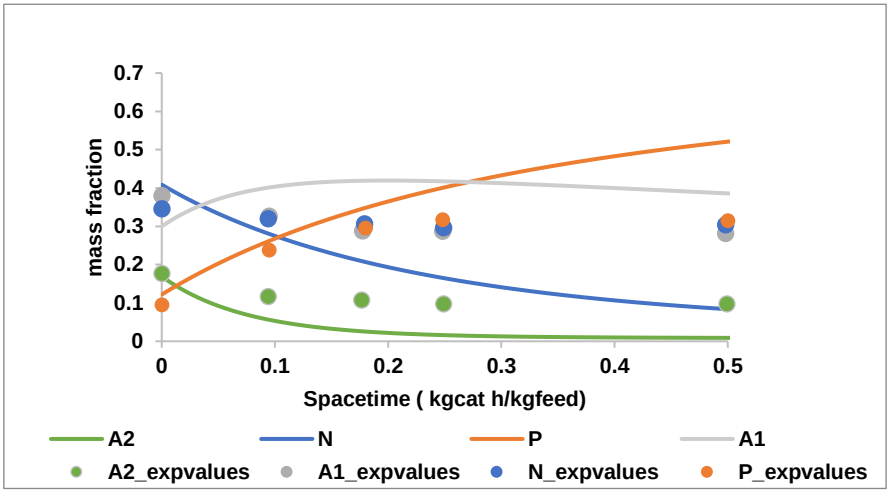

Figure 23 - Reproduction of Olmo 2015 experimental results and comparison of simulation and experimental data for 300 ºC and 65 bar for a vapor phase kinetic rate.

Analyzing Figure 23, it is possible to see that it is indeed possible to obtain more reasonable results compared to the previous situation since the curvature present in the experimental data is slightly captured. The same trends can be seen in Figure 46 (pag.85) for 340 and 375 ºC.

It is also possible to see in Figure 23 that the extension of the simulation results is clearly much higher than the experimental results. This can be justified by the excess of hydrogen present in the reactive mixture. Equations (32) - (34) are dependent on the concentration of hydrogen in the liquid phase. In a trickle-bed reaction, that concentration would depend on the mass transfer limitations between the gaseous and liquid phases present in the system, as shown in Figure 24. As it is considered that the entire reactive mixture is in one single phase, this means that the hydrogen concentration in equations (32) - (34) is probably much higher than its solubility in the liquid phase. This might be the reason as to why even though the curvature trend of the experimental data is slightly captured, the total average relative error increased from the previous approach to 37 %.

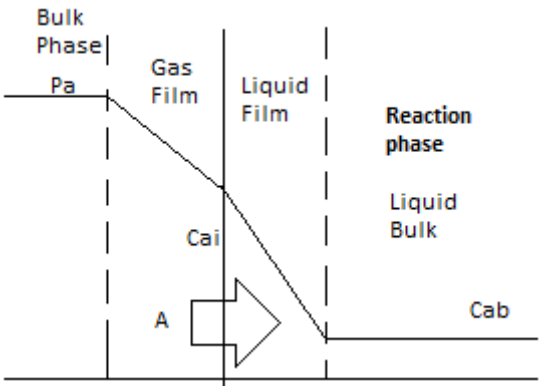

Figure 24 - Schematic of liquid-gas interface, where A is a gaseous compound, Pa is the partial pressure of A in the bulk (bar), Cai is the concentration of A in the interphase (mol/m^3), Cab is the concentration of A in the liquid bulk. (mol/m^3).

4.3.3 Reduction of the hydrogen ratio

Taking into account the previous results, the hydrogen-to-feed ratio was reduced, while keeping the reaction mixture in the vapor phase to confirm if the reduction of the hydrogen concentration would improve the results.

Figure 25 shows the simulation results and the experimental data for 300 ºC using a ratio of feed to hydrogen of 420 Nm^3/m^3. It is possible to see that the curvature of the A1 lump cannot be captured, but the curvature of the other lumps can. The simulation results are closer to the experimental data than before. The graphs containing the simulation results for 340 and 375 ºC can be seen in Figure 47 (pag.85).

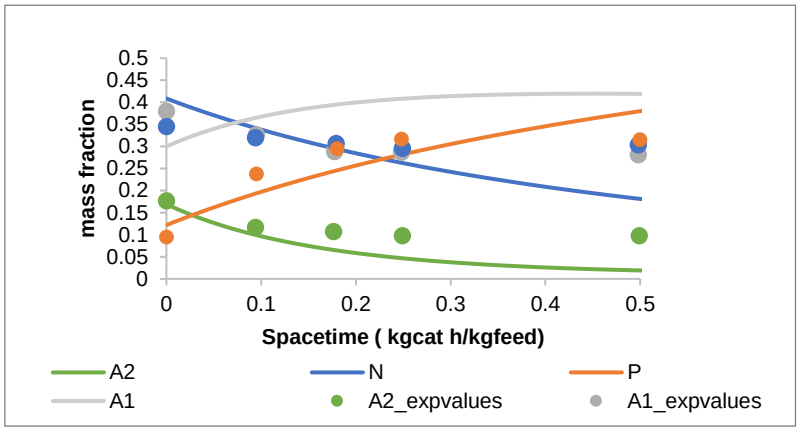

Figure 25 - Reproduction of *Olmo 2015* experimental results and comparison of simulation and experimental data for 300 ºC and 65 bar for the 420 Nm^3/m^3 ratio.

Table 10 shows the total average relative error obtained by reducing the H_2/feed ratio while maintaining the mixture in the vapor phase. to the results improve considerably, and the total average relative error reduces from 37% to 19%. This backs the previous assumption (reducing hydrogen quantity allows to emulate the solubility of hydrogen in the liquid phase in an industrial setting), and as a result, it can be said that reducing the amount of hydrogen allows for better modeling results.

Table 10 – Average Relative error values obtained for each H_2/feed ratios (Nm^3/m^3).

Ratio H_2/feed (Nm^3/m^3)	$\bar{\sigma}_{\text{Olmo 2015}}$ (%)
420	19
560	24
700	28
840	32
980	36
1000	37

4.3.4 Custom Term

Considering the idea of diminishing the mass fraction of hydrogen until a certain point to try and emulate the "solubility" of hydrogen in the oil, as previously mentioned, another route was considered. Because hydrogen is largely in excess, it can be assumed that is concentration in the liquid phase is constant. To implement this approach, it was necessary to add a custom term that would be constant and would not vary depending on the amount of hydrogen added. As such, using this method, the order of hydrogen in the reactions was set to zero because this custom term accounted for its fraction in the feed. Also, since the approach of simulating the kinetic in one phase, namely, the vapor phase, the amount of hydrogen influences the mass fraction of the lumping terms, as a result, this custom term, aside from the solubility, will also correct the mass fraction of the lumping terms. In summary, this means that in equations (29)-(34), x_H would be replaced by a constant value.

Figure 26 shows the simulation results and the experimental data for 300 ºC using a custom term of 0.023 for a H_2/feed ratio of 1000 Nm^3/m^3. The curvature trends and results obtained in the previous approach are similar to those obtained in this approach. The major difference between them is the reduction of the overshoot of the paraffin lump.

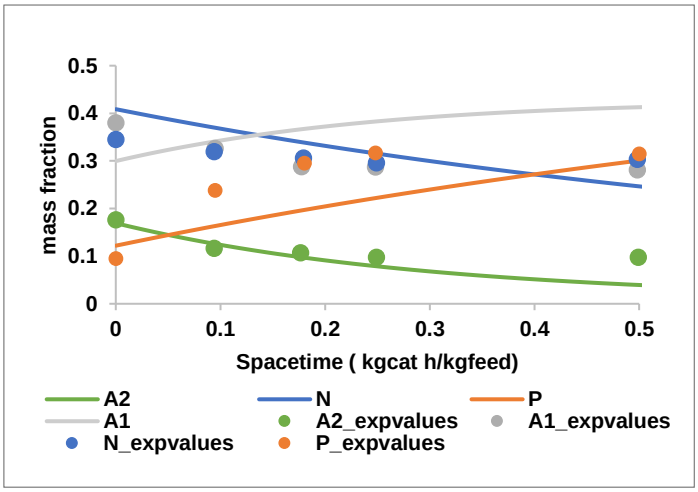

Figure 26 - Reproduction of *Olmo 2015* experimental results and comparison of simulation and experimental data for 300ºC and 65 bar, for the 0.023 custom term value.

Table 11 shows the various custom term values used and the resulting average relative error for each temperature and total average relative error. Through this approach a minimum for the total average error value is obtained, namely 0.023. In this study, 0.023 was assumed to be the minimum

value because it yielded the lowest error, and no optimization was performed to find the actual minimum value. For lower values than 0.023, the average error starts increasing, because a lower hydrogen concentration starts limiting the kinetics beyond what the experimental results indicate.

Table 11 – Average relative error for each temperature and the total average error value for each custom term, This results were obtained for a ratio of H_2/feed at 1000 Nm^3/m^3.

(%)	300 °C	340 °C	375 °C	$\bar{\sigma}_{\text{Olmo 2015}}$
0.001	38	37	34	36
0.01	25	23	19	22
0.023	20	17	12	16
0.0326	22	18	12	17
0.0375	24	19	13	19
0.0415	25	20	15	20
0.0562	29	26	21	25

It should be noted that in this approach, the solubility of hydrogen and the correcting term for the lumping terms are assumed to be constant across all temperatures. This could be a limitation because hydrogen solubility increases with the temperature. As a result, if the correcting term of the lumping terms was constant, the total term would increase with temperature. This concept, however, does not have any impact on the average relative error obtained for each temperature, as 0.023 is the lowest across all the temperatures.

In summary, the discrepancies between experimental and simulated values result from multiple approximations. The use of a different stream, the ratio of hydrogen to feed leading to total vaporization, using different compounds to reproduce the experimental data and the need to alter the kinetic model in order to model the experimental data in a better way, could account for the current discrepancy between the simulated and experimental values.

The method chosen to generalize the current results to the pyrolysis oil obtained from the simulation was to implement the current best custom term and consider it constant. This meant that hydrogen solubility was assumed to be constant, independent of the type of oil and temperature and that the correcting effect of naphthalene, aromatic, naphthene, and paraffin was also constant.

4.4 Lumping

For the sensitivity analysis, which uses a stream made of multiple compounds, to implement Olmo 2015 altered HDA model, the compounds must be grouped according to their chemical class in order to simulate the reaction.

In the scientific literature, lumping has been performed using the average molecular weight. By first agglomerating the compound and determining its average molecular weight, the compound with the molecular weight closest to the average molecular weight was selected as the representative of that lump. (Choe et al., 2021) Creating a pseudo component that mimics the compound that best represents the compounds grouped within a classification is an alternative method. In *Aspen Plus*®, this is accomplished by creating a pseudo component and providing three basic parameters (although only

two are required to generate the compound): the Average Normal Boiling Point (NBP), the average molecular weight (MW), and the specific gravity.

There are multiple metrics to calculate the average normal boiling point, in *Aspen Plus*® this value is represented by the mean average normal boiling point.

Both lumping procedures were compared using as basis the mass fraction of each lump at time 0 in Olmo 2015 work .The lumping methodology which allowed to have similar trends to the experimental work was used for the sensibility analysis.

It should be noted that the hydrotreater flowsheet shown in Figure 21 (pag.45) was used to conduct this comparison.

4.4.1 Lumping by Average Molecular Weight

The compounds present in the pyrolysis oil were classified as two-ring aromatic, one-ring aromatics and naphthene's. Table 21-Table 24 (pag.86,87) in the Appendix show their grouping and the average molecular mass.

Equation (39) was used to calculate the average molecular weight: (I. Martínez n.d.)

$$\bar{M} = \sum x_i M_i \tag{39}$$

Where xi = mol fraction and Mi = molecular weight of compound i

After determining the average molecular mass, each compound's relative error to the average molecular mass was calculated, and the compound with the lowest error was chosen. If there were compounds with similar low relative errors, the lump's representative compound was chosen arbitrarily. The compounds chosen to represent the oil mixture are listed in Table 12.

Table 12 – Compounds chosen to represent each lump, according to the average molecular weight.

A2	DIPHENYL
A1	XYLENE
N	LIMONENE
P	NC11

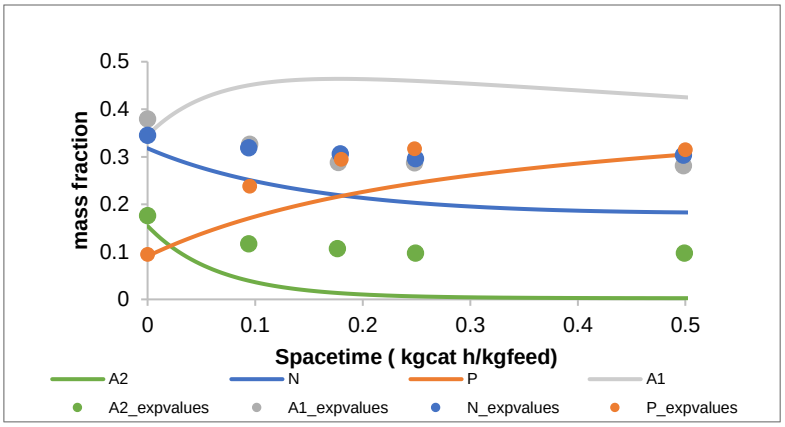

Figure 27 – Comparison of the experimental data with the lumping molecules representative, with the reactions in the vapor phase, at the ratio of 1000 Nm^3/m^3 without a custom term, for 300 ºC, 65 bar.

Analyzing Figure 27 it is possible to see that A2, N, P lump follows the trend in the experimental values. However, A1 does not as it increases and finally decreases.

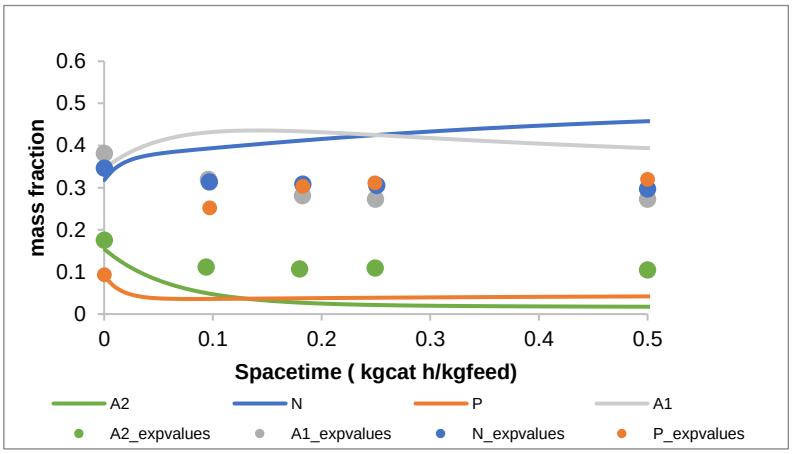

Figure 28 - Comparison of the experimental data with the lumping molecules representative, with the reactions in the vapor phase, at the ratio of 1000 Nm^3/m^3 without a custom term, for 340 ºC, 65 bar.

Figure 28 shows that an increase in temperature leads to the reverse trends between paraffin and naphthene lumps, indicating that instead of increasing, paraffin content decreases and vice versa. This is problematic because hydrotreatment process trends cannot be captured. This may suggest that this lumping method may not be the most appropriate for lumping the compounds in the oil.

4.4.2 Lumping by Pseudo components

To group the compounds into pseudo components, the basic information required to form them must first be obtained. Using the average NBP, molecular weight, and specific gravity, the pseudo components were created. It is also necessary to select the method used to create a pseudo component. Multiple methods are available in *Aspen Plus*®, and a metric was used to determine which one to use. The heat of vaporization was used in this case because it affects the amount of hydrogen used in the reaction model, as previously mentioned. The property method with the most accurate results was chosen by calculating the relative error between the pseudo component heat of vaporization resulting

from the property method and the heat of vaporization of the stream containing the compounds used to create the pseudo components. *Aspen Plus*® method was chosen because it has the lowest error and at the same time is the one recommended by *Aspen Plus*®. Table 25 (pag.87) in the Appendix shows the calculation for each property method.

Figure 29 shows that all the trends can be matched with the experimental trends except for the A1 lump, which increases and decreases, a similar situation has the one reported previously for 300 ºC.

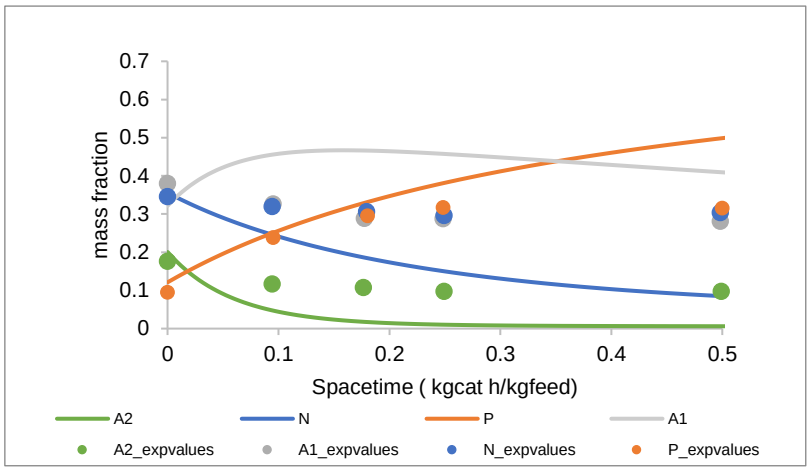

Figure 29 - Comparison of the experimental data with the pseudcomponents, with the reactions in the vapor phase, at the ratio of 1000 Nm^3/m^3 without a custom term, for 300 ºC, 65 bar.

In contrast to the average weight molecular weight lump, at higher temperatures, the same trends can be seen in Figure 30 rather than the previously observed switch in trends.

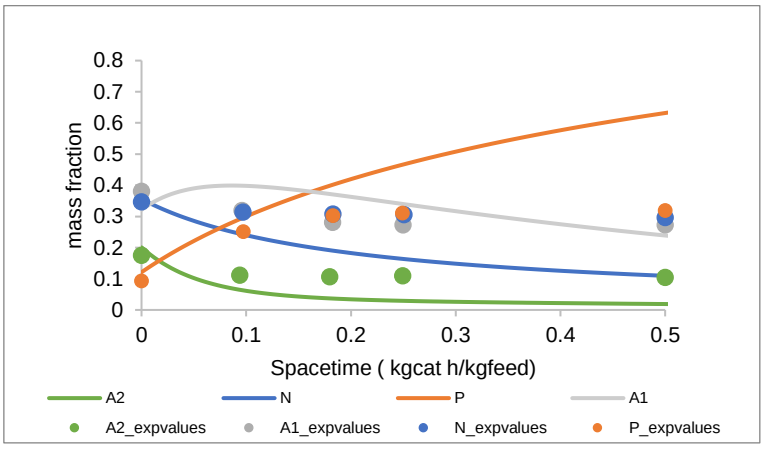

Figure 30 - Comparison of the experimental data with the pseudcomponents, with the reactions in the vapor phase, at the ratio of 1000 Nm^3/m^3 without a custom term, for 340 ºC, 65 bar.

In conclusion, using pseudo components to represent each stream lump yields better, more meaningful results than the average molecular weight lumping methodology.

4.5 Hydrotreatment Flowsheet

After choosing the hydrotreatment kinetic model to be used, and the lumping methodology, the hydrotreatment flowsheet was made.

4.5.1 HT Block

The entry towards the HT block (Figure 31) results from mixing the hydrogen recycle stream (RECYCLE) coming from the amine contactor explained below, the stream coming from the hydrogen purification system (H2), the makeup hydrogen which was assumed to be of the purity of 99.5% mol/mol for hydrogen, with the rest 0.5% being methane. This ratio was maintained by applying a design specification where the (H2F) stream, which was solely hydrogen, was mixed with the (CH4) stream, pure in CH_4, in a ratio to respect the previously mentioned purity. Finally, by adding the previous stream with the fresh feed (OILPYRO), the resulting stream (S5) was sent to a heater (B23).

The ratio 1000 Nm^3/m^3 hydrogen to oil was maintained at the entry of the RPlug block (B14) by a design specification that varies the amount of hydrogen makeup.

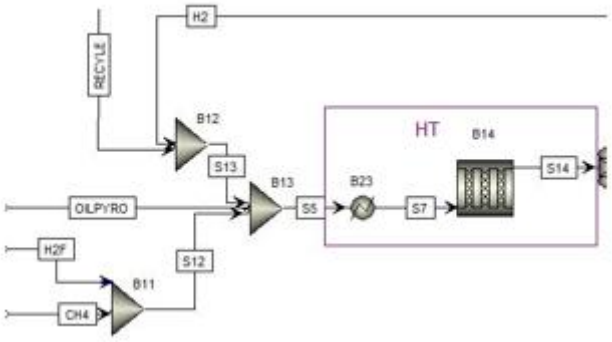

Figure 31 – HT kinetic zone in *Aspen Plus*®.

The reactor's temperature was varied by varying the (B23) heater block and allowing the (B14) block to be constant at the reactor inlet temperature. In this analysis, the reactor temperature was assumed to be constant, which is a limitation introduced in this simulation compared with real-world trickle bed reactors since the hydrotreating reactions happen in adiabatic conditions, using hydrogen to quench the reactor. Also, the hydrogen used was less than what would have been used in reality since no quenching hydrogen quantity was taken into consideration, only the hydrogen needed to maintain a ratio of 1000 Nm^3/m^3 of hydrogen to fresh feed.

4.5.2 HDS reaction zone

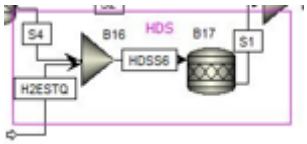

Figure 32 – HDS reaction zone in *Aspen Plus*®.

Since the kinetics for the current sulfur (Benzothiazole) compound were not found in the literature, it was decided to implement a stoichiometry reactor (B17), as seen in Figure 32, with the reaction present in equation (40) with the conversion found for the HDS pathway, 91,7%. (Olmo 2015)

$$Benzothiazole + H_2 \rightarrow Benzene + NH_3 + H_2S \quad (40)$$

A stoichiometric hydrogen stream (H2ESTQ) was mixed with the stream from the HT zone, (S4) in the (B16) block and sent to the stoichiometric reaction (B17). The hydrogen was introduced in a stoichiometric amount to the Benzothiazole compound present. This stoichiometry hydrogen stream was added to reduce the complexity of the design specifications used. Since no economic analysis was done, this added hydrogen would not impact the sensitivity analysis.

4.5.3 NH_4HS formation

In the literature (Piehl 1971), it has been mentioned that NH_4HS forms in the hydrotreatment process as a result of the reaction of NH_3 and H_2S. To model this reaction an RGibbs (B20) reactor was used to determine the quantity of NH3, H2S, and NH4HS produced, since the Olmo 2015 kinetic model does not take that into account and associated conversions for this reaction was not found.

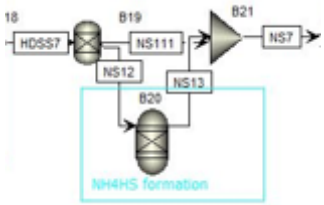

Figure 33 - NH_4HS formation zone in *Aspen Plus*®.

The stream resulting from the HT process and HDS process, HDSSS7, was sent to a separator block (B19), as seen in Figure 33, where all the compounds except NH_3 and H_2S were removed (NS111) and sent through stream (NS12) to the RGibbs reactor (B20). Afterward, the resulting stream (NS13) was mixed in a mixer (B21) with NS111, resulting in NS7.

4.5.4 Hydrotreatment Zone

The hydrotreating reaction was then assumed to take into account all the previously mentioned steps, namely the hydrotreating reaction with the Olmo 2015 model (HT block), the HDS pathway through a conversion step (HDS Block), and the formation of NH_4HS by minimizing Gibbs free energy (NH_4HS formation Block) is represented in Figure 34.

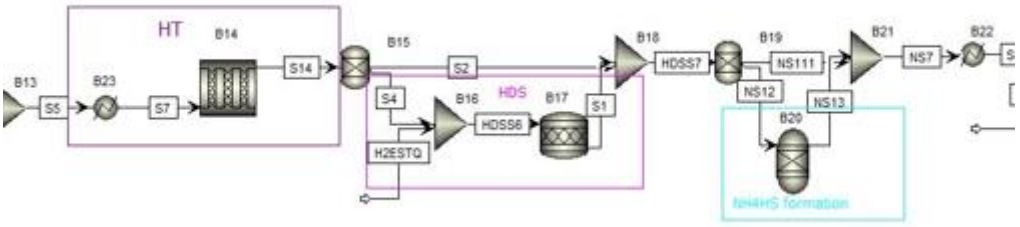

Figure 34 – HT zone in *Aspen Plus*®.

The resulting stream temperature from all these processes (NS17) is set to be the same as in the HT block to have the hydrotreatment zone with a constant temperature.

4.5.5 Wash water & Condenser

Wash water (WASHW) was added to the hydrotreated oil (S3), as seen in Figure 35 since this is the usual procedure in the industry to avoid the accumulation of solids in the pipes due to the presence of NH_4HS and NH_4Cl. Wash water was added in the ratio specified by Piehl 1971, where at least 5 pounds of water per pound of H2S must be added after the hydrotreater. In this simulation, only 5 pounds of water per pound of H2S were added, using a design specification.

Afterwards, the stream was sent to a condenser (B1), whose temperature was chosen based on the average range mentioned by Piehl 1971, namely 52ºC. Due to the limitations of the current methodology, no sensitivity analysis is performed to analyze the condenser temperature after the hydro treatment. As the liquid-vapor equilibrium is not being simulated through the equation of state, it makes no sense to conduct a sensibility analysis to determine the optimal condenser temperature for condensation, as latent and sensible heat that exists in the actual liquid-vapor equilibrium stream is not considered.

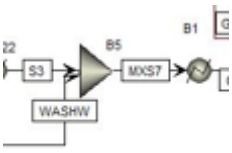

Figure 35 – Wash water and condenser zone in *Aspen Plus*®.

4.5.6 High pressure & Low-Pressure Sequence

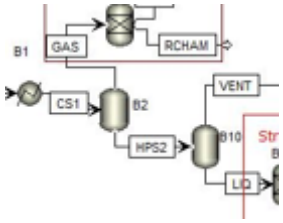

Figure 36 – High-pressure, low-pressure sequence in *Aspen Plus*®.

The condensed stream was then sent to a high-pressure, low-pressure flash sequence. In the high-pressure flash (B2), excess hydrogen was recovered, and light gases were removed in the low-pressure flash (B10). Figure 36 illustrates what has been previously mentioned.

4.5.7 Amine Contactor

The excess hydrogen stream (GAS) then passes through amine absorption columns. (Karre n.d.). This situation was implemented in *Aspen Plus*® through a separator block (B4), as seen in Figure 37, and the associated efficiency of amine absorption, as indicated in the literature for the H_2S, CO_2, and CH_4, namely 98, 87, and 99%. (Huertas, Giraldo, and Izquierdo 2011) A more accurate method would be to use a rate-based amine absorption column; however, convergence issues with this column were encountered, and a more simplistic method was selected.

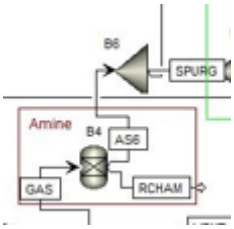

Figure 37 – Amine Contactor in *Aspen Plus*®.

The purified H_2S stream (AS6) leaving the amine contactor, 10 to 15 % of this stream, was sent to a hydrogen purification process. The block (B6) represents a splitter block that separates the entry stream into two according to the mass basis desired. In this case, 15%wt of this stream was sent to the purification process through the stream (SPURG), and the rest was recycled to the HT zone through the (RECYCLE) stream.

4.5.8 Hydrogen Purification process

The stream coming from the amine contactor, previously from entering the purification process, is purged. The splitter block (B8), as seen in Figure 38, was used to simulate this purge, where 20%wt of the stream (SPURG) was purged through stream (PSALST), and the rest (S9) was sent to a separator block (B9). This separator block, similar to the previous amine contactor situation, was used to model the hydrogen purification process. In this case, a hydrogen purification efficiency of 95%wt was used.

(Karre n.d.) This meant that 5 %wt of hydrogen present in the stream (S9) was present in (S11) and the rest in stream (H2).

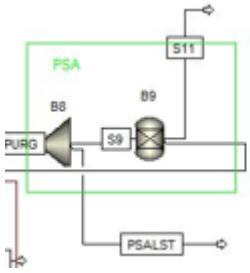

Figure 38 – Hydrogen purification process in *Aspen Plus*®.

The hydrogen stream obtained from the hydrogen purification process and part of the purified H_2S stream leaving the amine contactor were mixed with the makeup hydrogen and sent to the reactor.

4.5.9 Stripper

A Separator block (B7), as seen in Figure 39, was added at the end of the light-pressure separator to obtain a stream with only the lump compounds (aromatic, paraffinic, naphthene and naphthalene) to model Stripper equipment with 100% light gases removal efficiency. Stripper equipment is usual in the fractionation process to remove the light gases present in the fractionated oil and using that as basis, a stripper was implemented to remove the light gases present.

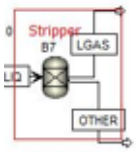

Figure 39 - Stripper process in *Aspen Plus*®.

The Hydrotreatment flowsheet can be seen in Figure 40 and the operating conditions used are available in Table 13.

Table 13 – Conditions of pressure and temperature of the blocks used in *Aspen Plus*®.

Block Type	Block	Temperature (ºC)	Pressure (bar)	Separation (mass basis)
Heater	B23	375	65	na
RPlug	B6	375	65	na
Rstoich	B17	375	65	na
Rgibbs	B20	375	65	na
Heater	B22	375	65	na
Condenser	B1	52	65	na
Flash	B2	52	65	na
Flash	B10	51.0	1	na
Separator	B4	0	0	CO_2,methane,H_2S (87%,99%,98%) to RCHAM
Spliter	B6	na	na	15% of AS6 SPURG
Spliter	B8	na	na	0.2 to PSALT
Separator	B9	na	na	95% H2 mass of s9 to H2stream
Separator	B7	na	na	100% A1,A2,N,P

na = doesn't apply, where A1, A2, N and P where the lumps of one ring, two ring aromatics, naphthene's and paraffins,

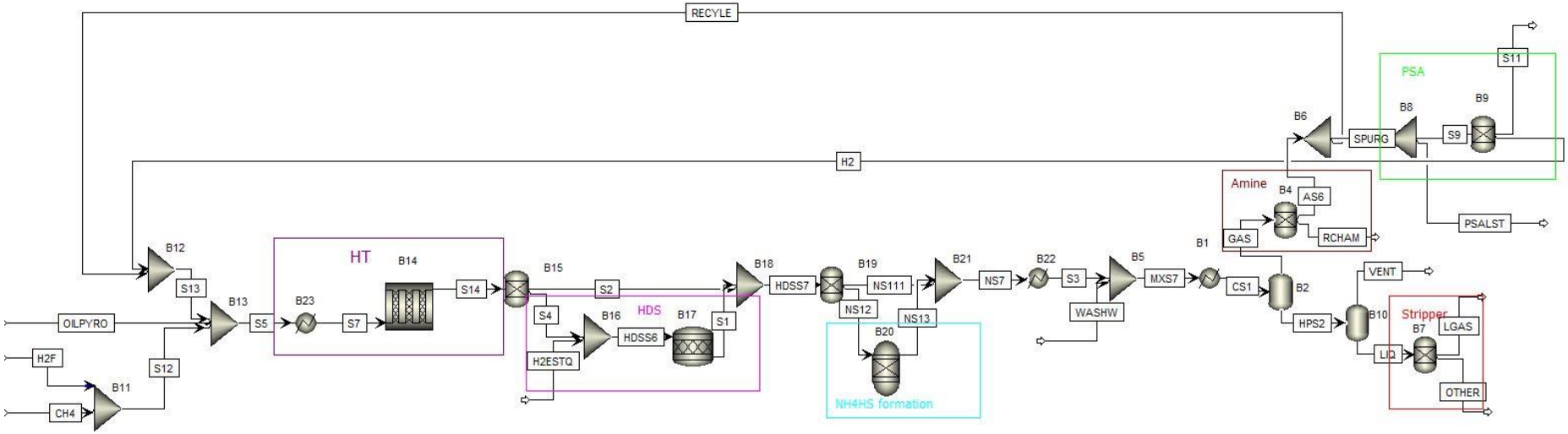

Figure 40 – *Aspen Plus*® hydrotreatment flowsheet schematic.

4.6 Sensitivity Analysis

After making the hydrotreatment flowsheet, some approximations were made regarding the lumping of the pyrolysis oil, namely the fact that compounds with more than two aromatic rings were allocated into the same group as the compounds with two aromatic rings and the fact that olefins were assumed to be hydrogenated and as such, the olefin compounds were allocated to lumps whose saturated product would be part of.

The base conditions for the sensibility study are seen in Table 14.

Table 14 – Reactor conditions, catalyst amount and hydrogen to feed ratio.

Temperature (ºC)	Pressure (bar)	Diameter (m)	Length (m)	Catalyst (kg)	H_2/Feed (Nm^3/m^3)
375	65	1	1	604	1000

The base stream used as feed for the hydrotreatment process matches the pyrolysis oil obtained from the pyrolysis reaction done at 500 ºC, 1 bar and condenser at 30ºC.

The amount of catalyst selected was based on the fact that it corresponds to the maximum amount of catalyst used in the Olmo 2015 experiment for a given amount of space and time (0.5 kgcat/kg feed). In terms of pressure, 65 bar is selected to be able to reproduce the kinetics accurately. The experiment's highest temperature, 375ºC, was used since it was at this temperature that the kinetics best matched the experimental data, as seen in Table 11 (pag.50), and allowed for a more precise prediction of the outcome. The kinetic model with the custom term presented in Section 4.3.4. was the one used to make the sensitivity analysis as previously indicated.

Finally, the sensibility analysis was done by varying the independent variables of the system, and its effect on the jet fuel specification were analyzed. It should be noted that the hydrotreated oil analyzed is the one obtained after the low-pressure separator, assuming a stripper with 100% efficiency in removing light gases.

4.6.1.1 Temperature

Temperature was varied within 300-415 ºC, and the results of the lumps change within the stripped hydrotreated oil with the temperature can be seen in Figure 41. Considering how the lumps change with temperature, it can be concluded that higher temperatures are more detrimental to the hydrotreatment, as the increase in temperature leads to the formation of two-ring aromatics (A2), which should be avoided. It can also be seen that aromatic one-ring (A1) content decreases with temperature, indicating that hydrogenation of this aromatic compounds is indeed occurring, resulting in an increase in naphthene (N) content and, consequently an increase in paraffin (P) content as well.

At temperatures above 380 ºC naphthene (N) and paraffin (P) content decrease, and the two ring aromatic compounds (A2) increase, which indicates that their formation is favored over the rest of the compounds as temperature increases.

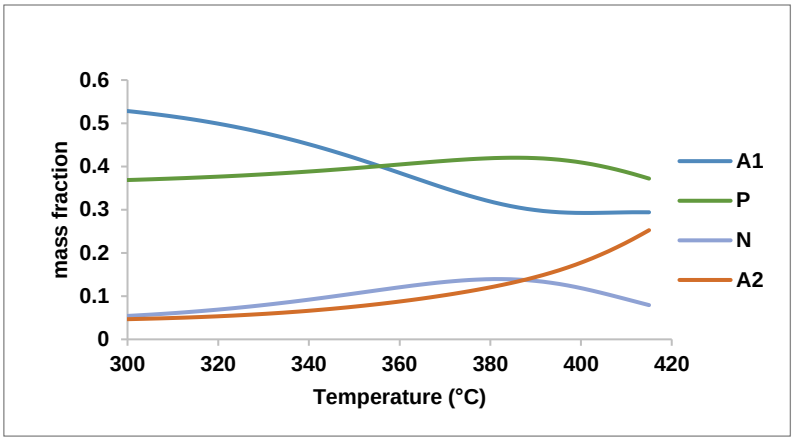

Figure 41 – Lumps mass fraction variation in the stripped hydrotreated oil within a temperature range of 300-415 ºC, using the custom term model.

Analyzing the jet fuel specification resulting from a change in temperature reveals, for instance, that the volume fraction of one-ring aromatic compounds (A1), as seen in Figure 42, is higher than the allowed amount for all the temperature ranges studied.

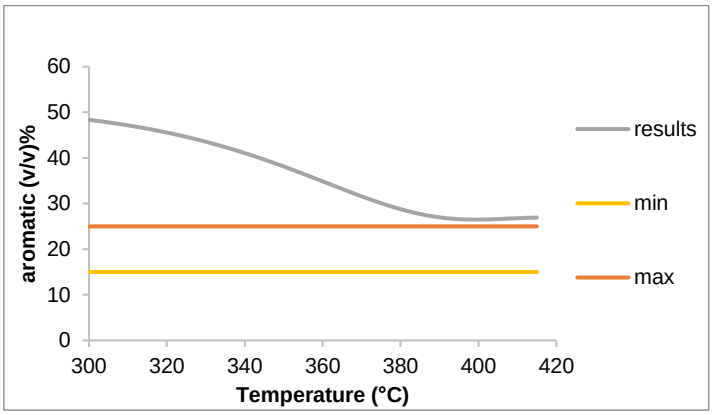

Figure 42 – Volumetric aromatic content (%) of the stripped hydrotreated oil.

This indicates that assuming a stripper with 100% efficiency and only changing the temperature variable, it is not possible to obtain a hydrotreated oil within the desired jet fuel specifications.

4.6.1.2 Pressure

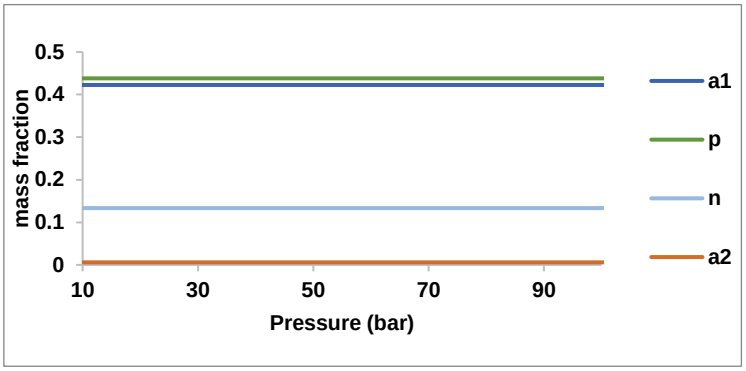

Figure 43 – Lumps mass fraction variation in the stripped hydrotreated oil within a pressure range of 10-100 bar, using the custom term kinetic situation, previously explained.

Since the kinetic model used is in the vapor phase and as no condensation occurs because the reaction is being simulated in an isotherm reactor, pressure has no influence on the product result as can be seen in Figure 43.

4.6.1.3 Catalyst Amount

The catalyst amount was varied between 10-1500 kg, and the results of the lumps change within the stripped hydrotreated oil with the catalyst change can be seen in Figure 44. It can be seen that increasing the catalyst amount leads to an increase in the paraffin content and naphthene content while decreasing the aromatic compounds.

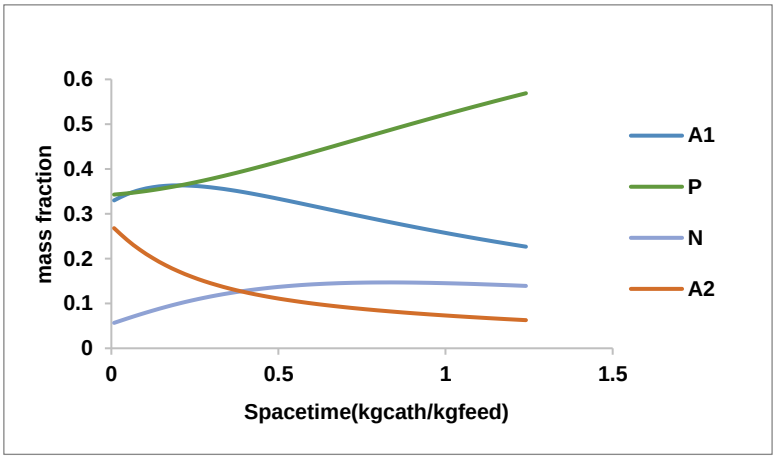

Figure 44 - Lumps mass fraction variation in the stripped hydrotreated oil within a catalyst range of 10-1500kg, using the custom termo model.

It can also be observed that altering the catalyst content while keeping all the base case scenario variables constant makes it difficult to meet all the jet fuel criteria, as seen by the volumetric content of two-ring aromatics in Figure 45, which is above the maximum allowable content in the jet fuel.

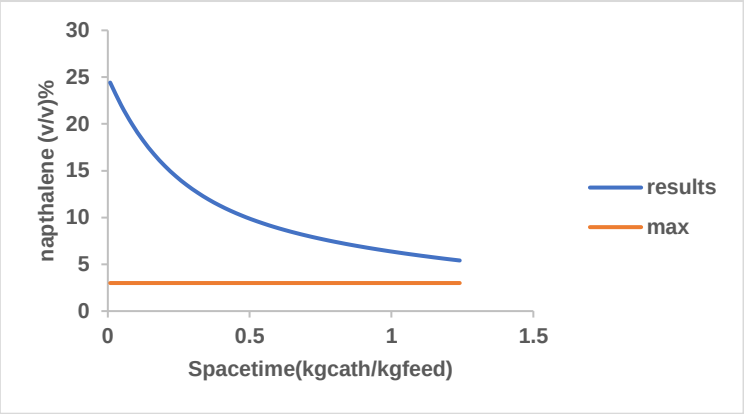

Figure 45 - Volumetric naphthalene content (%) of the stripped hydrotreated oil.

4.6.2 Best conditions

In order to find the best combination of temperature and catalyst amount to meet jet fuel criteria, a sensitivity analysis was conducted in which these two variables were varied. The temperature was varied between 300-415 ºC, and the catalyst amount was varied within the LSHV range, 0.5-3 hr^{-1}, assuming a catalyst density of 1500 kg/m^3. The temperature and LSHV range used were the ones mentioned in the literature review (pag.18) for the Ultra-low-sulfur diesel hydrotreatment process.

Table 15 – Values for the stripped hydrotreated oil matching the jet fuel specification for the aromatic volume, natpahelen volume, net heating value and flashpoint.

Catalyst (kg)	Temperature (ºC)	Density 15, kg/m^3	Viscosity -20 ºC cP	NHV (MJ/kg)	Flashpoint (ºC)	Naphthalene v/v%	Aromatic v/v%
1879	350.4	738.2	1.84	43.1	38.1	2.74	24.1
1879	350.8	738.0	1.84	43.1	38.3	2.76	23.9
1879	351.2	737.8	1.84	43.1	38.5	2.78	23.7
1879	351.5	737.6	1.84	43.1	38.7	2.80	23.5

The data were initially filtered by locating rows with a volumetric aromatic content between 15% and 25%, followed by rows with a naphthalene volume percentage below 3% and a flashpoint above 38 ºC. Finally, as density and viscosity minimum values could not be met, the top 4 values with the highest values were chosen to illustrate the properties of the stripped hydrotreated oil, present in Table 15.

It is possible to conclude that it is possible to obtain a near ready jet fuel through the hydrotreatment of pyrolysis oil and using a stripper with 100% efficiency. However, this stripped hydrotreated oil still needs to be tested for other jet fuel requirements which were not covered, such as freezing point. Regarding the viscosity and density values below the jet fuel requirements, a possible solution to increase their value is to add additives. However, if this addition does not lead to obtain a matching jet fuel oil, then distilling the oil and hydrocracking it might be an alternative as it would lead to decrease the aromatic and naphthalene content, and to an increase density and density.

The methodology employed to reach these values has multiple limitation and as a result, future work should done to guarantee the validity of the results presented.

The implementation of the kinetic model using a trickle bed reactor instead of a one plug flow reactor, to model the hydrotreatment process is a starting step. Either by implementing the kinetic model in the aspen modeler or implementing it in another software. Also, future work should go to obtain better thermodynamic parameters for the liquid-vapor equilibrium of the oil and the hydrogen compound as in *Aspen Plus*® this situation could not be well modeled. As a result, the liquid-vapor equilibrium present in the industry could be simulated and the kinetic model more realistically made.

There's also a need to consider the reactor in the adiabatic conditions instead of isothermal to verify the present conclusions.

5 Conclusion

The purpose of this study was to model the pyrolysis of waste tires and the hydrotreatment process of the pyrolysis oil to evaluate their potential for jet fuel applications. Chapter 1 introduced the waste tire problem. The potential application of waste tire as well as the jet fuel problem and the potential of using waste tire oil for jet fuel applications.

Chapter 2 discussed tire characterization, structural differences, jet fuel types, the main specifications required, the pyrolysis process, conditions, products, and the hydrotreatment process. Through a review of the literature, it was to find which different approaches are being taken to simulate the pyrolysis and hydrotreatment process in *Aspen Plus*® and how just one operating condition does not define the end product produced by the pyrolysis process.

Chapter 3 showed how the modeling of waste tires has been done in the literature and the simulations made in this thesis. It was found that the current thesis implementation of the Ismail 116 reaction kinetic model differs significantly from his stated results. This might occur due to the number of parameters to be introduced being many, and as a result, some might have been wrongly introduced in this work or in the article studied. This premise comes from the difference between the calculated average relative error reported in the literature for the Laresgoiti et al. 2004 values and the ones calculated in this thesis, which show a major discrepancy with what has been reported. Instead of a 20% average relative error, it was found that the true average relative error was of 89%. So, the literature might have some wrong parameters as seen by the faulty values given in some situations.

A parameter estimation was performed using the *gPROMS ModelBuilder* to improve the model used. It was discovered that the kinetic model with the fewest reactions (38 reactions) produced the best results. This could be because a low number of parameters to optimize helped in tuning the model more broadly, whereas a higher number of reactions resulted in a more tailored model to specific cases. Furthermore, because only the pre-exponential factors were changed, this may have affected the improvement overall that could have been achieved. Another reason could have been due to the use of data from two different types of reactors to obtain the parameters themselves. Furthermore, because the experimental data was obtained in a discontinuous situation, the kinetic parameter estimation was performed using a continuous model rather than a discontinuous one, which may have hampered a better outcome.

Chapter 4 showed the modelling of the hydrotreatment process. The model used to simulate the hydrotreatment process was based on the Olmo 2015 kinetic model, namely the HDA pathway. It was seen through the experimental reproduction that using the H_2 to oil ratios provided by the literature, the simulator could not model the vapor liquid equilibrium as it happens in reality, with the stream vaporizing. As a result, multiple studies were done to try to model this process. It was understood that it was needed to add a custom term that could take into account the solubility of hydrogen in the pyrolysis oil as well as correct the fraction of each lump in the vapor phase. Even though the stream used to reproduce the experimental data differed from the one used to obtain the experimental data, it was still possible to model the experimental data with a 20% average relative error. It should also be noted that in this thesis, the ideal plug flow reactor model was used instead of a trickle bed reactor since the latter model is not available in *Aspen Plus*®. This also possibly leads to a higher relative error.

Through the sensitivity analysis, it was possible to understand the importance of the temperature and catalyst amount. The increase in temperature leads to the formation of naphthalene content which is undesired. However, the increase in catalyst diminishes this increase, which means that a combination of both variables would allow to reach the desired jet fuel specifications. This situation was indeed found, by varying the temperature and catalyst variables at the same time and in that situation the jet fuel requirements were met by the stripped hydrotreated oil.

The conditions which produced a stripped hydrotreated oil which satisfied most of the jet fuel A requirements were, catalyst amount of 1879 kg and temperature of 350.4 ºC. This oil has a flashpoint of 38.1 ºC, net heating value of 43.1 Mj/kg, naphthalene volume of 2.74%, aromatic volume of 24.1%. The previously mentioned properties match the jet fuel requirements. However, viscosity and density were both below the minimum threshold, with 1.84 cP and 738.2 kg/m^3 respectively.

Future research should focus on utilizing additional datasets for parameter estimation. Implementing the current Olmo 2015 kinetic model with a trickle bed model reactor as opposed to a one plug flow reactor model, using either *Aspen Plus Custom Modeler*® or *gPROMS*® software and under adiabatic conditions. Validate the equation of state used for liquid-vapor equilibrium for the oil and hydrogen mixture. Conduct an economic analysis to determine the pyrolysis oil's economic potential for jet fuel replication.

References

Abbas-Abadi, Mehrdad Seifali, Marvin Kusenberg, Hamed Mohamadzadeh Shirazi, Bahman Goshayeshi, and Kevin M. Van Geem. 2022. “Towards Full Recyclability of End-of-Life Tires: Challenges and Opportunities.” *Journal of Cleaner Production* 374 (November): 134036. https://doi.org/10.1016/j.jclepro.2022.134036.

Adeniyi, Adewale George, and Joshua O Ighalo. 2020. “COMPUTER-AIDED MODELLING OF THE PYROLYSIS OF RUBBER SAW,” 4.

Akbas, Ahmed, and Nor Yuliana Yuhana. 2021. “Recycling of Rubber Wastes as Fuel and Its Additives.” *Recycling* 6 (4): 78. https://doi.org/10.3390/recycling6040078.

Alaei Kadijani, Javad, and Elhameh Narimani. 2016. “Simulation of Hydrodesulfurization Unit for Natural Gas Condensate with High Sulfur Content.” *Applied Petrochemical Research* 6 (1): 25–34. https://doi.org/10.1007/s13203-015-0107-0.

Alsaleh, Ali, and Melanie L. Sattler. 2014. “Waste Tire Pyrolysis: Influential Parameters and Product Properties.” *Current Sustainable/Renewable Energy Reports* 1 (4): 129–35. https://doi.org/10.1007/s40518-014-0019-0.

Alsheyab, Mohammad A.T., Daniel Schingnitz, Ali F. Al-Shawabkeh, and Sigrid Kusch. 2013. “Analysis of the Potential Use of Major Refuse-Derived Fuels in Jordan as Supplementary Fuel.” *Journal of the Air & Waste Management Association* 63 (8): 902–8. https://doi.org/10.1080/10962247.2013.776998.

Altayeb, Ryan K. 2015. “LIQUID FUEL PRODUCTION FROM PYROLYSIS OF WASTE TIRES: PROCESS SIMULATION, EXERGETIC ANALYSIS, AND LIFE CYCLE ASSESSMENT,” June, 96.

Antoniou, N., and A. Zabaniotou. 2013. “Features of an Efficient and Environmentally Attractive Used Tyres Pyrolysis with Energy and Material Recovery.” *Renewable and Sustainable Energy Reviews* 20 (April): 539–58. https://doi.org/10.1016/j.rser.2012.12.005.

Anuar Sharuddin, Shafferina Dayana, Faisal Abnisa, Wan Mohd Ashri Wan Daud, and Mohamed Kheireddine Aroua. 2016. “A Review on Pyrolysis of Plastic Wastes.” *Energy Conversion and Management* 115 (May): 308–26. https://doi.org/10.1016/j.enconman.2016.02.037.

Arabiourrutia, Miriam, Gartzen Lopez, Maite Artetxe, Jon Alvarez, Javier Bilbao, and Martin Olazar. 2020. “Waste Tyre Valorization by Catalytic Pyrolysis – A Review.” *Renewable and Sustainable Energy Reviews* 129 (September): 109932. https://doi.org/10.1016/j.rser.2020.109932.

Ariri, Ahmad, Sagir Alva, and Siti Aishah Hasbullah. 2020. “TIRE WASTE AS A POTENTIAL MATERIAL FOR CARBON ELECTRODE FABRICATION: A REVIEW.” *SINERGI* 25 (1): 1. https://doi.org/10.22441/sinergi.2021.1.001.

Aydın, Hüseyin, and Cumali İlkılıç. 2012. “Optimization of Fuel Production from Waste Vehicle Tires by Pyrolysis and Resembling to Diesel Fuel by Various Desulfurization Methods.” *Fuel*, Special Section: ACS Clean Coal, 102 (December): 605–12. https://doi.org/10.1016/j.fuel.2012.06.067.

Balaban, Eren, Ales Smejda, and Mehmet Inanç Onur. 2022. “Influence of Tire Crumbs on Mechanical Properties of Sand-Fine Soil Mixtures.” *Geomechanics and Geoengineering* 17 (1): 64–79. https://doi.org/10.1080/17486025.2019.1688870.

Bandyopadhyay, Rajarshi, and Sreedevi Upadhyayula. 2018. “Thermodynamic Analysis of Diesel Hydrotreating Reactions.” *Fuel* 214 (February): 314–21. https://doi.org/10.1016/j.fuel.2017.10.015.

Bi, Rongshan, Yan Zhang, Xiao Jiang, Haixing Yang, Kejia Yan, Min Han, Wenhua Li, et al. 2022. “Simulation and Techno-Economical Analysis on the Pyrolysis Process of Waste Tire.” *Energy* 260 (December): 125039. https://doi.org/10.1016/j.energy.2022.125039.

Blakey, Simon, Lucas Rye, and Christopher Willam Wilson. 2011. “Aviation Gas Turbine Alternative Fuels: A Review.” *Proceedings of the Combustion Institute* 33 (2): 2863–85. https://doi.org/10.1016/j.proci.2010.09.011.

Boesen, Rasmus Risum. 2011. *Investigation and Modelling of Diesel Hydrotreating Reactions*. Kgs. Lyngby, Denmark: Technical University of Denmark.

Bowles, A. J., and G. D. Fowler. 2022. “Assessing the Impacts of Feedstock and Process Control on Pyrolysis Outputs for Tyre Recycling.” *Resources, Conservation and Recycling* 182 (July): 106277. https://doi.org/10.1016/j.resconrec.2022.106277.

Campuzano, Felipe, Robert C. Brown, and Juan Daniel Martínez. 2019. “Auger Reactors for Pyrolysis of Biomass and Wastes.” *Renewable and Sustainable Energy Reviews* 102 (March): 372–409. https://doi.org/10.1016/j.rser.2018.12.014.

Cavalcanti, Cláudia J. S., Mauro A. S. S. Ravagnani, Luiz Stragevitch, Florival R. Carvalho, and Maria Fernanda Pimentel. 2022. “Simulation of the Soybean Oil Hydrotreating Process for Green Diesel Production.” *Cleaner Chemical Engineering* 1 (March): 100004. https://doi.org/10.1016/j.clce.2022.100004.

Cheng, Feng, and Catherine E. Brewer. 2017. “Producing Jet Fuel from Biomass Lignin: Potential Pathways to Alkyl-Benzenes and Cycloalkanes.” *Renewable and Sustainable Energy Reviews* 72 (May): 673–722. https://doi.org/10.1016/j.rser.2017.01.030.

Choi, Gyung-Goo, Su-Hwa Jung, Seung-Jin Oh, and Joo-Sik Kim. 2014. “Total Utilization of Waste Tire Rubber through Pyrolysis to Obtain Oils and CO2 Activation of Pyrolysis Char.” *Fuel Processing Technology* 123 (July): 57–64. https://doi.org/10.1016/j.fuproc.2014.02.007.

Cooper, C. David, Brian Kim, and John MacDonald. 1999. “Estimating the Lower Heating Values of Hazardous and Solid Wastes.” *Journal of the Air & Waste Management Association* 49 (4): 471–76. https://doi.org/10.1080/10473289.1999.10463816.

Costa, Sebastião M. R., David Fowler, Germano A. Carreira, Inês Portugal, and Carlos M. Silva. 2022. “Production and Upgrading of Recovered Carbon Black from the Pyrolysis of End-of-Life Tires.” *Materials* 15 (6): 2030. https://doi.org/10.3390/ma15062030.

D02 Committee. n.d. “Specification for Aviation Turbine Fuels.” ASTM International. Accessed August 27, 2022. https://doi.org/10.1520/D1655-20D.

Diebold, J. P., T. A. Milne, S. Czernik, A. Oasmaa, A. V. Bridgwater, A. Cuevas, S. Gust, D. Huffman, and J. Piskorz. 1997. “Proposed Specifications for Various Grades of Pyrolysis Oils.” In *Developments in Thermochemical Biomass Conversion: Volume 1 / Volume 2*, edited by A. V. Bridgwater and D. G. B. Boocock, 433–47. Dordrecht: Springer Netherlands. https://doi.org/10.1007/978-94-009-1559-6_34.

Elysium Press, Elysium. 2020. “Elysium » New Value from End-of-Life Tires.” November 30, 2020. https://elysiumnordic.com/news/6?locale=en.

ERJ. 2022. “Pyrolysis Hellas to Build Tire Recycling Plant in Greece | European Rubber Journal.” February 15, 2022. https://www.european-rubber-journal.com/article/2090949/pyrolysis-hellas-to-build-tire-recycling-plant-in-greece.

Eskandarinia, Milad, Mina Esmailzade, and Farhad Aslani. n.d. “Splitting Tensile Strength of Recycled Tire Steel Fiber-Reinforced Alkali-Activated Slag Concrete Designed by Taguchi Method.” *Structural Concrete* n/a (n/a). Accessed October 15, 2022. https://doi.org/10.1002/suco.202200306.

Fredenslund, Aage, Russell L. Jones, and John M. Prausnitz. 1975. “Group-Contribution Estimation of Activity Coefficients in Nonideal Liquid Mixtures.” *AIChE Journal* 21 (6): 1086–99. https://doi.org/10.1002/aic.690210607.

Goh, Brandon Han Hoe, Cheng Tung Chong, Hwai Chyuan Ong, Tine Seljak, Tomaž Katrašnik, Viktor Józsa, Jo-Han Ng, Bo Tian, Srinibas Karmarkar, and Veeramuthu Ashokkumar. 2022. “Recent Advancements in Catalytic Conversion Pathways for Synthetic Jet Fuel Produced from Bioresources.” *Energy Conversion and Management* 251 (January): 114974. https://doi.org/10.1016/j.enconman.2021.114974.

Goodchild, Stephen. 2022. “24/7 Operations Imminent at Carlton Forest Pyrolysis Plant.” Tyrepress. June 24, 2022. https://www.tyrepress.com/2022/06/24-7-operations-imminent-at-carlton-forest-pyrolysis-plant/.

Gupta, Goutam Kishore, and Monoj Kumar Mondal. 2022. “Chapter 14 - Pyrolysis: An Alternative Approach for Utilization of Biomass into Bioenergy Generation.” In *Biofuels and Bioenergy*, edited by Baskar Gurunathan, Renganathan Sahadevan, and Zainul Akmar Zakaria, 279–300. Elsevier. https://doi.org/10.1016/B978-0-323-85269-2.00024-1.

Gutiérrez-Antonio, Claudia, Araceli Guadalupe Romero-Izquierdo, Fernando Israel Gómez-Castro, Salvador Hernández, and A. Briones-Ramírez. 2016. “Simultaneous Energy Integration and Intensification of the Hydrotreating Process to Produce Biojet Fuel from Jatropha Curcas.” *Chemical Engineering and Processing: Process Intensification* 110 (December): 134–45. https://doi.org/10.1016/j.cep.2016.10.007.

Han, Yinglei, Filip Stankovikj, and Manuel Garcia-Perez. 2017. “Co-Hydrotreatment of Tire Pyrolysis Oil and Vegetable Oil for the Production of Transportation Fuels.” *Fuel Processing Technology* 159 (May): 328–39. https://doi.org/10.1016/j.fuproc.2017.01.048.

Hemighaus, Greg, Tracy Boval, John Bacha, Fred Barnes, Matt Franklin, Lew Gibbs, Nancy Hogue, et al. 2004. “Aviation Fuels - Chevron Corporation.”

Hita, Idoia, Andrés T. Aguayo, Martin Olazar, Miren J. Azkoiti, Javier Bilbao, José M. Arandes, and Pedro Castaño. 2015. “Kinetic Modeling of the Hydrotreating and Hydrocracking Stages for Upgrading Scrap Tires Pyrolysis Oil (STPO) toward High-Quality Fuels.” *Energy & Fuels* 29 (11): 7542–53. https://doi.org/10.1021/acs.energyfuels.5b01502.

Hoang, Anh Tuan, Tuan Hai Nguyen, and Hoang Phuong Nguyen. 2020. “Scrap Tire Pyrolysis as a Potential Strategy for Waste Management Pathway: A Review.” *Energy Sources, Part A:*

Recovery, Utilization, and Environmental Effects 0 (0): 1–18. https://doi.org/10.1080/15567036.2020.1745336.

Hossain, Muhammad Nobi, Myung Kyu Choi, and Hang Seok Choi. 2021. “A Review of the Desulfurization Processes Used for Waste Tire Pyrolysis Oil.” *Catalysts* 11 (7): 801. https://doi.org/10.3390/catal11070801.

Huertas, J.I., N. Giraldo, and S. Izquierdo. 2011. “Removal of H2S and CO2 from Biogas by Amine Absorption.” In *Mass Transfer in Chemical Engineering Processes*, edited by Jozef Marko. InTech. https://doi.org/10.5772/20039.

Hui, Xin, Weitao Liu, Xin Xue, and Chih-Jen Sung. 2021. “Sooting Characteristics of Hydrocarbon Compounds and Their Blends Relevant to Aviation Fuel Applications.” *Fuel* 287 (March): 119522. https://doi.org/10.1016/j.fuel.2020.119522.

iJET, and Sumaiya ijet. 2021. “The Different Types of Aviation Fuel – Jet Fuel & AVGAS.” *IJET* (blog). January 5, 2021. https://ijet.aero/ijet-blog/different-types-aviation-fuel-jet-fuel.

Ismail, Hamza Y., Ali Abbas, Fouad Azizi, and Joseph Zeaiter. 2017. “Pyrolysis of Waste Tires: A Modeling and Parameter Estimation Study Using Aspen Plus®.” *Waste Management* 60 (February): 482–93. https://doi.org/10.1016/j.wasman.2016.10.024.

Jadav, Kishan, Sivakumar Pandian, Anirbid Sircar, and Deepalakshmi Subramanian. 2022. “Investigation of Nano Catalyst to Enhance Fuel Quality in Waste Tyre Pyrolysis.” *Energy Sources, Part A: Recovery, Utilization, and Environmental Effects* 44 (1): 1468–77. https://doi.org/10.1080/15567036.2019.1645245.

Jansen, Arnold Alexander, Izak Jacobus van der Walt, and Philippus Lodewyk Crouse. 2022. “Waste-Tyre Pyrolysis and Gasification via the Reverse Boudouard Reaction: Derivation of Empirical Kinetics from TGA Data.” *Thermochimica Acta* 708 (February): 179104. https://doi.org/10.1016/j.tca.2021.179104.

Januszewicz, Katarzyna, Paweł Kazimierski, Wojciech Kosakowski, and Witold M. Lewandowski. 2020. “Waste Tyres Pyrolysis for Obtaining Limonene.” *Materials* 13 (6): 1359. https://doi.org/10.3390/ma13061359.

Kabir, Mohammed, Ashfaque Chowdhury, and Mohammad Rasul. 2015. “Pyrolysis of Municipal Green Waste: A Modelling, Simulation and Experimental Analysis.” *Energies* 8 (8): 7522–41. https://doi.org/10.3390/en8087522.

Kang, Dongil, Doohyun Kim, Vickey Kalaskar, Angela Violi, and André L. Boehman. 2019. “Experimental Characterization of Jet Fuels under Engine Relevant Conditions – Part 1: Effect of Chemical Composition on Autoignition of Conventional and Alternative Jet Fuels.” *Fuel* 239 (March): 1388–1404. https://doi.org/10.1016/j.fuel.2018.10.005.

Kapadia, Zarashpe Z., Dominick V. Spracklen, Steve R. Arnold, Duncan J. Borman, Graham W. Mann, Kirsty J. Pringle, Sarah A. Monks, et al. 2016. “Impacts of Aviation Fuel Sulfur Content on Climate and Human Health.” *Atmospheric Chemistry and Physics* 16 (16): 10521–41. https://doi.org/10.5194/acp-16-10521-2016.

Kar, Y. 2011. “Catalytic Pyrolysis of Car Tire Waste Using Expanded Perlite.” *Waste Management* 31 (8): 1772–82. https://doi.org/10.1016/j.wasman.2011.04.005.

Karonis, D., E. Lois, S. Stournas, and F. Zannikos. 1998. “Correlations of Exhaust Emissions from a Diesel Engine with Diesel Fuel Properties.” *Energy & Fuels* 12 (2): 230–38. https://doi.org/10.1021/ef9700588.

Karre, Avinashkumar. n.d. “Basics of Hydrotreating Units.” Worldofchemicals.Com. Accessed September 13, 2022. https://www.worldofchemicals.com/media/basics-of-hydrotreating-units/4340.html.

Klean. n.d. “Leading European Tyre Pyrolysis Recycling Technology | Klean Industries.” Accessed October 6, 2022. https://kleanindustries.com/waste-processing-projects/tire-pyrolysis-recycling/crr-germany-poland/.

Kushwaha, Nidhi, Debarun Banerjee, Khwaja Alamgir Ahmad, Nagaraj P. Shetti, Tejraj M. Aminabhavi, Kamal K. Pant, and Ejaz Ahmad. 2022. “Catalytic Production and Application of Bio-Renewable Butyl Butyrate as Jet Fuel Blend- A Review.” *Journal of Environmental Management* 310 (May): 114772. https://doi.org/10.1016/j.jenvman.2022.114772.

Laresgoiti, M.F, B.M Caballero, I de Marco, A Torres, M.A Cabrero, and M.J Chomón. 2004. “Characterization of the Liquid Products Obtained in Tyre Pyrolysis.” *Journal of Analytical and Applied Pyrolysis* 71 (2): 917–34. https://doi.org/10.1016/j.jaap.2003.12.003.

Larsen, M, L Schultz, P Glarborg, L Skaarupjensen, K Damjohansen, F Frandsen, and U Henriksen. 2006. “Devolatilization Characteristics of Large Particles of Tyre Rubber under Combustion Conditions.” *Fuel* 85 (10–11): 1335–45. https://doi.org/10.1016/j.fuel.2005.12.014.

Latchem, Robin. 2020. “UK Port to Host Innovative Tyre Recycling Plant • Recycling International.” Recycling International. August 21, 2020. https://recyclinginternational.com/rubber/uk-port-to-host-innovative-tyre-recycling-plant/31336/.

Lewandowski, Witold M., Katarzyna Januszewicz, and Wojciech Kosakowski. 2019. “Efficiency and Proportions of Waste Tyre Pyrolysis Products Depending on the Reactor Type—A Review.” *Journal of Analytical and Applied Pyrolysis* 140 (June): 25–53. https://doi.org/10.1016/j.jaap.2019.03.018.

Liu, Xiao-Jie, Feng Wang, Lu-Lu Zhai, Yu-Ping Xu, Long-Fei Xie, and Pei-Gao Duan. 2019. “Hydrotreating a Waste Engine Oil and Scrap Tire Oil Blend for Production of Liquid Fuel.” *Fuel* 249 (August): 418–26. https://doi.org/10.1016/j.fuel.2019.03.129.

Lødeng, Rune, Lenka Hannevold, Håkon Bergem, and Michael Stöcker. 2013. “Chapter 11 - Catalytic Hydrotreatment of Bio-Oils for High-Quality Fuel Production.” In *The Role of Catalysis for the Sustainable Production of Bio-Fuels and Bio-Chemicals*, edited by Kostas S. Triantafyllidis, Angelos A. Lappas, and Michael Stöcker, 351–96. Amsterdam: Elsevier. https://doi.org/10.1016/B978-0-444-56330-9.00011-5.

Lombardi, Lidia, Ennio Carnevale, and Andrea Corti. 2015. “A Review of Technologies and Performances of Thermal Treatment Systems for Energy Recovery from Waste.” *Waste Management* 37 (March): 26–44. https://doi.org/10.1016/j.wasman.2014.11.010.

López, Gartzen, Martin Olazar, Roberto Aguado, and Javier Bilbao. 2010. “Continuous Pyrolysis of Waste Tyres in a Conical Spouted Bed Reactor.” *Fuel* 89 (8): 1946–52. https://doi.org/10.1016/j.fuel.2010.03.029.

Marco Rodriguez, Isabel de, M. F Laresgoiti, M. A Cabrero, A Torres, M. J Chomón, and B Caballero. 2001. “Pyrolysis of Scrap Tyres.” *Fuel Processing Technology* 72 (1): 9–22. https://doi.org/10.1016/S0378-3820(01)00174-6.

Martín, María Teresa, Juan Luis Aguirre, Juan Baena-González, Sergio González, Roberto Pérez-Aparicio, and Leticia Saiz-Rodríguez. 2022. “Influence of Specific Power on the Solid and Liquid Products Obtained in the Microwave-Assisted Pyrolysis of End-of-Life Tires.” *Energies* 15 (6): 2128. https://doi.org/10.3390/en15062128.

Martínez, Isidoro. n.d. “Isidoro Martínez. Problems on Thermodynamics.” Accessed October 14, 2022. http://webserver.dmt.upm.es/~isidoro/pr4/index.htm.

Martínez, Juan Daniel. 2021. “An Overview of the End-of-Life Tires Status in Some Latin American Countries: Proposing Pyrolysis for a Circular Economy.” *Renewable and Sustainable Energy Reviews* 144 (July): 111032. https://doi.org/10.1016/j.rser.2021.111032.

Martínez, Juan Daniel, Neus Puy, Ramón Murillo, Tomás García, María Victoria Navarro, and Ana Maria Mastral. 2013. “Waste Tyre Pyrolysis – A Review.” *Renewable and Sustainable Energy Reviews* 23 (July): 179–213. https://doi.org/10.1016/j.rser.2013.02.038.

Mavukwana, Athi-enkosi, and Celestin Sempuga. 2022. “Recent Developments in Waste Tyre Pyrolysis and Gasification Processes.” *Chemical Engineering Communications* 209 (4): 485–511. https://doi.org/10.1080/00986445.2020.1864624.

Mederos-Nieto, Fabián S., Ignacio Elizalde-Martínez, Raúl Hernández-Altamirano, Fernando Trejo-Zárraga, Violeta Y. Mena-Cervantes, Edgar Ramírez-Jiménez, and Daniela E. Vallarta-Cardona. 2019. “Hydrotreating Model Comparison of Raw Castor Oil and Its Methyl Esters for Biofuel Production.” *Chemical Engineering & Technology* 42 (1): 167–73. https://doi.org/10.1002/ceat.201700619.

Mulaudzi, Lusani. 2017. “Process Modelling and Economic Evaluation of Waste Tyres to Limonene via Pyrolysis.” Thesis, Stellenbosch : Stellenbosch University. https://scholar.sun.ac.za:443/handle/10019.1/102990.

Nkosi, N., E. Muzenda, J. Gorimbo, and M. Belaid. 2021. “Developments in Waste Tyre Thermochemical Conversion Processes: Gasification, Pyrolysis and Liquefaction.” *RSC Advances* 11 (20): 11844–71. https://doi.org/10.1039/D0RA08966D.

Obando, Gabriel Andrés. 2016. “Condiciones de diseño de un Reactor de Pirolisis a escala de laboratorio para la obtención de biocarbón a partir de residuos orgánicos sólidos (ROS),” June. https://ridum.umanizales.edu.co/xmlui/handle/20.500.12746/2590.

Okoro, E.E., S.E. Sanni, M.E. Emetere, and D.O. Orodu. 2019. “Process Scheme for the Production of Liquid Fuel from Used Tires via Fast Pyrolysis.” *Procedia Manufacturing* 35: 847–53. https://doi.org/10.1016/j.promfg.2019.06.031.

Olazar, Martin, Gartzen Lopez, Miriam Arabiourrutia, Gorka Elordi, Roberto Aguado, and Javier Bilbao. 2008. “Kinetic Modelling of Tyre Pyrolysis in a Conical Spouted Bed Reactor.” *Journal of Analytical and Applied Pyrolysis* 81 (1): 127–32. https://doi.org/10.1016/j.jaap.2007.09.011.

Oliveira, Luís P. de, Damien Hudebine, Denis Guillaume, and Jan J. Verstraete. 2016. “A Review of Kinetic Modeling Methodologies for Complex Processes.” *Oil & Gas Science and Technology – Revue d’IFP Energies Nouvelles* 71 (3): 45. https://doi.org/10.2516/ogst/2016011.

Olmo, Idoia. 2015. “VALORIZATION OF SCRAP TIRES PYROLYSIS OIL (STPO) THROUGH A 2-STAGE HYDROTREATING-HYDROCRACKING STRATEGY. PROCESS VARIABLES AND KINETIC MODELING.,” March.

Ortega, Emmanuel. 2021. “An Overview of Hydrotreating | AIChE.” 2021. https://www.aiche.org/resources/publications/cep/2021/october/overview-hydrotreating.

Oßwald, Patrick, Julia Zinsmeister, Trupti Kathrotia, Maíra Alves-Fortunato, Victor Burger, Rina van der Westhuizen, Carl Viljoen, et al. 2021. “Combustion Kinetics of Alternative Jet Fuels, Part-I: Experimental Flow Reactor Study.” *Fuel* 302 (October): 120735. https://doi.org/10.1016/j.fuel.2021.120735.

Parthasarathy, Prakash, Hang Seok Choi, Hoon Chae Park, Jae Gyu Hwang, Ho Seong Yoo, Byeong-Kyu Lee, and Mukesh Upadhyay. 2016. “Influence of Process Conditions on Product Yield of Waste Tyre Pyrolysis- A Review.” *Korean Journal of Chemical Engineering* 33 (8): 2268–86. https://doi.org/10.1007/s11814-016-0126-2.

Pereira, Bruno Miguel Sousa Pisco. 2016. “Reaproveitamento de óleo queimado através do processo de Pirolise,” November. https://comum.rcaap.pt/handle/10400.26/28883.

Peters, Jens F., Diego Iribarren, and Javier Dufour. 2015. “Simulation and Life Cycle Assessment of Biofuel Production via Fast Pyrolysis and Hydroupgrading.” *Fuel* 139 (January): 441–56. https://doi.org/10.1016/j.fuel.2014.09.014.

Piehl, Robert L. 1971. Corrosion control in hydroconversion effluent piping by nh4 + control. United States US3583901A, filed February 3, 1969, and issued June 8, 1971. https://patents.google.com/patent/US3583901A/en.

Pires, Anamaria P. P., Yinglei Han, John Kramlich, and Manuel Garcia-Perez. 2018. “Chemical Composition and Fuel Properties of Alternative Jet Fuels.” *BioResources* 13 (2): 2632–57. https://doi.org/10.15376/biores.13.2.2632-2657.

Plazas-González, Meliza, Carlos Alberto Guerrero-Fajardo, and José Ricardo Sodré. 2018. “Modelling and Simulation of Hydrotreating of Palm Oil Components to Obtain Green Diesel.” *Journal of Cleaner Production* 184 (May): 301–8. https://doi.org/10.1016/j.jclepro.2018.02.275.

Rahman, Md. Maksudur, Yun Yu, and Hongwei Wu. 2022. “Valorisation of Waste Tyre via Pyrolysis: Advances and Perspectives.” *Energy & Fuels*, September. https://doi.org/10.1021/acs.energyfuels.2c02053.

Riazi, M. R. 2005. *Characterization and Properties of Petroleum Fractions*. W. Conshohocken, PA: ASTM International.

Riazi, M.R. 1986. “API Databook, 5th Ed., Procedure 2B7.1.”

Robinson, P.R. 2011. “Hydroconversion Processes and Technology for Clean Fuel and Chemical Production.” In *Advances in Clean Hydrocarbon Fuel Processing*, 287–325. Elsevier. https://doi.org/10.1533/9780857093783.3.287.

Santos, Ronaldo Gonçalves dos, Catharina Lucas Rocha, Fernanda Lopes Souza Felipe, Francielli Tonon Cezario, Paula Juliana Correia, and Sina Rezaei-Gomari. 2020. “Tire Waste Management: An Overview from Chemical Compounding to the Pyrolysis-Derived Fuels.” *Journal of Material Cycles and Waste Management* 22 (3): 628–41. https://doi.org/10.1007/s10163-020-00986-8.

Sathiskumar, C., and S. Karthikeyan. 2019. “Recycling of Waste Tires and Its Energy Storage Application of By-Products –a Review.” *Sustainable Materials and Technologies* 22 (December): e00125. https://doi.org/10.1016/j.susmat.2019.e00125.

Sbaaei, Eslam S., and Tamer S. Ahmed. 2018. “Predictive Modeling and Optimization for an Industrial Coker Complex Hydrotreating Unit – Development and a Case Study.” *Fuel* 212 (January): 61–76. https://doi.org/10.1016/j.fuel.2017.10.032.

Shemfe, Mobolaji B., Sai Gu, and Panneerselvam Ranganathan. 2015. “Techno-Economic Performance Analysis of Biofuel Production and Miniature Electric Power Generation from Biomass Fast Pyrolysis and Bio-Oil Upgrading.” *Fuel* 143 (March): 361–72. https://doi.org/10.1016/j.fuel.2014.11.078.

Somsri, Surapat. 2018. *Upgrading of Waste Tire Pyrolysis Oil*. http://urn.kb.se/resolve?urn=urn:nbn:se:kth:diva-228358.

Soria Baledón, Mónica, Marcel Trudel, and Nicolás Kosoy. 2022. “Alternative Jet Fuels and Climate Geopolitics: What, Why Does It and Who Matters in the Environmental Policy-Making Process.” *International Journal of Sustainable Transportation* 16 (6): 541–57. https://doi.org/10.1080/15568318.2021.1912225.

Speight, James G. 1999. *The Chemistry and Technology of Petroleum*. CRC Press.

T. Dick, Deinma, Oluranti Agboola, Augustine O. Ayeni, and Department of Chemical Engineering, College of Engineering, Covenant University, Ota, Nigeria. 2020. “Pyrolysis of Waste Tyre for High-Quality Fuel Products: A Review.” *AIMS Energy* 8 (5): 869–95. https://doi.org/10.3934/energy.2020.5.869.

Taylor, Bryan. 2022. “Scrap Tire Pyrolysis Plant to Be Built in Germany.” Recycling Today. July 25, 2022. https://www.recyclingtoday.com/article/pyrum-mcapital-tire-recycling-pyrolysis-bavaria-germany-investment/.

Ucar, Suat, Selhan Karagoz, Ahmet R. Ozkan, and Jale Yanik. 2005. “Evaluation of Two Different Scrap Tires as Hydrocarbon Source by Pyrolysis.” *Fuel* 84 (14): 1884–92. https://doi.org/10.1016/j.fuel.2005.04.002.

Why, Elaine Siew Kuan, Hwai Chyuan Ong, Hwei Voon Lee, Wei-Hsin Chen, N. Asikin-Mijan, Mahendra Varman, and Wen Jing Loh. 2022. “Single-Step Catalytic Deoxygenation of Palm Feedstocks for the Production of Sustainable Bio-Jet Fuel.” *Energy* 239 (January): 122017. https://doi.org/10.1016/j.energy.2021.122017.

Williams, Paul T. 2013. “Pyrolysis of Waste Tyres: A Review.” *Waste Management* 33 (8): 1714–28. https://doi.org/10.1016/j.wasman.2013.05.003.

Williams, Paul T., Serpil Besler, and David T. Taylor. 1990. “The Pyrolysis of Scrap Automotive Tyres.” *Fuel* 69 (12): 1474–82. https://doi.org/10.1016/0016-2361(90)90193-T.

Wu, Qijing, Qianqian Zhang, Xiaoyan Chen, Guohui Song, and Jun Xiao. 2022. “Integrated Assessment of Waste Tire Pyrolysis and Upgrading Pathways for Production of High-Value Products.” *ACS Omega* 7 (35): 30954–66. https://doi.org/10.1021/acsomega.2c02952.

Yadav, Ashutosh, and Sangram Roy. 2022. “Modelling of Hydrodesulphurization in Industrial Trickle Bed Reactor Using Mixing Cell Network Approach.” *The Canadian Journal of Chemical Engineering* 100 (8): 1764–70. https://doi.org/10.1002/cjce.24280.

Zhang, Guohao, Feng Chen, Yuhao Zhang, Liang Zhao, Jingye Chen, Liyuan Cao, Jinsen Gao, and Chunming Xu. 2021. “Properties and Utilization of Waste Tire Pyrolysis Oil: A Mini Review.” *Fuel Processing Technology* 211 (January): 106582. https://doi.org/10.1016/j.fuproc.2020.106582.

Zhang, Xin, Jiyun Tang, and Juan Chen. 2022. “Behavior of Sulfur during Pyrolysis of Waste Tires: A Critical Review.” *Journal of the Energy Institute* 102 (June): 302–14. https://doi.org/10.1016/j.joei.2022.04.006.

Zhang, Yeshui, Chunfei Wu, Mohamad A. Nahil, and Paul Williams. 2015. “Pyrolysis–Catalytic Reforming/Gasification of Waste Tires for Production of Carbon Nanotubes and Hydrogen.” *Energy & Fuels* 29 (5): 3328–34. https://doi.org/10.1021/acs.energyfuels.5b00408.

Zhu, Frank Xin X., Richard Hoehn, Vasant Thakkar, and Edwin Yuh. 2017. *Hydroprocessing for Clean Energy: Design, Operation, and Optimization*. Hoboken, New Jersey: John Wiley & Sons, Inc. https://doi.org/10.1002/9781119328261.

Appendix

Table 16 - Industries that treat waste tires.

Working Since	Continent	Company	Capacity of Waste Tires to treat tonne/year	Location	Reference
	Europe	Pyrum Innovations AG	18143.695	Germany. Bavaria	(Taylor 2022)
Dec.2021	Europe	Carlton Forest Renewables	8760	Worksop. UK	(Goodchild 2022)
2023	Europe	Elysyum nordic	*30.000*	Nyborg Harbor. Denmark	(Elysium Press 2020)
2016	Europe	Klean Industries	20.000	Poland	(Klean n.d.)
	Europe	Pyrolysis Hellas	20 000	Greece	(ERJ 2022)
2022 2nd half	Europe	*Wastefront*	65700	UK	(Latchem 2020)

Pyrolysis

Parameter Estimation

Table 17 – Ismail et al. 2017 116 reaction rates parameters, Aspen Plus® 38 reaction reactions parameters the best parameter estimation parameter (38 reactions).

			Classification	A	Aspen 38	Parameter estimation (38)	E (kJ/mol)	n (Temperature coefficient)
1	Methane	$C + 2\ H_2 \rightarrow CH_4$	gas	4.877	5.3	2.69862	23.01	0
2	Ethane	$2\ C + 3\ H_2 \rightarrow C_2H_6$	gas	0.52	0.52	0.265213	23.01	0
3	Ethene	$2\ C + 2\ H_2 \rightarrow C_2H_4$	gas	2.386	2.386	1.21516	23.01	0
4	Propane	$3\ C + 4\ H_2 \rightarrow C_3H_8$	gas	0.277	0.277	0.141506	23.01	0
5	Propene	$3\ C + 3\ H_2 \rightarrow C_3H_6$	gas	0.446	0.446	0.227541	23.01	0
6	Butane	$4\ C + 5\ H_2 \rightarrow C_4H_{10}$	gas	0.122	0.122	0.062599	23.01	0
7	Butene	$4\ C + 4\ H_2 \rightarrow C_4H_8$	gas	0.144	0.144	0.073799	23.01	0
8	Butalyne	$4\ C + 3\ H_2 \rightarrow C_4H_6$	gas	0.981			23.01	0
9	Carbon Dioxide	$C + O_2 \rightarrow CO_2$	gas	0.226	0.096	0.320293	23.01	0
10	Carbon Monoxide	$C + 0.5\ O_2 \rightarrow CO$	gas	0.096	0.226	0.267984	23.01	0
11	Hydrogen Sulfide	$H_2 + S \rightarrow H_2S$	gas	Equilibirum	0.4	0.232977	Equilibirum	0
12	Pentane	$5\ C + 5\ H_2 \rightarrow C_5H_{10}$	gas	0.339			23.01	0
13	Pentalyne	$5\ C + 5\ H_2 \rightarrow C_5H_{10}$	gas	0.066			23.01	0
14,15	Methylcyclopentene	$6\ C + 6\ H_2 \rightarrow C_6H_{12}$	non_aromatic	0.009,0.009			1.59	0
16	Methylhexadiene	$8\ C + 7\ H_2 \rightarrow C_8H_{14}$	non_aromatic	0.016			1.59	0
17,19	Trimethylpentane	$8\ C + 9\ H_2 \rightarrow C_8H_{18}$	non_aromatic	0.023,0.019	0.0231	0.050388	1.59	0
18	Dimethylcyclopentane	$7\ C + 7\ H_2 \rightarrow C_7H_{14}$	non_aromatic	0.015			1.59	0
20	Dimethylhexane	$8\ C + 9\ H_2 \rightarrow C_8H_{18}$	non_aromatic	0.044			1.59	0
21	Ethylcyclopentane	$7\ C + 7\ H_2 \rightarrow C_7H_{14}$	non_aromatic	0.008			1.59	0
22	Methylcyclohexene	$7\ C + 7\ H_2 \rightarrow C_7H_{14}$	non_aromatic	0.045			1.59	0
23	Dimethylcyclohexane	$8\ C + 8\ H_2 \rightarrow C_8H_{16}$	non_aromatic	0.01	0.01	0.07439	1.59	0
24	Octene	$8\ C + 8\ H_2 \rightarrow C_8H_{16}$	non_aromatic	0.007			1.59	0

25	Dimethylhexadiene	8 C + 7 H_2 → C_8H_{14}	non_aromatic	0.011			1.59	0
26,27	Ethylcyclohexane	8 C + 8 H_2 → C_8H_{16}	non_aromatic	0.054,0.007			1.59	0
28	Trimethylcyclohexane	9 C + 9 H_2 → C_9H_{18}	non_aromatic	0.003			1.59	0
29	Nonene	9 C + 9 H_2 → C_9H_{18}	non_aromatic	0.017			1.59	0
30	Methylocatene	9 C + 9 H_2 → C_9H_{18}	non_aromatic	0.164	0.164	0.260338	1.59	0
31	Dlimonene	10 C + 8 H_2 → $C_{10}H_{16}$	non_aromatic	0.035			1.59	0
32	Pinene	10 C + 8 H_2 → $C_{10}H_{16}$	non_aromatic	0.064			1.59	0
33	Limonene	10 C + 8 H_2 → $C_{10}H_{16}$	non_aromatic	0.619	0.35	0.286891	1.59	0
34	Benzene	6 C + 3 H_2 → C_6H_6	aromatic	1.654	4.708	2.39725	33.89	0
35	Toluene	7 C + 4 H_2 → C_7H_8	aromatic	7.305	12	7.84012	33.89	0
36	Ethylbenzene	8 C + 5 H_2 → C_8H_{10}	aromatic	4.708	4.708	2.43545	33.89	0
37	Xylene	8 C + 5 H_2 → C_8H_{10}	aromatic	4.476	4.476	2.31728	33.89	0
38	Styrenetyrene	8 C + 4 H_2 → C_8H_8	aromatic	4.049	4.049	5.94432	33.89	0
39	Dimethylbenzene	8 C + 5 H_2 → C_8H_{10}	aromatic	1.084			33.89	0
40	Cumene	9 C + 6 H_2 → C_9H_{12}	aromatic	1.07			33.89	0
41	Ethylmethylbenzene	9 C + 5 H_2 → C_9H_{10}	aromatic	0.5	0.5	0.631691	33.89	0
42	Propylbenzene	9 C + 6 H_2 → C_9H_{12}	aromatic	1.117			33.89	0
43,44	Ethylbenzene	9 C + 6 H_2 → C_9H_{12}	aromatic	1.189,2.128	4.708	2.43545	33.89	0
45	Trimethylbenzene	9 C + 6 H_2 → C_9H_{12}	aromatic	0.424			33.89	0
46	Phenol	6 C + 3 H_2 → C_6H_6	aromatic	0.497			33.89	0
47,51,52	Methylethenylbenzene	9 C + 5 H_2 → C_9H_{10}	aromatic	1.532,0.634,0.344	1.532	1.25507	33.89	0
48	Benzonitrile	7 C + 2.5 H_2 → C_7H_5	aromatic	0.528			33.89	0
49	Propenylbenzene	9 C + 5 H_2 → C_9H_{10}	aromatic	0.567			33.89	0

50	C3-benzene	9 C + 6 H_2 → C_9H_{12}	aromatic	1.808			33.89	0
53	Isopropyltoluene	10 C + 7 H_2 → $C_{10}H_{14}$	aromatic	3.85	0.769	1.19228	33.89	0
54	C3-benzene	9 C + 6 H_2 → C_9H_{12}	aromatic	0.392			33.89	0
55	Dihydro-1H-indene	9 C + 5 H_2 → C_9H_{10}	aromatic	0.922			33.89	0
56	1H-indene	9 C + 4 H_2 → C_9H_8	aromatic	1.278	1.278	7.87142	33.89	0
57	Butylbenzene	10 C + 7 H_2 → $C_{10}H_{14}$	aromatic	1.058			33.89	0
58	Ethyldimethylbenzene	10 C + 7 H_2 → $C_{10}H_{14}$	aromatic	0.338			33.89	0
59,61	Isopropylmethylbenzene	10 C + 7 H_2 → $C_{10}H_{14}$	aromatic	0.769,0.678	3.85	2.76076	33.89	0
60	Ethyldimethylbenzene	10 C + 7 H_2 → $C_{10}H_{14}$	aromatic	0.397			33.89	0
62,7,9,73	Dihydromethyl-1H-indene	9 C + 5 H_2 → C_9H_{10}	aromatic	0.516,0.759,3.694,0.433			33.89	0
63	Tetramethylbenzene	10 C + 7 H_2 → $C_{10}H_{14}$	aromatic	0.383			33.89	0
64	Tetramethylbenzene	10 C + 7 H_2 → $C_{10}H_{14}$	aromatic	0.4			33.89	0
65	Ethylisopropylbenzene	10 C + 7 H_2 → $C_{10}H_{14}$	aromatic	0.198			33.89	0
66	Dimethylphenol	8 C + 5 H_2 + 0.5 O_2 → $C_8H_{10}O$	aromatic	0.316			33.89	0
68	Benzoic acid	7 C + 3 H_2 + O_2 → $C_7H_6O_2$	aromatic	0.549			33.89	0
70	Methyl-1H-indene	10 C + 5 H_2 → $C_{10}H_{10}$	aromatic	0.439			33.89	0
71	Tetrahydronaphalene	10 C + 6 H_2 → $C_{10}H_{12}$	aromatic	0.562			33.89	0
72	C4-benzene	10 C + 7 H_2 → $C_{10}H_{14}$	aromatic	0.165			33.89	0
74	Naphthalene	10 C + 4 H_2 → $C_{10}H_8$	aromatic	0.979	0.979	1.34644	33.89	0
75	Isopropylphenol	10 C + 7 H_2 + 0.5 O_2 → $C_{10}H_{14}O$	aromatic	0.056			33.89	0

76	Benzothiazole	7 C + 2.5 H_2 + 2 S+0.5 N_2 → $C_7H_5NS_2$	aromatic	1.2	1.2	4.53823	33.89	0
77	Tetrahydroethylnaphthalene	12 C + 8 H_2 → $C_{12}H_{16}$	tar	47.264			6.3	-1.089
78	C6-benzene	12 C + 9 H_2 → $C_{12}H_{18}$	tar	47.815			6.3	-1.089
79,80	Methylnaphthalene	11 C + 5 H_2 → $C_{11}H_{10}$	tar	125.001,156.807	125	161.844	6.3	-1.089
81,2	Trimethylindene	12 C + 7 H_2 → $C_{12}H_{14}$	tar	9.307,95.891			6.3	-1.089
83	Diphenyl	12 C + 5 H_2 → $C_{12}H_{10}$	tar	142.201	142.2	152.924	6.3	-1.089
84,5	Ethylnaphthalene	12 C + 6 H_2 → $C_{12}H_{12}$	tar	97.289, 37.367	97.283	165.24	6.3	-1.089
86,7,8	Dimethylnaphthalene	12 C + 6 H_2 → $C_{12}H_{12}$	tar	85.169, 83.486, 119.843	85.169	165.917	6.3	-1.089
89	Ethylquinoline	10 C + 4.5 H_2 + 0.5 N_2 → $C_{10}H_9N$	tar	184.356			6.3	-1.089
90	n-C14	14 C + 14 H_2 → $C_{14}H_{28}$	tar	118.294	118.294	165.666	6.3	-1.089
91	Acenaphthene	12 C + 5 H_2 → $C_{12}H_{10}$	tar	36.147			6.3	-1.089
92	n-C15	15 C + 16 H_2 → $C_{15}H_{32}$	tar	56.974	56.974	143.373	6.3	-1.089
93,4,5	Trimethylnaphthalene	15 C + 9 H_2 → $C_{15}H_{18}$	tar	88.852, 31.429, 29.175	22.6	14.7977	6.3	-1.089
96	Fluorene	13 C + 5 H_2 → $C_{13}H_{10}$	tar	47.77			6.3	-1.089
97,8	Dimethyldiphenyl	15 C + 8 H_2 → $C_{15}H_{16}$	tar	60.554, 11.521	60.554	36.3494	6.3	-1.089
99	Pentadecene	15 C + 15 H_2 → $C_{15}H_{30}$	tar	17.88			6.3	-1.089
100	n-C16	16 C + 17 H_2 → $C_{16}H_{34}$	tar	46.822	46.822	54.8564	6.3	-1.089
101	Phenanthrene	14 C + 5 H_2 → $C_{14}H_{10}$	tar	34.666			6.3	-1.089

102	Anthracene	14 C + 5 $H_2 \rightarrow C_{14}H_{10}$	tar	38.059			6.3	-1.089
103	Methylphenanthrene	15 C + 6 $H_2 \rightarrow C_{15}H_{12}$	tar	36.925	36.925	151.693	6.3	-1.089
104	Pentadecanoic acid	15 C + 15 H_2 + $O_2 \rightarrow C_{15}H_{30}O_2$	tar	64.017			6.3	-1.089
105,6,7	Methylphenanthrene	15 C + 6 $H_2 \rightarrow C_{15}H_{12}$	tar	41.028, 46.908, 82.056	36.925	151.693	6.3	-1.089
108	n-C19	19 C + 20 $H_2 \rightarrow C_{19}H_{40}$	tar	12.247			6.3	-1.089
109	Trimethylphenanthrene	19 C + 8 $H_2 \rightarrow C_{19}H_{16}$	tar	22.599			6.3	-1.089
110	Isopropylmethylphenanthrene	19 C + 19 $H_2 \rightarrow C_{19}H_{38}$	tar	51.627			6.3	-1.089
111	n-C20	20 C + 21 $H_2 \rightarrow C_{20}H_{42}$	tar	13.594	13.594	31.2239	6.3	-1.089
112	n-C21	21 C + 22 $H_2 \rightarrow C_{21}H_{44}$	tar	15.524			6.3	-1.089
113	n-C22	22 C + 23 $H_2 \rightarrow C_{22}H_{46}$	tar	12.028			6.3	-1.089
114	n-C23	23 C + 24 $H_2 \rightarrow C_{23}H_{48}$	tar	15.641			6.3	-1.089
115	n-C24	24 C + 25 $H_2 \rightarrow C_{24}H_{50}$	tar	3.029			6.3	-1.089
116	n-C11	11 C + 12 $H_2 \rightarrow C_{11}H_{24}$	tar	35.684	35.584	130.31	6.3	-1.089

Compounds Classification

Table 18 – Compounds classification.

Aspen Nomenclature	Characterization	Chemical name
C	Solid	Carbon
H_2	Gas	Hydrogen
O_2	Gas	Oxygen
N_2	Gas	Nitrogen
S	Solid	Sulfur
Methane	Gas	Methane
Ethane	Gas	Ethane
Ethene	Gas	Ethene
Propane	Gas	Propane
Propene	Gas	Propene
Butane	Gas	Butane
Butene	Gas	Butene
CO	Gas	Carbon Monoxide
CO_2	Gas	Carbon Dioxide
H_2S	Gas	Hydrogen Sulfide
TRIMPENT	isoparaffin	2.2.3-Trimethylpentane
DMCHEX	Cycloparaffin	1.1-Dimethylcyclohexane
ETHBENZ	Aromatic	Ethylbenzene
DMNAPHTA	naphtalene	1.2-Dimethylnaphthalene
METYBENZ	Aromatic	1-Methyl-2-Ethylbenzene
ISPROTOL	Aromatic	1-Methyl-2Isopropylbenzene
METNAPH	naphtalene	1-Methylnaphthalene
METETBEN	Aromatic	P-Methyl-Stirene
MPHENANT	naphtalene	4-Methylphenanthrene
TRIMTNAF	naphtalene	1.2.6Trimethylnaphthalene
ISPRMBEN	Aromatic	1-Methyl-4Isopropylbenzene
INDENE	Aromatic	Indene
ETNAPHTA	naphtalene	1-Ethylnaphthalene
DIPHENYL	naphtalene	Diphenyl
MBIPHENY	naphtalene	Biphenyl.-4-Methyl-
NAPHTALE	naphtalene	Naphthalene
BENZTHIA	Aromatic	Benzothiazole
NC11	N-Alkane	N-Undecane
NC14	N-Alkane	N-Tetradecane
NC15	N-Alkane	N-Pentadecane
NC16	N-Alkane	N-Hexadecane
NC20	N-Alkane	N-Eicosane
MOCTENE	Olefin	7-Methyl-1-Octene
LIMONENE	Olefin	D-Limonene
TRIMTNAF	naphtalene	1.2.6Trimethylnaphthalene
ISPRMBEN	Aromatic	1-Methyl-4Isopropylbenzene
BENZENE	Aromatic	Benzene
TOLUENE	Aromatic	Toluene
XYLENE	Aromatic	O-Xylene
STYRENE	Aromatic	Stirene

Composition of different tires

Table 19 – Ultimate analysis of different tires. (J. D. Martínez et al. 2013)

	Motorcycle Tire	Bus Tire	Truck tire	Passenger car tire 1	Passenger car tire 2
Carbon	77.85	84.34	78.98	75.56	83.92
Sulphur	1.29	1.97	1.37	1.59	0.92
Hydrogen	7.30	7.07	7.31	6.43	6.83
Oxygen	5.09	0.62	5.85	0.64	3.39
Nitrogen	0.92	0.24	1.42	0.23	0.78
Ashes	7.54	5.76	5.07	15.56	4.16

Hydrotreatment

Kinetic parameters

Table 20 - Kinetic parameters, pre-exponential constant for the reference temperature, 390 ºC and the activation energy values.

	ki	ki,390ºC (gfeed/gcath)	E (kJ/mol)
Hydrogenation	k1	(3.71±0.15)·102	0.61±0.29
Dehydrogenation	k-1	(1.49±0.15)·102	
Hydrogenation	k2	(1.57±0.36)·102	92.01±11.43
Dehydrogenation	k-2	(1.66±0.36)·102	
Ring Opening	k3	(1.71±0.11)·102	22.78±2.15
Cyclization	k-3	16.3±0.11	
Chain sicssion	k4	1.71±0.11	69.73±2.56

Hydrotreater – Reproducing experimental data

Vapor Phase (1000 Nm^3/m^3)

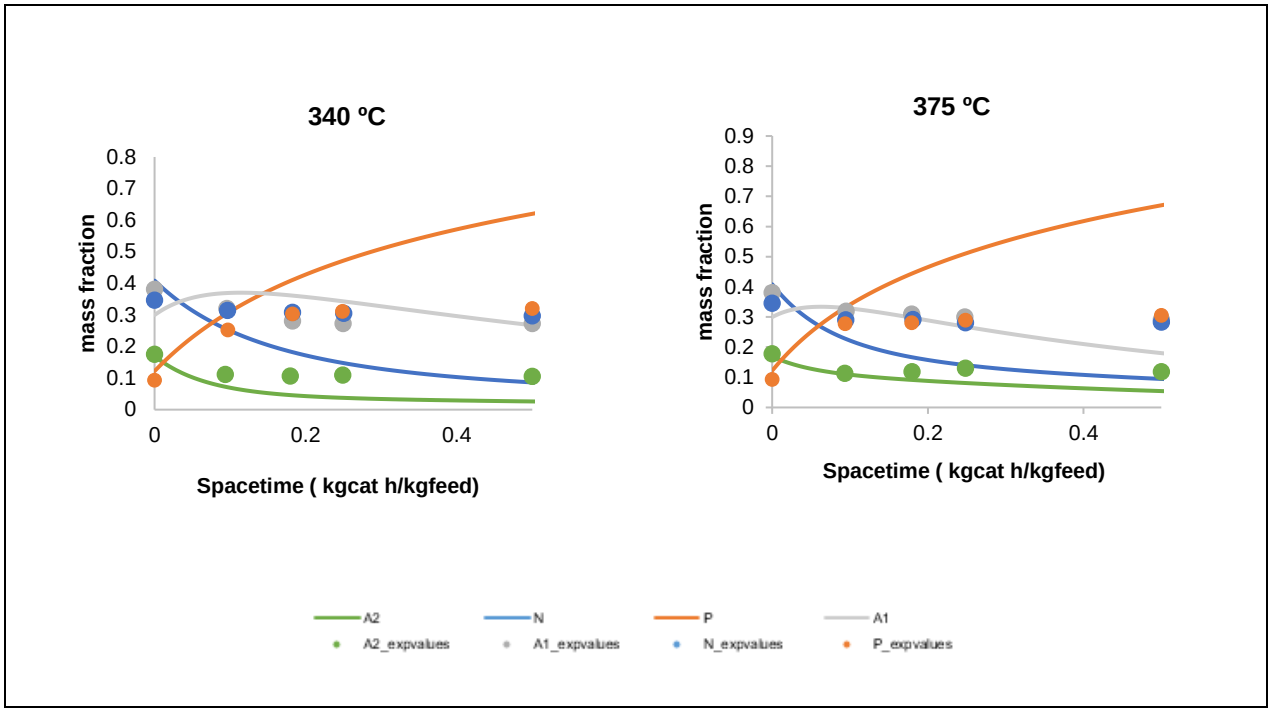

Figure 46 - Reproduction of Olmo 2015 experimental results and comparison of simulation and experimental data for 340 (63% vaporized), 375 ºC (100% vaporized) and 65 bar, for a vapor phase kinetic.

Reduction of the hydrogen ratio

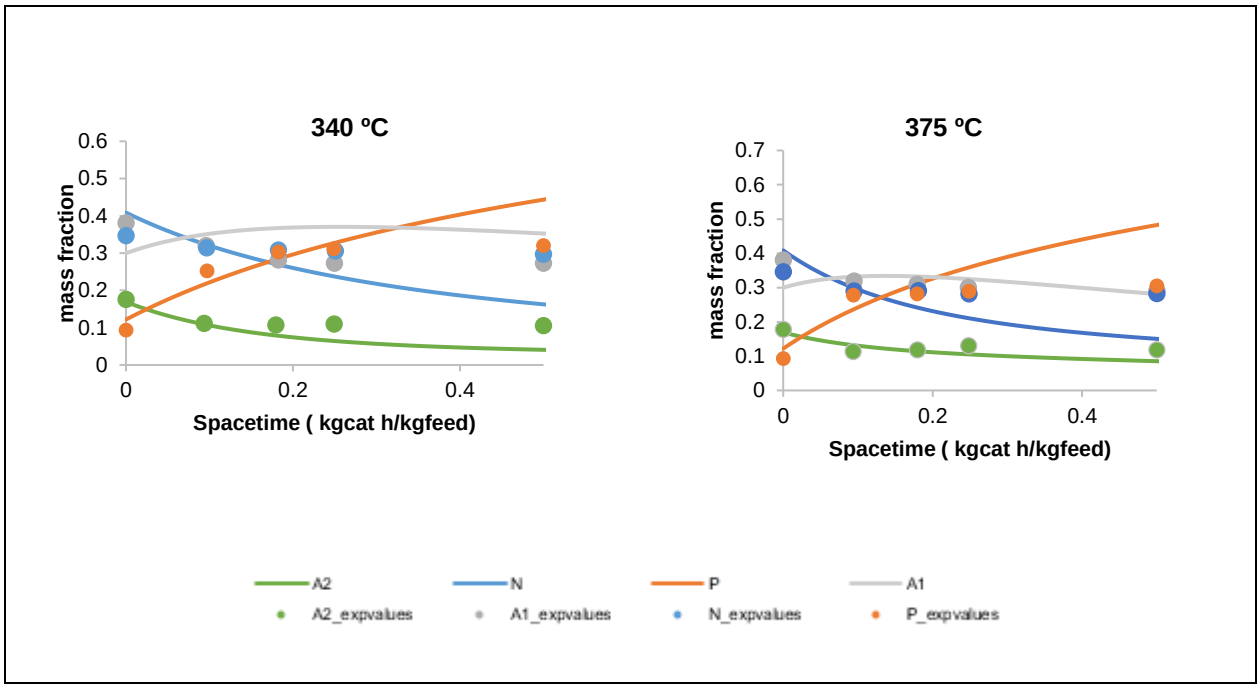

Figure 47 - Reproduction of Olmo 2015 experimental results and comparison of simulation and experimental data for 340. 375 ºC and 65 bar, for the 420 Nm3/m3 ratio.

Lumping

A1 lumping

Table 21 – A1 lumping molar fraction.

	MW	Fraction	Relative Error
TOLUENE	92.1405	0.191	15%
XYLENE	106.167	0.105	2%
STIRENE	104.152	0.171	4%
ETHBENZ	106.167	0.104	2%
METYBENZ	120.194	0.057	11%
ISPROTOL	134.221	0.099	24%
METETBEN	118.178	0.160	9%
BENZENE	78.1136	0.058	28%
ISPRMBEN	134.221	0.056	24%
Average MW	108.579		

A2 lumping

Table 22 – Molecular weight of each compound that is part of the A2 lump, their molar fraction and their relative error to the average molecular weight.

	MW	Fraction	Relative Error
INDENE	116.163	0.180	23.4%
MPHENANT	192.26	0.135	26.8%
DMNAPHTA	156.227	0.151	3.0%
METNAPH	142.2	0.144	6.2%
TRIMTNAF	170.254	0.025	12.3%
ETNAPHTA	156.227	0.152	3.0%
DIPHENYL	154.211	0.130	1.7%
MBIPHENY	168.238	0.050	10.9%
NAPHTALE	128.174	0.033	15.5%
Average MW	151.644		

N lumping

Table 23 - Molecular weight of each compound that is part of the N lump, their molar fraction and their relative error to the average molecular weight.

	MW	Fraction	Relative Error
DMCHEX	112.215	0.240	14%
LIMONENE	136.237	0.760	4%
Average MW	130.467		

P lumping

Table 24 - Molecular weight of each compound that is part of the P lump, their molar fraction and their relative error to the average molecular weight.

	MW	Fraction	Relative Error
TRIMPENT	114.231	0.143	26%
NC11	156.312	0.108	1%
NC14	198.392	0.126	28%
NC15	212.419	0.113	37%
NC16	226.446	0.042	46%
NC20	282.553	0.029	82%
MOCTENE	126.242	0.439	19%
Average MW	155.37		

Pseudcomponents Method Choosing

Table 25 - Heat of vaporization Gcal/hr relative error.

	P	A1	A2	N	Average Relative Error
Aspen	31.68%	6.76%	24.21%	14.45%	19%
API-METH	31.68%	6.76%	24.21%	14.45%	19%
LK	33.42%	7.53%	25.66%	16.06%	21%
API-TWU	33.92%	7.92%	26.13%	15.96%	21%
EXTTWU	33.78%	8.11%	26.08%	16.04%	21%
EXTAPI	33.79%	8.12%	26.10%	16.05%	21%
EXTCAV	35.77%	7.40%	27.27%	17.24%	22%
HYSTWU	33.89%	8.23%	26.20%	16.18%	21%